ABSTRACT

Title of Dissertation: ENTROPIC APPROACHES FOR ASSESSMENT OF METAL FATIGUE DAMAGE

Huisung Yun, Doctor of Philosophy, 2019

Dissertation directed by: Professor Mohammad Modarres
Center for Risk and Reliability
Department of Mechanical Engineering

Prognostics and Health Management (PHM), a promising technique assessing individual life of engineering systems, requires metrics that indicate the current level of degradation and aging. However, traditional methods of fatigue life estimation have a restriction to apply to PHM due to scale dependency of measurements. An alternative to the conventional fatigue assessment is the entropic approach, initially derived from the second law of thermodynamics. The entropic approach is scale-independent and able to monitor degradation and aging from the early periods of life. The entropic endurance indicates a certain level of damage that a component can tolerate before failure. Not only the thermodynamic theory but also information and statistical mechanics laws introducing entropy apply to the various modes of energy dissipations. This dissertation introduces the extension of the entropic approaches as the representation of damage by empirically examining the theoretical basis of three entropic theorems. Metallic cou-

pons were fatigue tested to confirm the applicability of three entropic measures: irreversible thermodynamic entropy, information (Shannon) entropy, and Jeffreys divergence, by measuring variables used to compute energy dissipations during fatigue. In addition to the entropic approaches to damage, short-term loading process (STLP) is designed to minimize the difficulties associated with acoustic emission background noise when used to measure information entropy of the generated signals. Without damaging the material, high-frequency/low-amplitude loading is expected to generate acoustic signals through quiet background noise excitation loading to infer the current damage status. The results of this research help identifying multiple damage measurement methods and will broaden understanding and selecting practical applications, and reduce the prognosis uncertainty in PHM applications.

ENTROPIC APPROACHES FOR ASSESSMENT OF METAL FATIGUE DAMAGE

by

Huisung Yun

Dissertation submitted to the Faculty of the Graduate School of the
University of Maryland, College Park, in partial fulfillment
of the requirements for the degree of
Doctor of Philosophy
2019

Advisory Committee:
Professor Mohammad Modarres, Chair
Professor Aris Christou
Professor Katrina M. Groth
Professor Sung Lee
Professor Christopher Jarzynski (Dean's Representative)

Acknowledgements

Ministry of National Defense, Republic of Korea provided the finance and time to study at University of Maryland. The commissioned education program to the active army officer was invaluable, and I should acknowledge this policy.

Reliability and Mechanics Laboratory team was my stalwart supporter. Christine Sauerbrunn was my co-researcher since the beginning of my experimental studies. Mehdi Amiri and Ali Kahirdeh were the best advisors in approaching to the studies, from the theoretical understanding to experimental settlement.

In broadening knowledge, from fundamentals to the state-of-art techniques related to reliability engineering, course instructors, when I was taking those courses and working as the Teaching Assistant, provided lots of opportunities to review the studies related to my research. Notably, Dr. Vasiliy Krivtsov showed the reliability data analysis tools applicable to the present and gave more chance to profoundly understanding the linkage between the theory and application. Dr. Peter Chung reminded fundamental statistical tools by teaching undergraduate students.

Dr. Christopher Jarzynski advised the part of statistical mechanics studies. As the founder of Jarzynski equality, his lectures and discussions enriched my research to address the applicability limitation and understand the gap between natural science and engineering approaches.

Above all, I heartily acknowledge my advisor, Dr. Mohammad Modarres, he unconditionally guided and supported my research. Without his support, it is unimaginable to complete my Ph.D. studies.

Table of Contents

List of Tables

List of Figures

List of Abbreviations

AA: Aluminum alloy
AE: Acoustic emission
AST: Automatic sensor test
CI: Criticality index
CIE: Cumulative information entropy
CTE: Classical thermodynamic entropy
DEG: Degradation-entropy generation
EDM: Electro discharge machining
ECG: Electro-cardiogram
FEM: Finite element method
HVDC: High-voltage direct current
IE: Information entropy
JD: Jeffreys divergence
LEFM: Linear elastic fracture mechanics
MaxEnt: Maximum entropy
MDD: Modulus degradation damage
NDT: Non-destructive testing
PHM: Prognostics and health management
PoF: Physics of failure
RE: Relative entropy
RNA: Ribo-nucleic acid
RUL: Remaining useful life
SD: Standard deviation
SE: Squared error
SS: Stainless steel
STLP: Short-term loading process
XRD: X-ray powder diffraction

Chapter 1: Motivation of Research

Empirically-based probabilistic models have been the main tools in engineering materials to assess the extent of degradation and damage, including the likelihood of failure occurrence. Of particular interests in recent years has been the physics of failure (PoF) approach, whereby surrogates or markers of damage are empirically correlated with the time-varied agents (stresses) that cause or induce the damage. In supplementing traditional PoF models, the entropic damage assessment has emerged as an alternative. Different from the traditional life assessment methods, e.g., deterministic life models and observable markers, entropic methods can utilize real-time irreversible energy dissipation during the damaging process to indicate the amount of total damage.

Well-known experimental proof of the entropic approach in fatigue is available through the use of irreversible strain energy and temperature [1]. Various researchers have proved the existence of an entropic endurance, which indicates a certain level of entropy around which materials and structures fail [2,3] regardless of the path to failure. Not only fatigue but other failure mechanisms have also shown the same behavior of endurance, e.g., wear and corrosion [1,4-12].

Most of the entropic approaches have been investigated in the context of thermodynamic frameworks. On the other hand, not only the second law of thermodynamics but other entropic theories, e.g., information theory, introduce entropy as metrics of disorder or uncertainty. By using information theory, acoustic emission (AE) waveform from fatigue damage may be characterized by the information entropy, and that may prove comparably a better indicator of damage than the traditional AE features such as the count of exceedingly large signals (threshold) [13].

Fluctuation theorem of G. E. Crooks in statistical mechanics introduces another concept to compute entropy from the forward/reverse works [14,15]. This theorem has been empirically verified from smaller-scale experiments only involving thermal energy dissipation [16,17]. Therefore, a question arises whether the fluctuation theorem can be empirically useful for application to a macro-scale fatigue process in which multiple energy dissipation modes exist. Accordingly, this expands entropic methodologies of damage as characterized empirically from the statistical mechanics theorem.

There is a need and opportunity to explore the three entropic theorems further, and their applications to PHM. In order to address this need, the applicability of three entropic theorems to predict incipient failures and the amount of fatigue damage needs to be demonstrated through empirical studies. Exploring entropic approaches using collected empirical data of energy dissipation during controlled experiments provide the core motivation in this study. As such, this research seeks to develop and compare various measures of entropy to assess fatigue failures. Ultimately, an effective damage representation during the application of the three entropic approaches to the metallic materials fatigue damage introduced in this research will enhance the PHM process.

Chapter 2: Introduction and Objectives

Prognostics and health management (PHM) is a promising method in reliability engineering to supplement traditional life assessments. The traditional damage measurements in fatigue, for example, crack growth and load-carrying capacity reduction, are detectable only in the later stages of life and are ineffective in characterizing damage during the earlier periods of life [18]. In contrast, PHM-based life estimation and prognosis incorporates related monitored damage variables into deterministic physics of failure (PoF) models [19-23]. In data-driven prognostics in PHM, observed damage precursors, such as initiation of very small cracks, are collected during system operation and are used to estimate the so-called remaining useful life (RUL) [22,24]. Among the approaches used to meet the requirements of early life prediction, entropy has appeared as a robust option according to degradation-entropy generation (DEG) theorem [11].

Entropy in DEG theorem is based on the irreversible thermodynamics and can be used to depict the endurance to failure, such as cycles to crack initiation or fracture [11,25,26]. Pioneering works in entropic approaches have verified successful applications to several failure mechanisms such as fatigue, corrosion, and wear. These entropies are derived from sources of irreversible energy dissipation [1,25-27]. In the case of fatigue damage, irreversible energy dissipations include plastic mechanical work, heat, and acoustic emission (AE) [28]. A popular entropic approach in fatigue is to use plastic strain energy and temperature [2,3]. In this approach, the existence of a fixed entropic endurance, irrespective of the underlying conditions that lead to fatigue damage and failure, is experimentally verified. It has resulted in good agreement with the

DEG theorem. Another approach has been to use acoustic energy dissipation during fatigue in the form of generated AE waveforms, where associated information entropy typically correlates well with the amount of fatigue damage [13].

Strain energy dissipation during the cyclic fatigue loading and unloading also appears to apply to the relative entropy. Crooks et al. [29] have shown that the Kullback-Leibler divergence computed from loading/unloading distributions is equivalent to the thermodynamic entropy when distributions of loading/unloading processes are measurable. This concept was demonstrated by Collin et al. [16], who measured thermal dissipation in the unfolding/folding process of an RNA (ribo-nucleic acid) strand. Loading/unloading work distributions were also used by Douarche et al. [17] to measure a brass wire's cyclic torsional work and to assess the Helmholtz free energy difference. In practical applications, relative entropy in cyclic mechanical work can be computed without the need for temperature information, which provides a potentially simpler entropic damage assessment than the classical thermodynamics. Not only mechanical work, but AE waveform can also be applied to the relative entropy by using a reference waveform. The assumption is that relative entropy discounts the AE background noise routinely embedded in an AE waveform.

In PHM using energy dissipation data during operation, several passive sensors are employed, e.g., load cell, strain gauge, thermocouple, and acoustic emission sensor. However, this process would be vulnerable to the noise generated during the operation or damaging process. On the other hand, non-destructive testing (NDT) of inspection uses active sensors, which has both signal transmitter and receiver, e.g., ultrasonic, x-ray powder diffraction (XRD), and eddy-currents. The investigation of these active

measurements may be performed in the controllable environment [30,31]. Instead of using additional active sensors, passive sensors can be used if an exciting signal is generated in the system. Short-term loading process (STLP) can be designed to generate high-frequency and low-amplitude loading and generate the signal representing the instantaneous damage status without damaging effect, using passive sensors. The STLP allows the application of low-amplitude/high-frequency loads that will not cause much of any damage to avoid background noise shortcomings which are notorious in the detection of AE signals during normal applications. Ultimately, the behaviors of waveforms and their information entropies during the STLP loading would provide a clear and noise-free prediction of fatigue damage.

This dissertation presents the entropic damage measurements from the dog-bone coupons that were fatigue tested using the three energy dissipations discussed: plastic mechanical work, thermal energy, and acoustic emission (AE). STLP method also supplements the entropic measures. In these approaches, use of the classical thermodynamics, information (Shannon), and relative entropy (Kullback-Leibler divergence) may be applied, evaluated in the context of PHM applications. This research objectives to the understanding of entropic fatigue damage are as follows:

1. Understand sources of irreversible energy dissipation in the metallic fatigue mechanisms, i.e., mechanical, thermal, and acoustic.
2. Develop and assess measures of entropy for each energy dissipation induced damage representing in materials based on thermodynamic, information, and statistical mechanics laws and theorems.

3. Develop experimental short-term loading process (STLP) and evaluate the usefulness of STLP method in fatigue damage measure.
4. Draw conclusions about the appropriateness of each method in PHM applications to fatigue damage measures.

The key contributions of this research are as follows:

1. Jeffreys divergence (JD) shows an excellent correlation to the measured damage. The usefulness of JD in macro-scale fatigue measurement was presented by the consistent pseudo-Boltzmann constant (k_{pB}).
2. AE information entropy provides a statistically better relation than conventional AE features by correlating to the measured damage.
3. STLP method detected the upcoming fatigue failure by the criticality index processed from cumulative AE information entropy.
4. Temperature rise and rise rate measured during the fatigue loading process indicate crack growth by the transition point.

This dissertation continues with six more chapters: Chapter 3 details the theoretical backgrounds based on previous related studies. Chapter 4 presents the experiment setup and analysis procedure. The results are discussed through chapters 5 to 7 by applications to fatigue crack growth (a macro-scale marker) analysis, entropic damage assessments, and STLP and temperature measurements. Finally, Chapter 8 summarizes and concludes the research and its findings, and presents recommendations for future expansions of this dissertation research.

Chapter 3: Literature Review

This chapter reviews related studies to make up the bases of this research: Entropic damage measures and STLP method.

3.1 Damage measurement in fatigue

According to Lemaitre [18], measurements of fatigue damage include changes detected in crack length, elastic modulus, micro-hardness, ultrasonic wave, and electric resistance. These measurements, also called markers of damage, are often only detectable when 10 - 20 % of life remains, which is too late for effective prognostic and corrective actions [24]. During the early period of life, assessment of damage must rely on deterministic life models, which tend to be highly uncertain, variable, and conservative [1].

Amiri and Modarres [1] have summarized and delineated fatigue damage scales and process into:

1. Nano-scale: The grain boundary, where atoms are more loosely packed, is a likely location for damage. At this scale, the states of material damage are physically determined by the configuration of the atomic bonds.
2. Micro-scale: Damage is the accumulation of the slip irreversibility that results in strain localizing in a small region within the materials, i.e., persistent slip bands and dislocation cells/bundles.
3. Meso-scale: Damage is the growth and coalescence of micro-cracks that initiate a crack.

4. Macro-scale: Damage is the growth of macro-cracks that results in final fracture of the structure.

Thus, the damage measurement scale evolves from the very small to larger scales, and it is only in the macro-scale that damage can be detected. As such, the lack of detectable damage is highly scale-dependent. However, damage measurement through the second law of thermodynamics suggests a universal methodology that applies to all the scales discussed above.

3.2 Degradation-entropy generation (DEG) theorem

Entropic metrics of damage have been proposed and utilized in engineering applications. Basaran [27,32] and Bryant [26] introduced thermodynamic concepts to assess damage in specific failure modes. Based on irreversible thermodynamic processes, these studies considered the degradation-induced dissipated energy or entropy as a reflection of the cumulative damage process. Amiri and Modarres [1] reviewed entropy for various failure mechanisms including fatigue, corrosion, and wear, and discussed the corresponding irreversible thermodynamic forces and fluxes used to calculate entropy generation. They reviewed in more detail the DEG theorem, including the concept of entropic endurance introduced by Imanian and Modarres [33], described as follows:

1. Entropic endurance of different units (or structural materials) is different.
2. Entropic endurance of the same unit is equal.
3. Entropic endurance of different units is different.
4. Entropic endurance can be measured experimentally, and depending on the accuracy of the experiments, it will involve stochastic variability.

Following the DEG theorem, it is expected that entropic endurance determines the amount of cumulative entropy that a unit can hold before failure, including variability.

Experimental results have supported this theorem for fatigue failures [2,3,25] by demonstrating that fatigue fracture occurs at a relatively fixed entropic endurance level regardless of the underlying loading profiles. **Figure 1** presents an example confirming this entropic theorem.

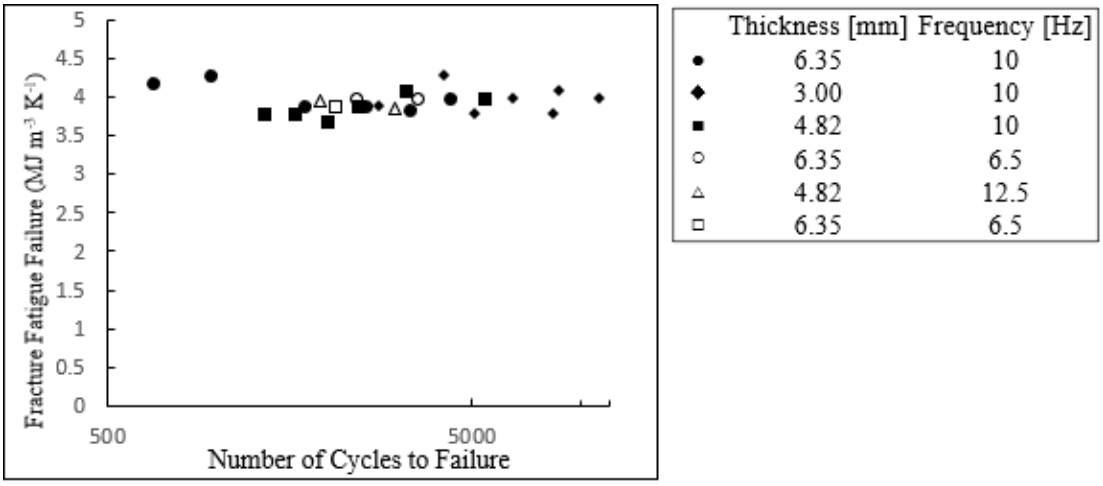

Figure 1. Cumulative entropy for various fatigue test conditions. The entropic data points show that the thermodynamic entropy has the endurance to failure, irrespective of the path to failure [2]. The cyclic bending loading was applied to each specimen with an amplitude of 25 - 50 mm.

The empirical validation of the DEG theorems has been demonstrated through the uses of classical thermodynamic entropy based on irreversible thermodynamics. In this study, entropic damage approaches are extended to other entropies. Information theory and fluctuation theorem in statistical mechanics will be mainly reviewed in the next sections, to apply in terms of the DEG theorem.

3.3 Irreversible energy dissipation in fatigue damage and entropy

From the irreversible thermodynamics, dissipative entropy generation may be expressed in the form of Equation (1) [1,25,33]:

$$\sigma = \sum_i X_i J_i. \quad (1)$$

This equation is bilinear, where X_i is the thermodynamic force, and J_i is the flux due to the dissipation mechanism i. Depending on the sources of energy dissipation, Amiri and Modarres [1] presented the entropy generation in its most general form, as shown by Equation (2) [25]:

$$\sigma = \frac{1}{T^2}\boldsymbol{J}_q \cdot \nabla T - \sum_k \boldsymbol{J}_k \left(\nabla \frac{\mu_k}{T}\right) + \frac{1}{T}\boldsymbol{\tau}: \dot{\boldsymbol{\varepsilon}}_P + \frac{1}{T}\sum_j \nu_j A_j + \frac{1}{T}\sum_m c_m \boldsymbol{J}_m(-\nabla\psi). \quad (2)$$

Where σ is the entropy generation rate, $\boldsymbol{J}_q$ is the thermodynamic flux due to heat conduction, $\boldsymbol{J}_k$ is the thermodynamic flux due to diffusion, μ_k is the chemical potential, $\boldsymbol{\tau}$ is the mechanical stress, $\boldsymbol{\varepsilon}_P$ is the plastic strain, ν_j is the chemical reaction rate, A_j is the chemical affinity, c_m is the coupling constant, $\boldsymbol{J}_m$ is the thermodynamic flux due to external field, and ψ is the potential of the external field.

In this equation, the sources of thermodynamic entropy generation terms from left are heat, diffusion, mechanical work, chemical reaction, and external field effect, respectively. In the fatigue damaging process, heat and mechanical work terms are involved. Naderi et al. [2] numerically calculated the dissipative entropy by using only the mechanical work term assuming that plastic deformation is the dominant term and the heat conduction effect is negligible, as presented in **Figure 1**. This assumption was also empirically verified by Imanian et al. [25] and Ontiveros et al. [3]. In addition, the concept of entropic endurance was further confirmed by Imanian et al. [25], who measured the interacting thermodynamic forces in a coupled failure mechanism, corrosion-fatigue. Summation of entropies from both mechanical work (fatigue) and chemical

reaction (corrosion) contributed to the total entropic endurance at the point of fatigue failure.

According to the previous researchers, thermodynamic entropy is computed during metallic material's fatigue damaging process may be used to predict crack initiation and fracture. The entropic endurance based on thermodynamics is quantitatively shown in **Figure 1**. This thermodynamic entropy is shown to measure damage adequately. The uses of thermodynamic entropy in the multiple phases of fatigue damage starting from nucleation, crack initiation, to the fracture is an open area of research. Further, other measures of entropy such as the information theory and fluctuation theorem in statistical mechanics are additional entropic measures that need to be further explored.

3.4 Acoustic emission (AE) and transformation to entropy

In addition to the heat and mechanical work, AE has been considered another source of irreversible energy dissipation. Kahirdeh and Khonsari [28] regarded AE absolute energy as an AE waveform feature and a damage indicator. However, the entropic approach was not investigated as a part of their AE-based damage research.

AE has been used as non-destructive testing (NDT) information source for characterizing material damage. It is applied to real-time monitoring systems undergoing damage by tracking the AE signal (waveform) features and correlate them with the observed or calculated damage metrics, such as crack growth [34-38]. For example, Keshtgar et al. [38] have shown a log-linear relation to micro-crack growth rate with a key AE feature (count), as shown in **Figure 2**.

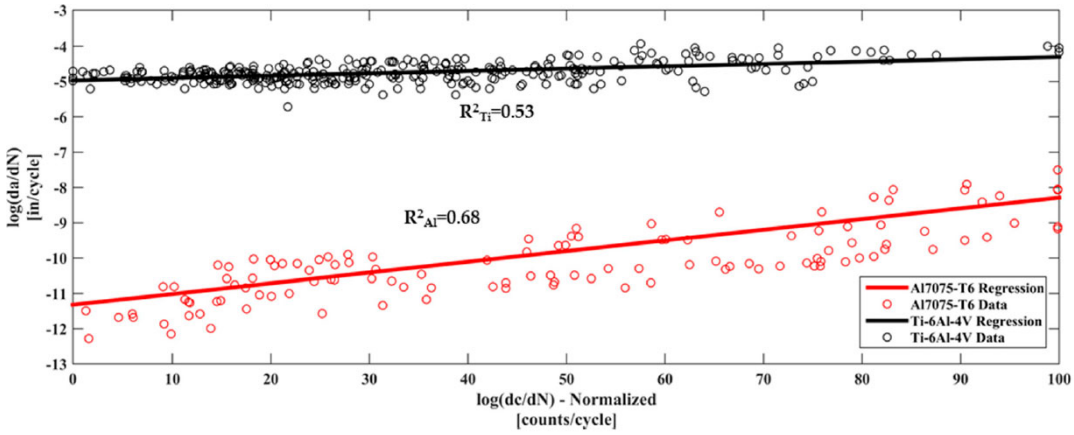

Figure 2. Correlation of AE count to crack growth rate [38]. Count and crack growth rate presented a log-linear relation for two material types.

The recorded data from the AE sensor is digitized into the so-called waveforms. The AE information (Shannon) entropy may be characterized by the associated probability distribution in the form of a histogram representing each recorded waveform. Hughes [39] introduced information entropy from digitized waveform data collected from ultrasonic tests. Likewise, specific features of the waveforms such as the count rate, information entropy has been applied to AE waveforms to assess the entropy of the waveform signals and empirically establish any correlation between the increasing entropy and the ensuing progression of the fatigue damage observed. Digitized data is processed to a corresponding discrete histogram (expressed in $p(x_i)$), and entropy is computed by using Equation (3):

$$S = -\sum_i p(x_i) \log p(x_i). \quad (3)$$

Sauerbrunn et al. [13] used Equation (3) to calculate information entropy using collected AE waveforms from many fatigue tests. In their research, the AE was shown to be a more appropriate damage indicator than the traditional AE features, such as count and energy, as shown in **Figure 3**.

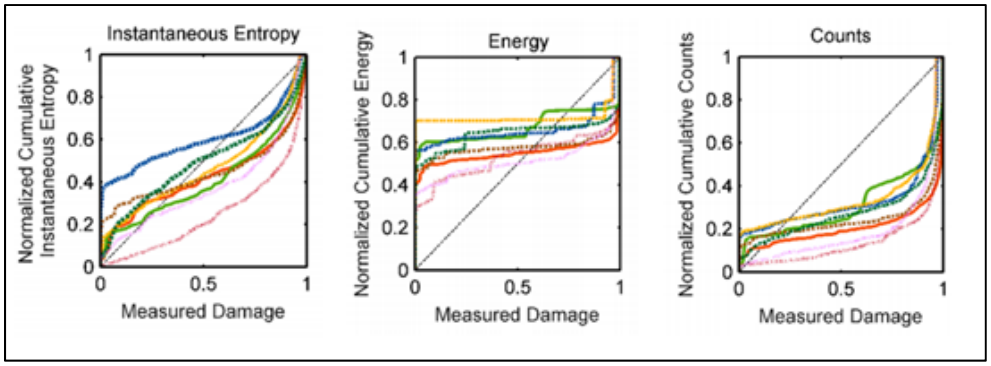

Figure 3. Evaluation of AE features. Information entropy (in this paper, instantaneous entropy) presents better appropriateness of damage representation compared to AE energy and count by correlating with measured damage degradation (MDD) [13].

Another applicable entropic method characterizing waveform data is the relative entropy, also known as the Kullback-Leibler divergence. The mathematical expression for the relative entropy in discrete distribution form is shown in Equation (4).

$$S = \sum_i p_a(x_i) \log \frac{p_a(x_i)}{p_b(x_i)}. \quad (4)$$

In Equation (4), the relative entropy is mathematically interpreted as the comparison of the information content of distribution "a" relative to distribution "b". According to Caticha [40], relative entropy is a fundamental quantity of entropic inference used as a formal information inference and updating process. In practical applications, Lin et al. [41] introduced the relative entropy concept characterizing abnormal voltage signal in high-voltage direct current (HVDC) transmission system, and He et al. [42] used the relative entropy as a candidate to filter electro-cardio-gram (ECG) wavelet in the de-noising process. As acquired AE waveform from fatigue damaging can be transformed into a distribution, relative entropy is a robust candidate to characterize damage.

In this dissertation, both information and relative entropies were applied to assess fatigue damage. The waveform information from the acoustic energy dissipation

is converted to the probability density function (or histogram), and the probability density function is converted to the corresponding information entropy using Equations (3) and (4). The reference distribution, $p_b(x_i)$ in Equation (4), is considered the probability density of noisy AE signal, and the relative entropy (Kullback-Leibler divergence) approach is expected to filter out AE noise [42].

3.5 Crooks fluctuation theorem and Kullback-Leibler divergence

In addition to the thermodynamic entropy and AE entropies, the third approach to entropic damage explored as a new damage metric relies on the statistical mechanics definition of entropy, which provides relative entropy from energy dissipation modes during the fatigue damage process. Forward and reverse work distribution functions applied during the cyclic loading in fatigue can be related to the thermodynamic work and free energy. The so-called Crooks fluctuation theorem expressed in Equation (5) is one such relationship [14]:

$$\frac{\pi_f(+W)}{\pi_r(-W)} = \exp\left[\frac{W-\Delta F}{k_B T}\right], \tag{5}$$

where $\pi_f(+W)$ and $\pi_r(-W)$ in the content of the fatigue damage process may be interpreted as the forward and reverse work distributions over many load cycles, respectively. W is the net strain energy dissipated, ΔF is the Helmholtz free energy difference, k_B is the Boltzmann constant (1.381×10^{-23} J/K), and T is the temperature. Equation (5) has been applied to nano-scale systems such as RNA (ribo-nucleic acid) strands, by introducing forward/reverse works to measure the Helmholtz free energy difference (ΔF) as the RNA system's inherent property [16]. **Figure 4** presents the distributions of RNA strand unfold/fold test results. This dissertation introduces an extension of this

notion into a macro-scale system (i.e., fatigue) and examines its consistency with the fatigue damage assessment by the traditional thermodynamic entropy and information entropy.

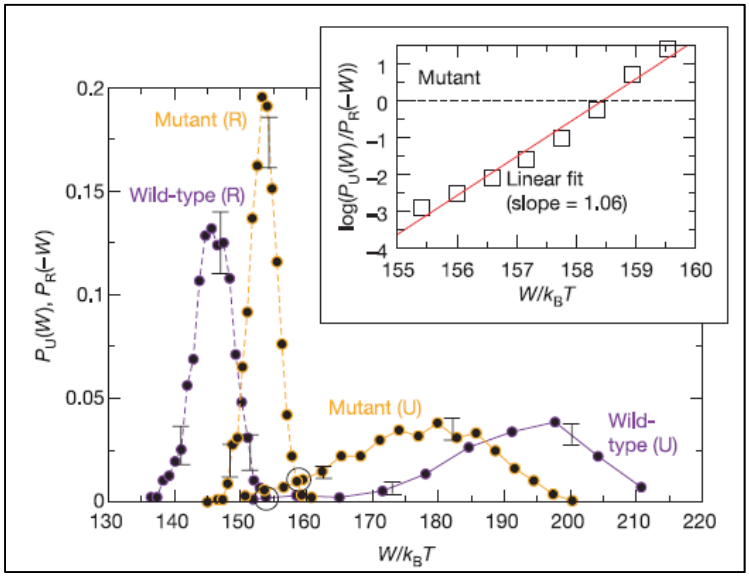

Figure 4. Distributions of forward/reverse loading process from two types of RNA strands [16].

By using the second law of thermodynamics and the Helmholtz free energy definition, Equation (5) could be converted to calculate the total entropy, as shown in Equation (6).

$$\Delta S_{tot} = k_B \ln\left(\frac{\pi_f(+W)}{\pi_r(-W)}\right). \quad (6)$$

According to the fluctuation theorem, the unloaded/fully-loaded points should be determined in thermodynamic equilibrium, whereas the loading/unloading in the fatigue process does not require equilibrium condition. In addition, the source of the fluctuation is only thermal energy dissipation. However, these conditions may be invalid when applied to the macro-scale fatigue damage evaluation. Not only the thermodynamic conditions but also mathematical applications may have limitations. Regardless of the

unsettled extension of this theorem to macro-scale, this research is inspired by the forward/reverse work convention and seeks to investigate the application of this notion to assess fatigue damage empirically. Crooks and Sivak [29] discuss measures of trajectory ensemble. Consistent with Crooks and Sivak results, relative entropy and Jeffreys divergence (JD) effectively capture the symmetric hysteresis properties of the fatigue phenomenon. Further, in the molecular scale, JD is related to the classical thermodynamic entropy through the Boltzmann constant.

The relative (divergence) entropy in continuous distribution form is shown in Equation (7) [29,43-45]:

$$\mathrm{D}(\pi_\mathrm{f}||\pi_\mathrm{r}) = \int \pi_f(+W) \ln\left(\frac{\pi_\mathrm{f}(+\mathrm{W})}{\pi_\mathrm{r}(-\mathrm{W})}\right) dW. \tag{7}$$

Relative entropy may be interpreted in the classical thermodynamics as the total entropy difference [29]:

$$\begin{gathered}\mathrm{D}(\pi_\mathrm{f}||\pi_\mathrm{r}) = \frac{1}{k_B T}\left(\langle W\rangle_f - \Delta F\right) = \frac{1}{k_B T}\left(\langle W_{diss}\rangle_f\right) = \frac{1}{k_B T}\left(\langle W\rangle_f - \Delta\langle E\rangle_f + k_B T \Delta S_f^{sys}\right) = \\ -\frac{1}{k_B T}\langle Q\rangle_f + \Delta S_f^{sys} = \Delta S_f^{env} + \Delta S_f^{sys} = \Delta S_f^{tot},\end{gathered} \tag{8}$$

wherein the nano-scale, k_B is the Boltzmann constant (1.381×10^{-23} J/K), T is the temperature, $\langle W\rangle_f$ is the mean work in the process f (forward work), $\langle W_{diss}\rangle_f$ is the mean dissipative work, $\Delta\langle E\rangle_f$ is the mean internal energy difference, $\langle Q\rangle_f$ is the mean heat dissipation, ΔS_f^{sys} is the entropy change within the system, ΔS_f^{env} is the entropy dissipated to the environment, and ΔS_f^{tot} is the total entropy during the process f. The relative entropy in the process f is interpreted as the product of the thermodynamic dissipative work ($\langle W\rangle_f - \Delta F$) and the constant $\left(\frac{1}{k_B T}\right)$. Consistent with its definition, the

Helmholtz free energy difference, ΔF, expands to the sumo of internal energy $\left(\Delta\langle E\rangle_f\right)$ and the product of system entropy difference $\left(\Delta S_f^{sys}\right)$ and the constant $(-k_BT)$. Considering the first law of thermodynamics, the mean work and mean internal energy difference become the product of the mean heat dissipation $\left(\langle Q\rangle_f\right)$ and the constant $\left(-\frac{1}{k_BT}\right)$, which is expressed in terms of the entropy difference dissipated to the environment. Therefore, the relative entropy in the process, f, is expressed by the total entropy difference $\left(\Delta S_f^{tot}\right)$. The relative entropy of the reverse process is:

$$\mathrm{D}(\pi_\mathrm{r}||\pi_\mathrm{f}) = \frac{1}{k_BT}(\langle W\rangle_r + \Delta F) = \frac{1}{k_BT}(\langle W_{diss}\rangle_r) = \frac{1}{k_BT}\left(\langle W\rangle_r - \Delta\langle E\rangle_r + k_BT\Delta S_r^{sys}\right) = -\frac{1}{k_BT}\langle Q\rangle_r + \Delta S_r^{sys} = \Delta S_r^{env} + \Delta S_r^{sys} = \Delta S_r^{tot}. \quad (9)$$

For the reverse process r, it should be noted that, unlike the forward process, the Helmholtz free energy difference, ΔF, should be expressed with the positive sign.

Summing Equation (8) and Equation (9) is defined as the JD and represents the dissipative thermodynamic entropy as related to the hysteresis associated with the cyclic loadings in fatigue [29]:

$$\mathrm{Jeffreys}(\pi_\mathrm{f};\pi_\mathrm{r}) = \mathrm{D}(\pi_\mathrm{f}||\pi_\mathrm{r}) + \mathrm{D}(\pi_\mathrm{r}||\pi_\mathrm{f}) = \Delta S_f^{env} + \Delta S_f^{sys} + \Delta S_r^{env} + \Delta S_r^{sys} = \Delta S_f^{env} + \Delta S_r^{env} = \Delta S^{\mathrm{env}}. \quad (10)$$

In Equation (10), the terms ΔS_f^{sys} and ΔS_r^{sys} are canceled out, and the only term remaining is dissipative entropy. Therefore, JD from the statistical mechanics corresponds to the thermodynamic entropy as described in the classical thermodynamics. Also, JD is computed only by strain energy distributions in fatigue.

A statistical hysteresis can interpret and correlate JD to the classical thermodynamic entropy. **Figure 5** presents a statistical hysteresis from the loading/unloading process. The straight line inside the hysteresis is the path of the reversible (elastic) process represented by Helmholtz free energy. The hysteresis area above and below the reversible line represents relative entropy of forward and reverse process, respectively. In this illustration, Jeffreys divergence is defined by summing the two relative entropies, and Boltzmann constant is the converting factor from JD to the classical thermodynamic entropy.

To demonstrate and assess the JD for the metallic material's fatigue damage process, fatigue tests were repeated in several controlled conditions (mostly loading amplitude and ratio). Within the repeated tests, corresponding strain energies of forward and reverse processes were collected to construct the distribution, as shown in equations (5) to (7). The JD from forward/reverse work distributions is also assessed by using the reference damage.

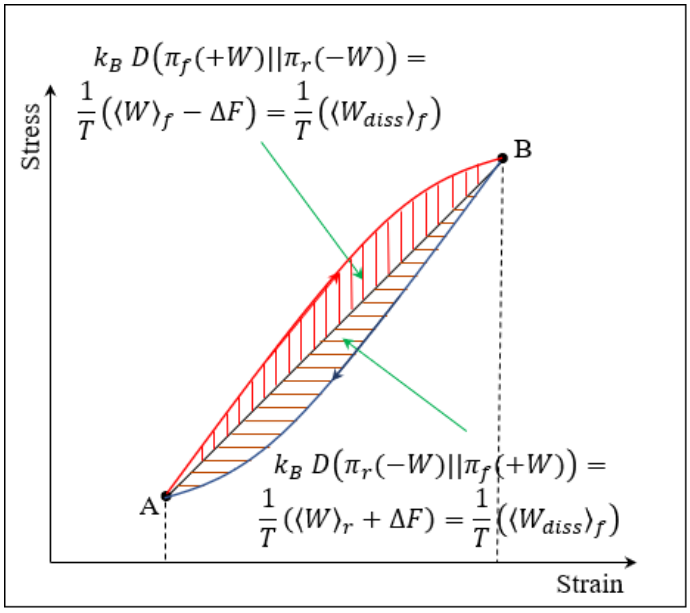

Figure 5. Conceptual statistical hysteresis and interpretation in terms of classical thermodynamics.

3.6 Acoustic emission noise and short-term loading process (STLP)

Dissipative energy, generated from the damaging process, is collected during the system's operation. Passive sensors such as load cell, thermocouple, and acoustic emission sensor collect the dissipative energy and are used in PHM for monitoring instantaneous damage status [1,2,28,33]. These passive sensors are prone to noise that is mixed with a valid energy dissipation signal. Damage-related acoustic emission (AE) signal, for example, is generated from internal deformation, micro-crack, dislocation, debonding of inclusions, phase transitions, recrystallizations, slipping, twinning, and the interaction between the cracked surfaces [28, 46-51]. Not only these damage-related signals but also external signals (background noise) transmit through the material medium due to the load-applying system (e.g., hydraulic actuator) and friction from connected devices [52].

In order to address this background noise problem, noise reduction processes have to be designed. As the pre-processes, mechanical damping and analog filtering were applied [53,54]. In the post-processes, filtering accepting only valid burst AE signal (e.g., delta T method [55]) and signal processing with wavelet transformation or spectral subtraction were used [56,57]. However, noise-free information may not be possible due to the background noise environment. This gap is addressed in this research by introducing a new concept called short-term loading process.

The AE signal using controllable excitation loading that is the introduced short-term loading process (STLP) is applicable. Without damaging the system (or in the damage-negligible process), excitation loading may be applied to investigate the mate-

rial damage state. The concept of the excitation method in AE was introduced by Parsons and Staszewski [58] where a crack was identified by the AE signal using piezoceramic vibration generator. The mode of excitation loading using mechanical loading frame was introduced by Amiri and Khonsari [59] that low-amplitude and high-frequency mechanical loading convention was regarded as a non-destructive procedure. In this research, excitation loading is combined in the cyclic loading process to investigate the validity of this alternative damage measure.

Chapter 4: Research Approach and Experimental Setup

A series of experiments were planned and performed to present entropies analyzed from various dissipation modes during metallic material's fatigue damaging process. This chapter depicts the analyses and experimental procedures. Also, the measurement limitation of stress/strain curve is stated, and the analysis of collected data for each tested specimen is discussed.

4.1 Research Approaches for entropic analyses and STLP

Figure 6 shows the overall research approaches. This flow chart describes three parts: Measurements, analyses, and assessments.

Experimental process collected three dissipative energies such as strain energy, heat dissipation (temperature behavior), and acoustic emission. Each dissipative energy data was converted to damage-representing entropy and assessed. Particularly, classical thermodynamic entropy (CTE) is used as the reference damage measure and used to assess the performance of the other two entropic approaches.

The crack length was also monitored using the images taken by an optical microscope. The measured crack length and the corresponding life in cycles are used to define the life of failure at a certain crack length. In this research, the failure point in crack length is differently determined at initiation, 250 μm crack, 500 μm crack, 1000 μm crack, the transition from region II to III (following linear elastic fracture mechanics (LEFM) [60]), and fracture. These failure determinations are used in each entropic approach's assessment.

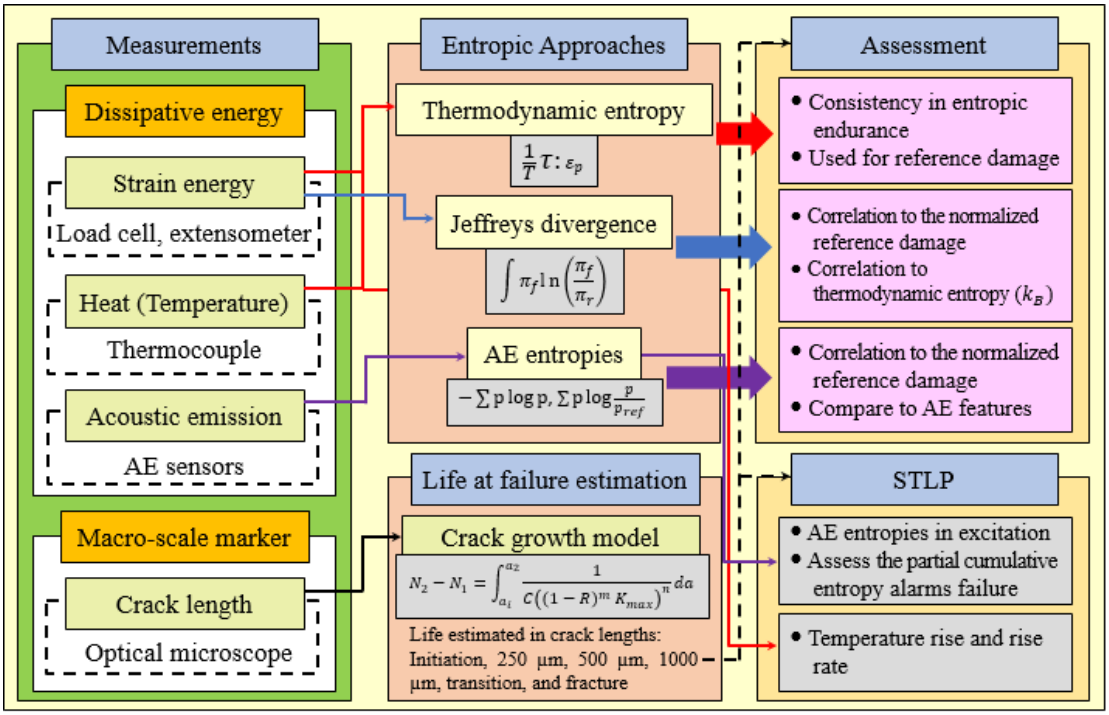

Figure 6. The research flow chart. Four measurements (three dissipative energies and crack length), collected during each fatigue test, are the sources of overall analyses. Entropic approaches and their assessments are presented according to each dissipated energy and entropic theorems. The life at the failure is determined by the crack length, and the life estimation is used in both assessment of entropies and STLP.

4.2 Specimen preparation: design, evaluation, manufacturing, and surface processing

In a series of uniaxial tensile fatigue experiments, aluminum alloy (AA) 7075-T6 and stainless steel (SS) 304L were selected as the testing materials and for the development of test specimens. AA7075-T6 is the high-strength and light-weight material, which is usually used in the aircraft fuselages. SS304L is a widely used structural material, especially in highly acidic environments. The properties of these alloys are shown in **Table 1** and **Table 2**.

Table 1. Mechanical properties and chemical composition of specimen material AA7075-T6.

Mechanical Properties											
σ_U [MPa]			σ_U [MPa]			Elongation [%]			Hardness [RB]		
584.0			515.5			11.65			53.50		
Chemical Composition [w%]											
Al	Si	Fe	Cu	Mn	Mg	Cr	Zn	Ti	V	Zr	Other
89.74	0.07	0.17	1.5	0.03	2.4	0.19	5.8	0.03	0.01	0.01	0.05

Table 2. Mechanical properties and chemical composition of specimen material SS304L.

Mechanical Properties									
σ_U [MPa]		σ_U [MPa]			Elongation [%]			Hardness [RB]	
613.8		325.7			54.06			85.00	
Chemical Composition [w%]									
C	Cr	Cu	Mn	Mo	N	Ni	P	S	Si
0.0243	18.06	0.3655	1.772	0.2940	0.0713	8.081	0.0300	0.0010	0.1930

The dogbone-shape specimen was selected and designed for fatigue testing under the ASTM 406 guideline [61]. To induce the crack formation at the center of the specimen, a V-shaped notch with $K_T = 4.04$ was designed. The stress concentration factor was calculated using the Peterson plot, provided on the efatigue.com website[1]. The V-shape notch, which has a higher concentration effect than the round-shaped notch, was selected in order not to have the crack around the loading hole (with the $K_T = 3.44$). This was designed to minimize the AE noise by reducing the contact area from the noise source. **Figure 7** shows the shape and dimensions of the specimen.

After the design was selected, uniaxial stress distribution was investigated using the finite element method (FEM) with ANSYS Workbench version R16.2 [62]. The specimen and loading rigs were drawn by AutoCAD 2018 [63]. **Figure 8** presents the specimen's stress mapping with 24 kN uniaxial tensile load applied on the inner surface

[1] https://www.efatigue.com/constantamplitude/stressconcentration/#a. Last accessed in 3/10/2019.

of the hole. From the analysis, no abnormal stress was detected in the overall geometry, and the maximum stress was detected at the center of the notch.

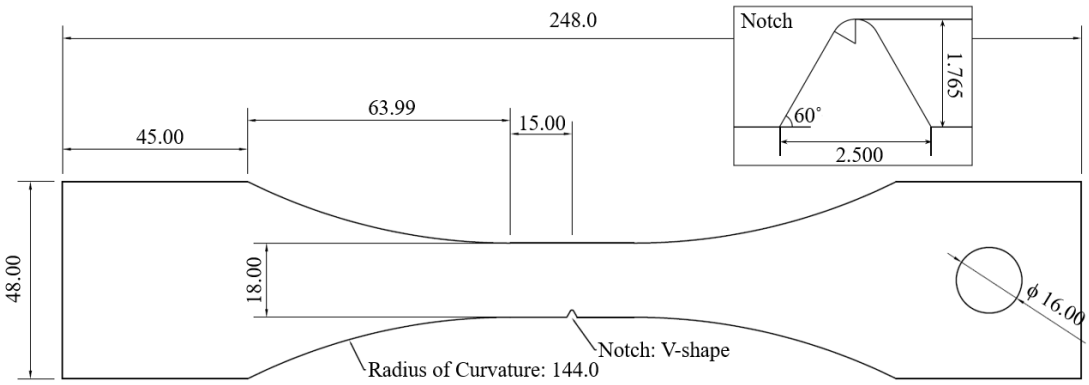

Figure 7. The geometry of the dogbone specimen. The specimen has a hole for loading with a 16-mm diameter pin and stress concentrated by a V-shape notch. Theoretical stress concentration factors (K_T) are 4.04 for the notch and 3.44 for the hole (pin in tension condition), respectively. The length unit is millimeter.

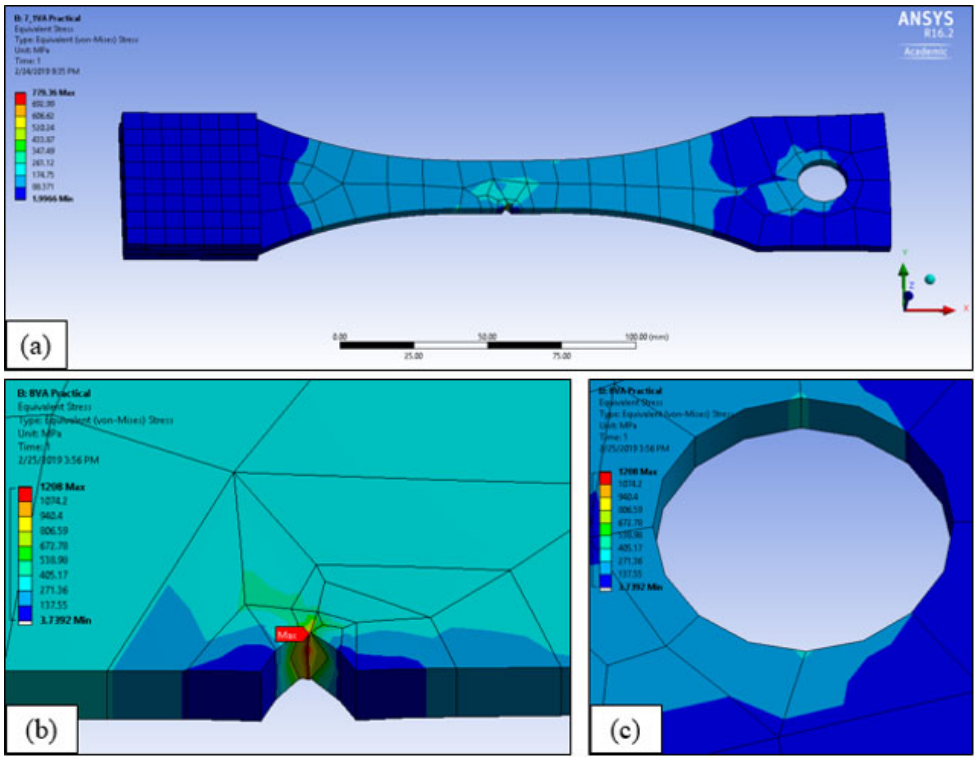

Figure 8. Stress mapping result with 24 kN uniaxial tensile load. (a) Overall stress distribution. No abnormal stress was detected. (b) Magnified observation around the notch. The maximum stress locates at the center of the notch. (c) Stress mapping in the hole area.

Additional quantitative analyses proceeded. First, the stress concentration factor was computed in various tensile loading conditions. **Figure 9** shows the stress concentration factor computed by the maximum stress at the notch for both two materials. The slight difference from the theoretical concentration factor is due to the Poison ratio (AA7075-T6: 0.33 and SS304L: 0.31) and the numerical calculation process in the mesh formation. Another analysis was the maximum stress applied at the hole area to investigate whether the stress is exceeding the material's yield strength. **Figure 10** presents the result, and no case of exceeding yield strength was found.

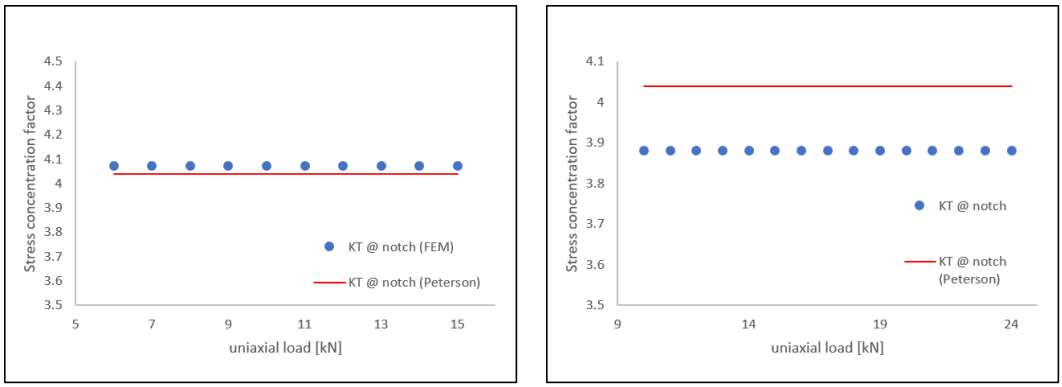

(a) **(b)**

Figure 9. Comparison between theoretical stress concentration factor (K_T) and the concentration factor computed from the FEM result. (a) Specimen made by AA7075-T6 (concentration factor: 4.07) and (b) Specimen made by SS304L (concentration factor: 3.88).

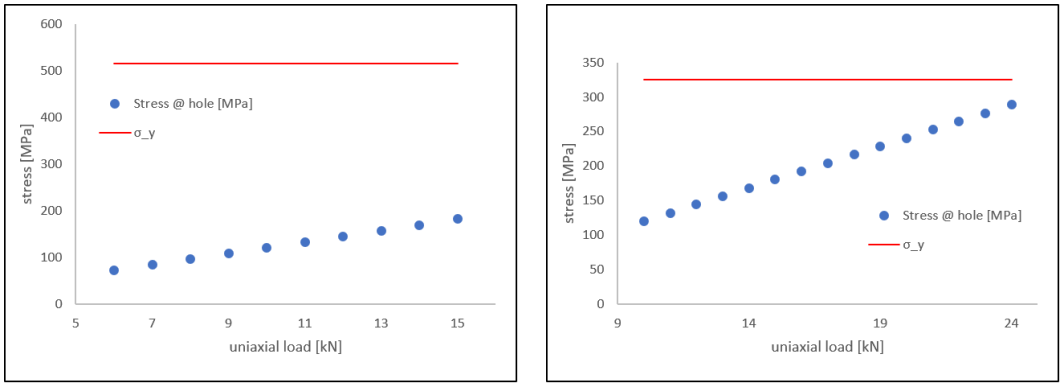

(a) **(b)**

Figure 10. Maximum stress around the loading hole and yield strength. (a) AA7075-T6 and (b) SS304L specimens. The maximum stress around the loading hole did not exceed each material's yield strength from any tensile loading condition.

The specimens were manufactured using electro-discharge machining (EDM). Twenty-four (AA7075-T6) and fifty-two (SS304L) specimens were prepared for the series of fatigue tests under different loading conditions. After cutting out the specimens, the specimen surface around the crack growth area was processed to clarify the surface image. First, the surface was sanded with increasingly larger grit numbers (grit # 400 → 800 → 2000), then the surface was polished with a polishing pad using 1 μm alumina solution. Finally, the etching process was employed by using Keller etchant (for AA7075-T6) and Carpenters etchant (for SS304L). **Figure 11** illustrates the sanding process, and **Figure 12** shows the polishing.

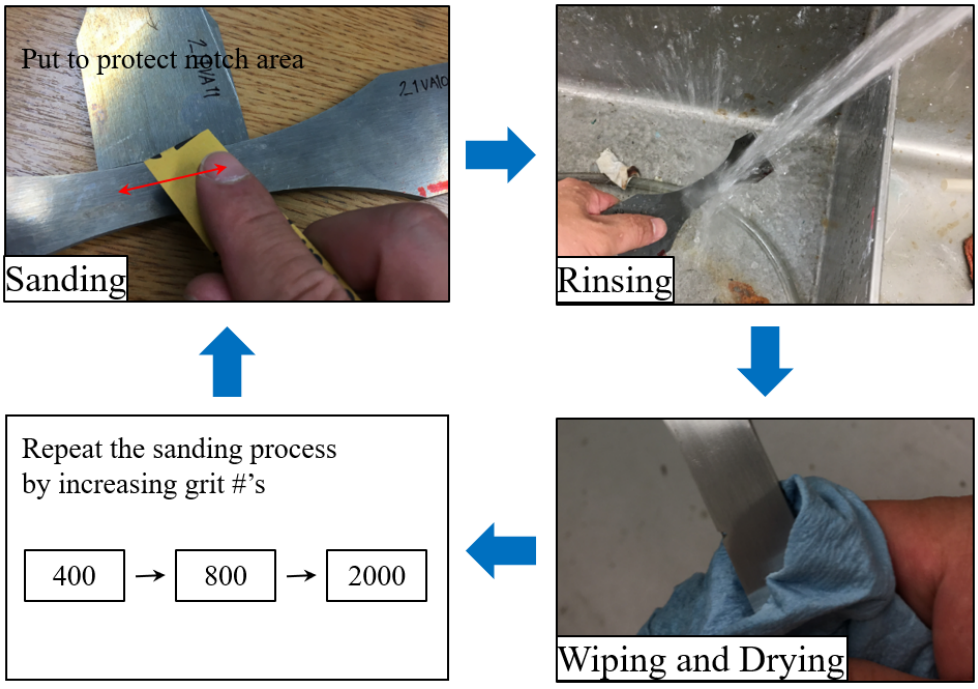

Figure 11. The illustration of the specimen sanding procedure. The sanding process was repeated with softer sandpapers to proceed to the next step, polishing.

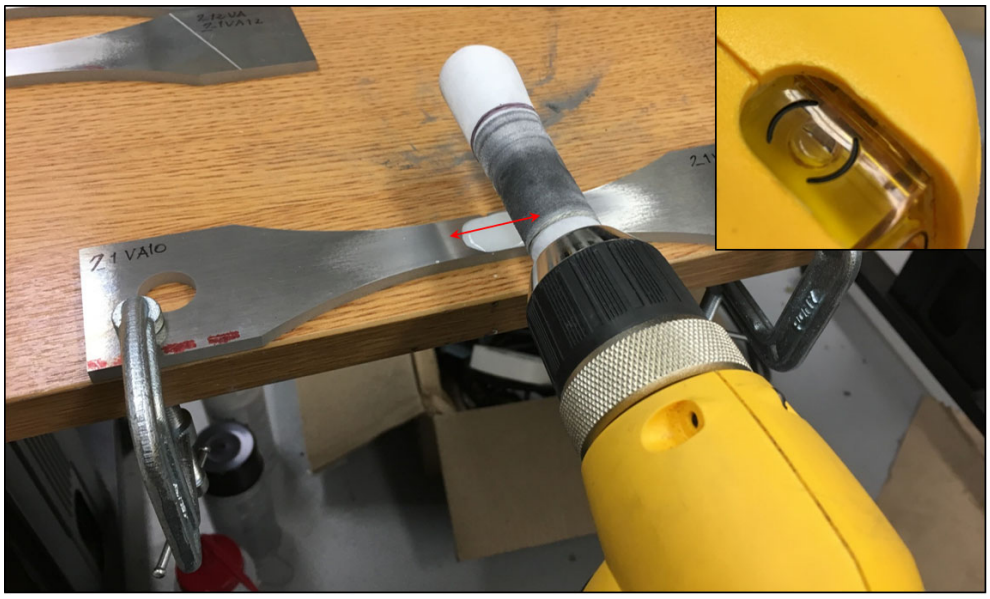

Figure 12. The snapshot of the polishing process. The rolled polishing pad, plugged in the electric drill, was utilized to polish the specimen's surface. During the polishing process, the level (magnified on the upper right) was maintained to keep balance.

After the surface processing, the area around the notch tip was observed using higher-resolution optical microscope (Zeiss Primo Star optical microscope), as shown in **Figure 13**. The images show the grain boundaries and inclusions. However, no significant defect, such as crack caused by the machining process, was detected.

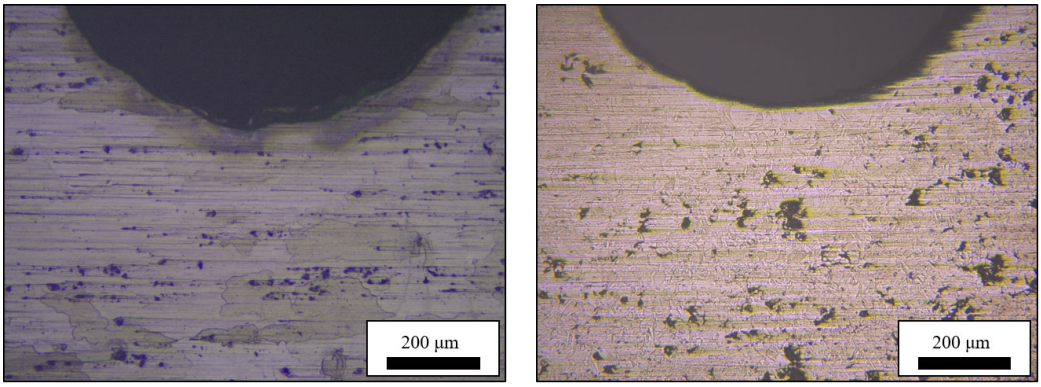

(a) **(b)**

Figure 13. Microscope images of notch area. (a) An AA7075-T6 specimen (7VA24) and (b) a SS304L specimen (8VA32). Grain boundaries and inclusions are observed on the specimens' surface.

4.3 Cyclic loading process

In this uniaxial loading test, a servo-hydraulic testing system was used. An Instron 8800 system retrofitted on an MTS 311.11 frame. Each specimen was held and loaded by upper and lower wedge grips, and the actuator was connected to the lower wedge grip to apply cyclic uniaxial tensile loading. The loading conditions were in the range of 9 ~ 15 kN (for AA7075-T6) and 16 ~ 24 kN (for SS304L) maximum loads, 0.1 stress (or loading) ratio, and 5 Hz frequency. For applications to STLP, every 1000-cycles, cyclic loading was paused, and 500-cycles of excitation loading were applied with 25 Hz, 6 kN (AA7075-T6), and 10 kN (SS304L) maximum loads. Between damaging and excitation loading process, a 2-minute of pause time was applied. The pause time allowed the specimen's cooling and provided the ability for capturing clearer microscope images. **Figure 14** presents the stepwise loading procedure. Each test stopped at the pre-set limitation of actuator position (+1.5 mm from the initial position). **Table 3** presents the maximum load for each specimen. Ten SS304L specimens were grouped for repetitions to make up forward/reverse work distribution applying to JD.

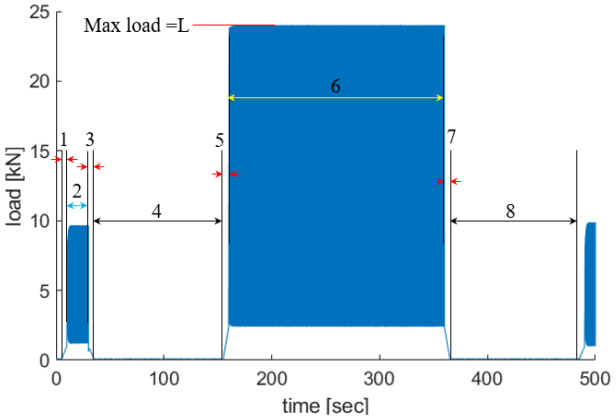

Step	Loading Mode	Loading	Duration
1	Linear	0.1 → 1 kN	5 sec
2	Sinusoidal	1 ↔ 10 kN	20 sec
3	Linear	1 → 0.1 kN	5 sec
4	Linear	0.1 → 0.1 kN	120 sec
5	Linear	0.1 → 0.1×L kN	5 sec
6	Sinusoidal	0.1×L ↔ L kN	200 sec
7	Linear	0.1×L → 0.1 kN	5 sec
8	Linear	0.1 → 0.1 kN	120 sec

Figure 14. Description of the loading process for a block (example: 8VA10). The loading mode for each step is detailed on the right chart. A load block represents one repetition of a series of steps (step 1 to 8) and corresponds to the damage loading of 1000 cycles (e.g., two blocks correspond to 2000 cycles of damage loading).

Table 3. The maximum load applied to each specimen. 7VA and 8VA stand for the specimens of AA7075-T6 and SS304L. SS304L specimens were grouped in ten repetitions for the JD analysis. 7VA05 and 7VA15 were excluded from the list due to the test failure.

Specimen ID	Load [kN]	Specimen ID	Load [kN]	Specimen ID	Load [kN]
7VA03	14	7VA13	9	7VA23	13
7VA04	13	7VA14	11	7VA24	14
7VA06	11	7VA16	12	8VA03 – 12	24
7VA07	10	7VA17	10	8VA13 – 22	22
7VA08	12	7VA18	9	8VA23 – 32	20
7VA09	14	7VA19	11	8VA33 – 42	18
7VA10	15	7VA20	9	8VA43 – 52	16
7VA11	13	7VA21	9		
7VA12	11	7VA22	11		

4.4 Experimental setup and measurements

Figure 15 illustrates the experimental system, including loading frame and measurement devices, and **Figure 16** shows the attachment of the sensors to the specimen. Measurements are described in the next sub-sections.

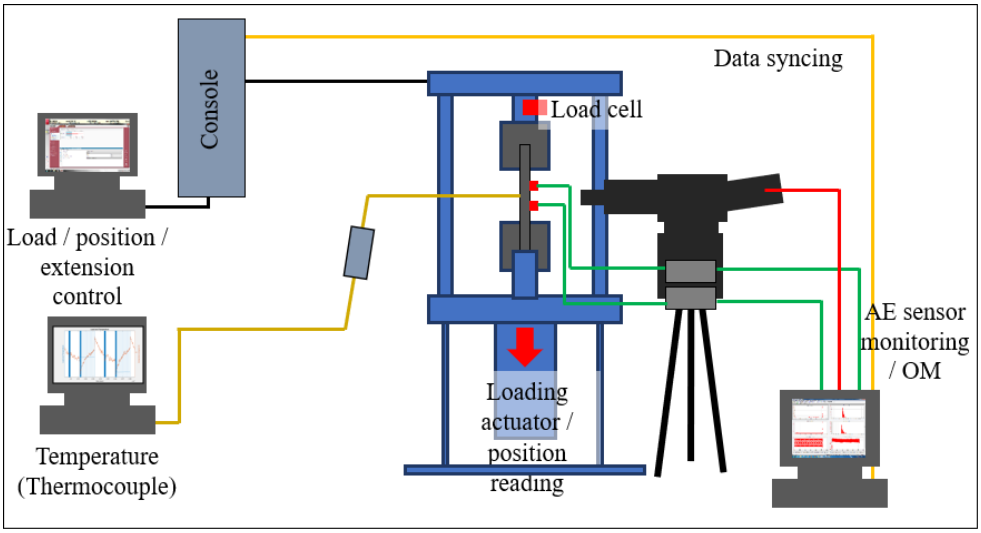

Figure 15. The schematics of the experimental setup. The specimen was fixed by two wedge grips, and the servo-hydraulic actuator applied the tensile loading. Several sensors were attached to the specimen to collect dissipative energies and crack length data.

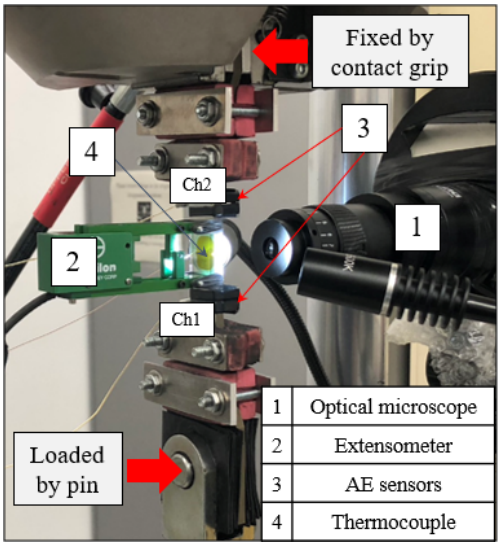

Figure 16. Specimen settlement in the fatigue loading system and the sensor attachments. The specimen was loaded by the pin-in-hole method to reduce the contact area, resulting in AE noise reduction. Two AE sensors, an extensometer, and a thermocouple were attached to the specimen.

4.4.1 Stress and strain

Load and extension data were collected by the Instron 8800 system [64,65]. A LEBOW 3116-103 load cell monitored loading applied in the specimen and an Epsilon extensometer model 3542 measured extension. The gauge length was 25 mm, and several rubber bands attached the extensometer to the specimen, centering it over the specimen's notch. The Instron 8800 system tabulated load and extension data with 200 Hz frequency. The raw data of load and extension were converted to stress and strain using the specimen geometry information (i.e., cross-sectional area and gauge length).

4.4.2 Acoustic emission

Two Physical Acoustics Micro-30s resonant sensors were symmetrically attached to the specimen surface 23 mm from the specimen center. The symmetric sensor placement made it possible to apply the delta T filtering technique [66]. In attaching AE sensors, Sonotech Ultragel II filled the contact area between the sensor and the

specimen surface to maintain the sensors' sensitivity. The electric current signal from the piezoelectric AE sensors (measured in volts) was amplified by the preamplifier in 40 dB gain mode. Overall control and recording of the AE signal were operated by the AEWin software [66]. The detailed AE sensor setup is shown in **Table 4**. The threshold amplitude was determined by the background noise survey, and timing parameters were determined based on the default values from the manual [67] and pencil lead breaking tests [68-70].

Table 4. AE sensor setups (primary, filtering/waveform, and timing parameters).

Primary setup						
Threshold			Gain	Preamp		
Type	dB	FTBnd	dB	Type	Gain dB	Voltage
Fixed	40 (AA7075-T6) 45 (SS304L)	6	0	2/4/6	40	28

Filtering/waveform						
Analog filter		Digital filter		Waveform setup		
Lower	Upper	Lower	Upper	Sample rate	Pre-trigger	Length
1 kHz	3MHz	None	None	5 MSPS	256.0000	10 k

Timing parameters			
Peak definition time (PDT) [μs]	Hit definition time (HDT) [μs]	Hit lockout time (HLT) [μs]	Max. duration [ms]
300	600	1000	100

Acoustic emission noise reduction methods were applied to maximize the AE signals' validity in damage measurement. The methods were divided into pre- and post-processes. The pre-process is to reduce the level of noise amplitude by minimizing the submerged valid AE signals, and the post-process filtered out the AE waveforms that were proved unrelated to the fatigue damage.

In the pre-process, two methods were applied following the research by Miller [53]. He introduced the concept of AE background noise and two strategies to eliminate the background noise. First, he inserted multi-material layers in building load train. This method reflected and diminished the noise by the different material layers in his experiments. From empirical verification with multi-layer blocks, the effect of amplitude reduction was not observed. Instead, contact area (between the specimen and the load train) was reduced by changing the grip (direct wedge grip contact to pin-in-hole holding). In a preliminary test, AE amplitude reduction effect was significant, as shown in **Figure 17**. Second, Miller used mechanical damper made by polymer blocks. Damper effect was also reported by Sauerbrunn [54] who used hard erasers to reduce AE noise. Both two pre-process methods were used in this experimental study, as shown in **Figure 16**.

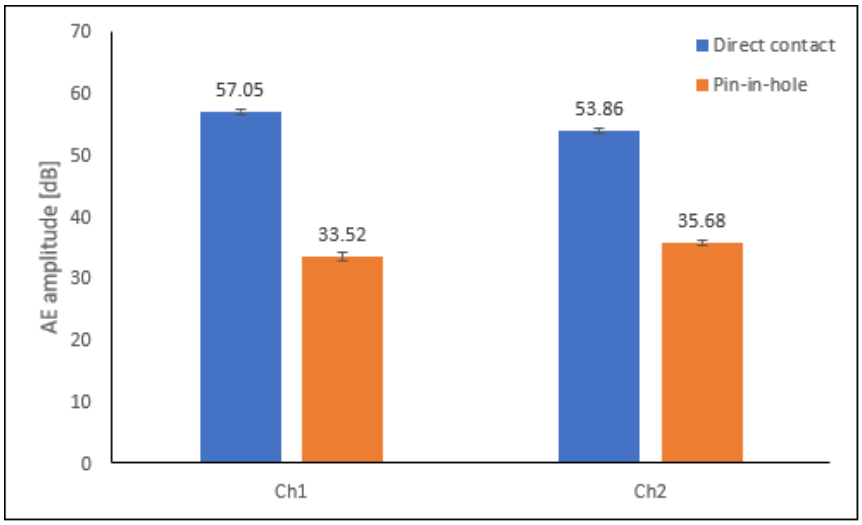

Figure 17. AE noise reduction effect by changing the loading method. The pin-in-hole tensile loading method was very useful in reducing the amplitude of AE noise. In this preliminary test, an AA7075-T6 specimen was used.

After each fatigue test, the post-process filtered waveform data following several steps. First, only valid AE waveform data pair (the data collected from the same

source) was accepted using delta T method. Delta T is a technique localizing AE generation using the waveform arrival time difference measured from two AE sensors [66] [71]. **Figure 18** shows the concept of delta T method, and the reference time ($t_R = 10^{-5}$ sec) was determined by the travel time between two sensors measured using automatic sensor tests (AST). This filtering process accepted only the waveform data pair, of which the delta T is less than the reference time (t_R). The second step used the attenuation [66]. Two absolute energies within the pair were compared. The pair was accepted when the absolute value difference was less than five times. The last step of the post-process was to use the cyclic loading profile. As shown in **Figure 19**, the AE data generated during the loading process and at the higher values of the load were accepted. The post-process was executed by a Matlab [72] script, and the script is written in A.1.1.

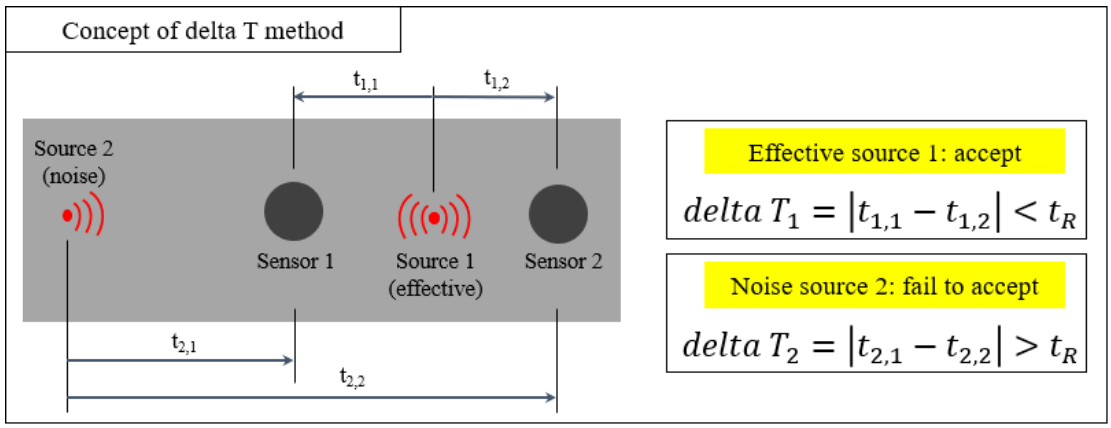

Figure 18. The concept of delta T method. The signal generated away from the area of interest (noise) was evaded from the acceptable data, using delta T method.

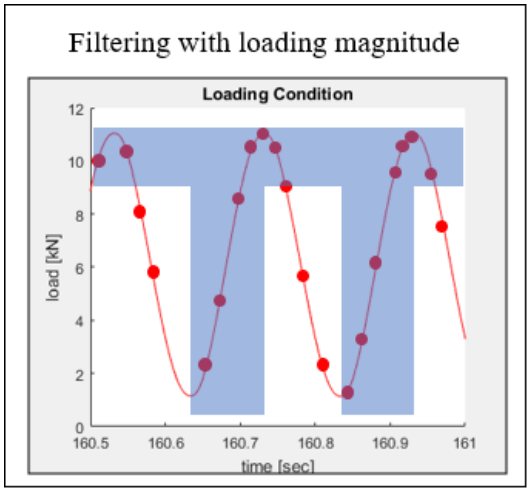

Figure 19. Filtering method using cyclic loading profile. AE data generated during the loading process and staying in higher load (AE data in the highlighted area) were accepted in this filtering step.

Table 5 presents the post-processing result for each test by the number of accepted AE data for each step. A large portion of the AE data was noise, although the AE data were collected under the reduced background noise.

4.4.3 Surface temperature

A thermocouple (Omega 5TC-TT-K-40-36) [73] was attached to the surface of the specimen (close to the notch tip). The thermocouple was connected to a National Instrument 9211A module and controlled by NI Labview software [74]. The surface temperature was recorded every half second.

Table 5. The post-processing results of the AE noise reduction. The number of data points accepted from each filtering step is shown for each test. The process for each step is as follows: step1 is the delta T method, step 2 is the filtering by the comparison of paired signals' absolute energy, and step 3 is the filtering with loading amplitude.

Test	Raw data		Step1	Step2	Step3	Test	Raw data		Step1	Step2	Step3
	Ch1	Ch2					Ch1	Ch2			
7VA03	55549	54373	24688	24385	21067	8VA18	65609	74390	8649	8634	8621
7VA04	35577	35063	18462	18322	7293	8VA19	64177	88953	12987	12977	12434
7VA06	29533	28812	17284	17147	13263	8VA20	62509	66178	19932	19881	19729
7VA07	111589	117098	55196	54153	44685	8VA21	27002	19406	3422	3418	2952
7VA08	148169	206375	51077	48238	12701	8VA22	35072	46538	9747	9743	9724
7VA09	84282	102123	22174	21733	14992	8VA23	25769	19581	11764	11757	10210
7VA10	25090	34971	10003	9879	8274	8VA24	93312	86537	25762	25760	24433
7VA11	56625	66249	23244	22767	12713	8VA25	47868	63534	21462	20846	19165
7VA12	37679	51837	9756	9441	8622	8VA26	6060	7850	2379	2371	1882
7VA13	93678	114512	42499	40717	31931	8VA27	25567	24393	12909	12872	12735
7VA14	26856	35011	16701	16193	7746	8VA28	4484	4396	3278	3275	2575
7VA16	18252	16559	6642	6613	6176	8VA29	8258	3151	1972	1769	1398
7VA17	30278	11850	5600	5548	5215	8VA30	31508	26746	7141	7139	6421
7VA18	13040	16348	5836	5805	4935	8VA31	157878	161776	40424	40369	18383
7VA19	18563	9233	4810	4692	4422	8VA32	214325	217915	100433	100132	90095
7VA20	17363	46798	11685	11608	6243	8VA33	183826	195913	34895	34819	30612
7VA21	75624	37454	19220	19137	15412	8VA34	46906	26625	3958	3947	1671
7VA22	9456	6801	4802	4765	700	8VA35	55236	53237	15070	15025	1469
7VA23	52972	56539	24186	24078	22393	8VA36	410012	390780	91290	91245	78575
7VA24	9202	6197	3727	3680	3152	8VA37	53318	41643	10238	10224	3465
8VA03	217962	249959	52908	49213	46641	8VA38	293956	295016	74249	73958	6586
8VA04	92919	118249	15681	15508	15429	8VA39	22094	23035	6340	6339	6296
8VA05	2883	960	121	120	25	8VA40	177866	195397	75401	75148	58674
8VA06	187782	150342	47345	44687	44612	8VA41	342483	383409	108566	107858	89161
8VA07	64237	19845	6895	6893	6865	8VA42	43447	50716	16278	16260	14975
8VA08	174861	186975	28459	26245	26163	8VA43	73030	80889	17778	17321	15604
8VA09	117281	146657	21765	21118	21038	8VA44	250005	322996	23557	23375	20132
8VA10	111142	110072	29062	28884	28865	8VA45	48193	32671	25177	25148	19885
8VA11	29789	7210	878	878	401	8VA46	219132	265493	164934	164535	144733
8VA12	24421	43981	2015	2006	1986	8VA47	71935	38068	29617	29094	24989
8VA13	4688	2894	89	89	66	8VA48	265432	287476	62600	62472	60448
8VA14	7289	3604	2334	2333	653	8VA49	74996	69653	11695	11666	11005
8VA15	16155	21427	920	907	672	8VA50	73957	48652	18557	18401	12072
8VA16	7310	9739	1215	1194	1140	8VA51	128955	140956	57365	57300	56661
8VA17	10898	18423	809	808	638	8VA52	358995	448836	53063	52775	47817

4.4.4 Crack length measurement

During the fatigue tests, an optical microscope system (Edmond 2.5-10X microscope body combined with OptixCam Pinnacle Series CCD digital camera) took images of the crack growth area. Images were taken every 5 seconds, controlled by OCView SW [75]. Every 1000 cycles, crack initiation and propagation were investigated using the taken images. The crack length was monitored to collect data on the observable damage, and the material fatigue life was defined by specific crack lengths, e.g., 250 μm.

4.5 Measurement and analysis limitations

Sauerbrunn [54] and Ontiveros [76] reported that the stress-strain curve, made from AA7075-T6 fatigue tests, was very close to the linear line when using the extensometer to measure strain. Hence, the plastic strain energy was very close to zero. Likewise, the hysteresis of AA7075-T6 fatigue tests, in this study, showed a similarly linear trend, as shown in **Figure 20**(a). On the other hand, SS304L fatigue tests had comparably more apparent hysteresis loop representing plastic deformation, as shown in **Figure 20**(b). Therefore, the entropic approaches and assessments proceeded only for SS304L test data due to the limitation of AA7075-T6 strain energy calculation. STLP and temperature effect analyses were conducted for both two materials.

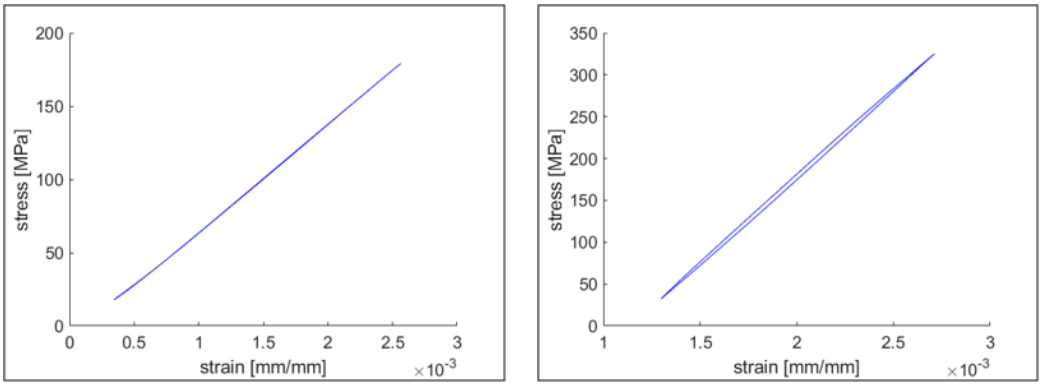

(**a**) (**b**)

Figure 20. Stress-strain curves at the 2500th cycle. The curves were drawn from the tests of (a) 7VA03 and (b) 8VA03.

Chapter 5: Crack Growth Analysis

5.1 Life determination by crack length

Fatigue crack length is one of the macro-scale damage measurements [18]. According to fracture mechanics [60,77], failure is determined by the fracture toughness (K_C). The critical crack length determining failure is calculated by the pre-determined critical fracture toughness (K_C) using Equation (11) [60]:

$$a_f = \frac{1}{\pi}\left[\frac{K_C}{\sigma f(g)}\right]^2, \tag{11}$$

where, σ is the stress applied in the material, and $f(g)$ is the correction factor that depends on the specimen and cracks geometry.

In practical engineering application, the fatigue failure is determined by a specific crack length for the scale-dependent measurement limitation and convenience. For example, the retirement criterion for United States Navy aircraft fuselage was reported to 250 μm [78]. Schijve [79] categorized the crack size in nucleation, micro-crack, and macro-crack, and determined 1 mm crack length as the critical small crack size to identify. Depending on material and geometry, the critical small crack length varies from hundreds of micron to 1 mm [78-81].

In this study, the popular small crack lengths (250 μm, 500 μm, and 1000 μm) are used in determining life. In addition, crack growth model based critical life at initiation, transition (from region II to III based on the linear elastic fracture mechanics (LEFM) [60]), and fracture, are also estimated using the crack propagation model.

5.2 Crack length measurement from specimen images

During each experiment, the microscope took images of the specimen surface (focused on the notch tip) every 5 seconds. Due to specimen moves, the images taken during the cyclic loading process were not clear enough to measure a crack length. Instead, the images taken during the non-cyclic loading period (step 8, shown in **Figure 14**), were used in crack measurements. **Figure 21** compares the images of loading and non-loading periods. After detecting the crack, the crack length was manually measured using Adobe Photoshop-CC [82] software.

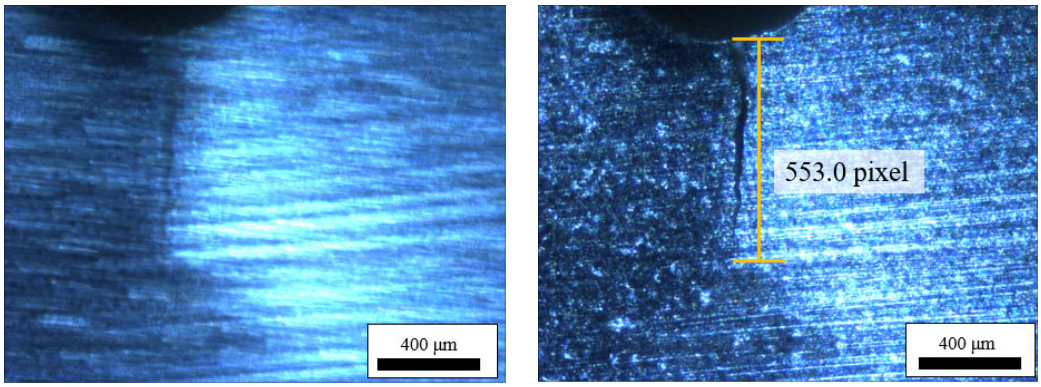

(**a**) (**b**)

Figure 21. Real-time surface images taken by the microscope (test: 8VA10). (a) Image taken during the cyclic loading (16th block). (b) Image taken a right after the 16th block. The crack growth was detected, and the crack length was measured in the pixel unit.

The crack lengths in pixel were converted to the measured physical lengths (µm) using the factor converting pixel to the micron. The notch depth was designed to be 1765 µm, and the corresponding pixel unit was measured for each test. **Figure 22** shows the converting factor for each test. The converting factor shows consistency, although existing variability.

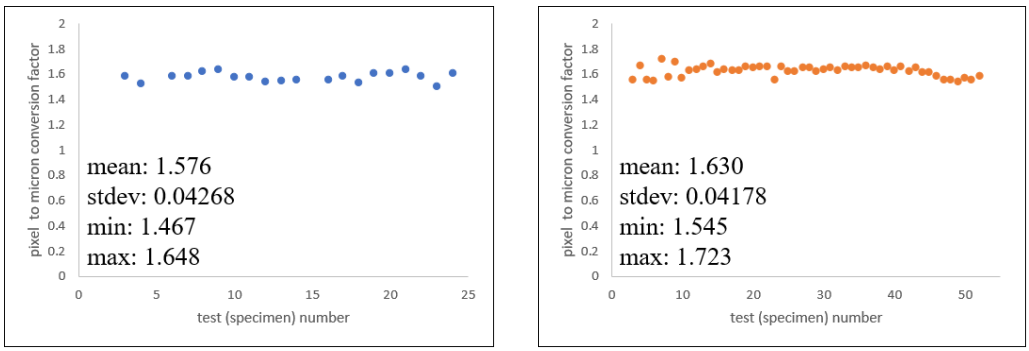

(**a**) (**b**)

Figure 22. Pixel to the micron conversion factor for each test. (a) Conversion factors from the tests of AA7075-T6 specimens and (b) conversion factors from the tests of SS304L specimens.

The measured minimum and maximum crack lengths from the crack detected images within each test are shown in **Figure 23**. In several fatigue experiments (7VA21 - 24 and all the SS304L tests), the optical microscope was manually adjusted to track the crack growth. Hence, the crack length measurement was possible up to the end of the experiment. The crack growth model estimation was applied for all the tests, regardless of how large the measured maximum crack length.

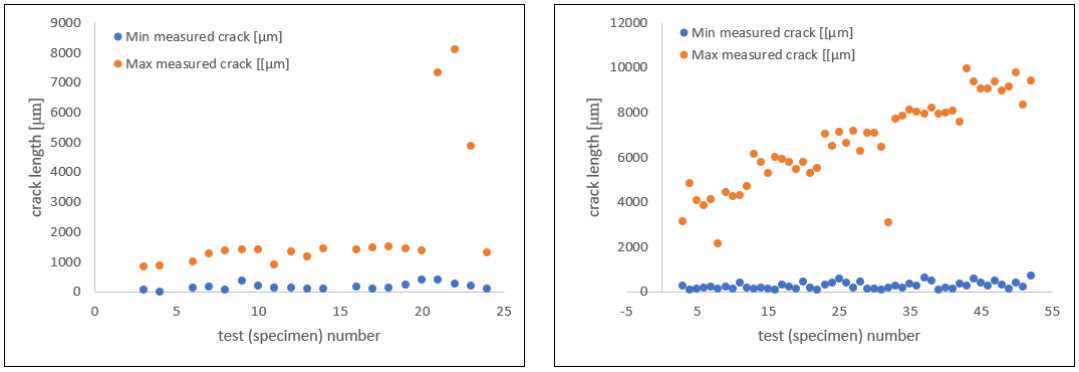

(**a**) (**b**)

Figure 23. Minimum and maximum measured crack lengths for each test. (a) Crack length data of AA7075-T6 specimens' tests and (b) data of SS304L specimens' tests.

5.3 Crack Growth Model estimation

After measuring the crack length over time, the crack growth model parameters were estimated for each test. In this estimation, the Walker model [60,83], as shown in Equation (12), was used. Walker model extends Paris-Erdogan equation [84] by making it applicable to any stress ratio.

$$\frac{da}{dN} = C((1-R)^m K_{max})^n \rightarrow N_2 - N_i = \int_{a_i}^{a_2} \frac{1}{C((1-R)^m K_{max})^n} da, \quad (12)$$

where a is the crack length (including the notch depth), a_i is the crack length at the crack initiation (same to notch depth), and a_2 is the current crack length in the model estimation process. N_i is the life at the crack initiation, N_2 is the current life in the model estimation process, R is the stress ratio (0.1 for this research), K_{max} is the maximum stress intensity factor, and C, m, and n are the model parameters to be estimated from the measured crack growth data. This equation was converted to the integration form to apply the measured crack data directly. In using the data from experiments, the four parameters (C, m, n, and N_i) were then estimated.

In the optimal parameter estimation process, the least-square method was used. The error in the least-square was computed by the difference between the measured and model lives, corresponding to the crack length of interest. The four parameters were estimated by minimizing the summation of errors.

Figure 24 and **Figure 25** show the estimated parameters for the separate two materials tests. **Figure 26** presents the measured data and the model-based crack growth curve as an example (8VA45). The crack growth model showed close to the measured (observed) cracks for each test.

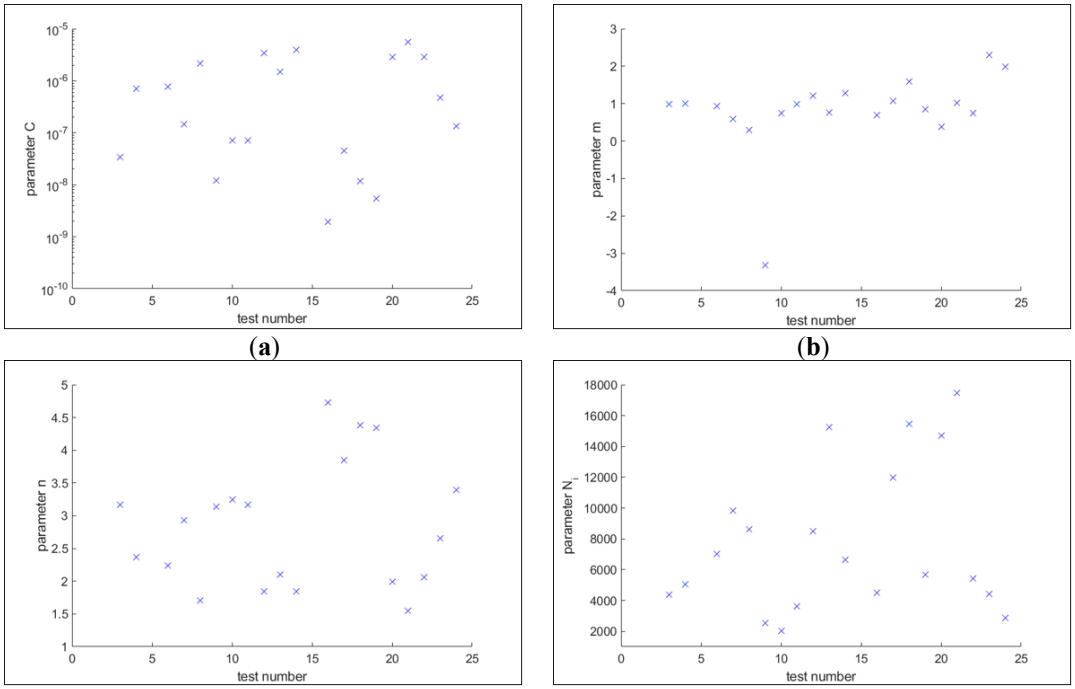

(a) (b) (c) (d)

Figure 24. Walker model parameter estimations of AA7075-T6 material tests. (a) Estimation of parameter C, (b) estimation of parameter m, (c) estimation of parameter n, and (d) estimation of parameter N_i.

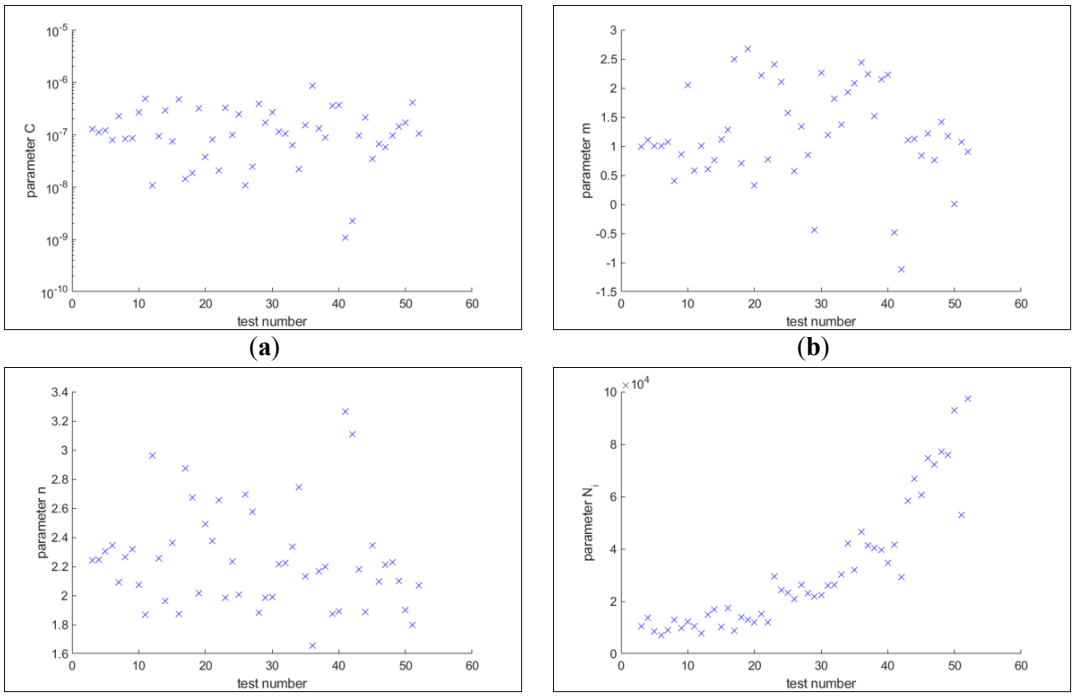

(a) (b) (c) (d)

Figure 25. Walker model parameter estimations of SS304L material tests. (a) Estimation of parameter C, (b) estimation of parameter m, (c) estimation of parameter n, and (d) estimation of parameter N_i.

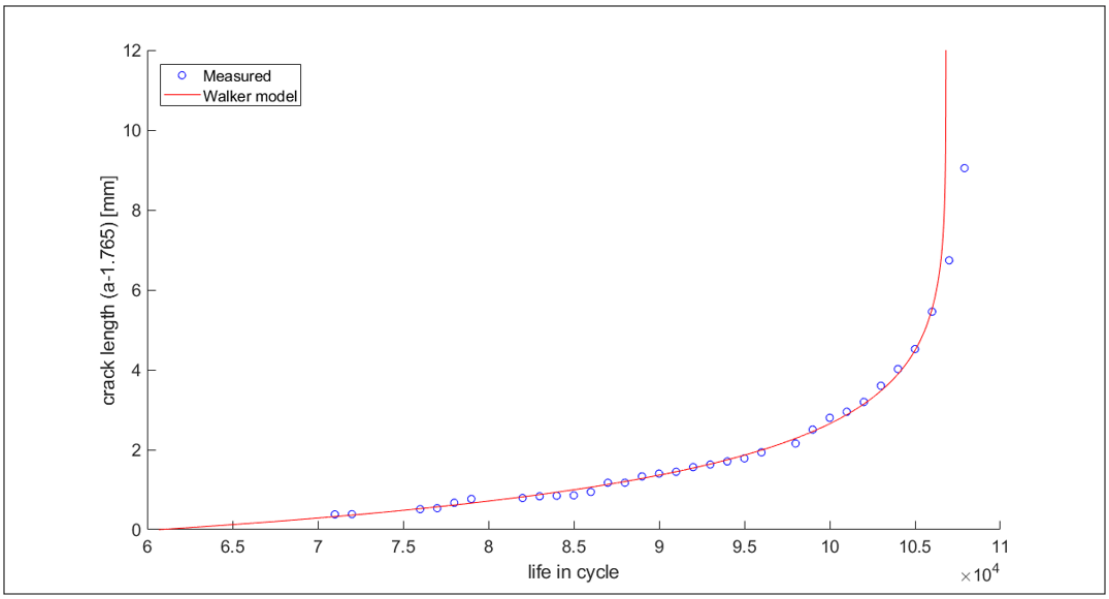

Figure 26. Measured crack lengths and fitted result in Walker model (test: 8VA45).

5.4 Life estimation in crack lengths

The fatigue life of each test was estimated for specific crack lengths and crack propagation phases. The criteria for life determination were initiation, 250 µm, 500 µm, 1000 µm, transition (from region II to III), and fracture. The life at crack initiation was N_i, which indicates the life at the beginning of crack growth. Next three lives corresponding to the crack lengths were calculated using the numerical integration using Equation (12). Lives at transition and fracture were estimated using graphical analyses. Transition point was found using the offset method inspired by the offset yield strength [85]. Fracture point was read from the extension of the nearly vertical crack growth line at the end of the test. **Figure 27** illustrates the procedure of pointing the lives at the transition and fracture, and **Figure 28** summarizes the crack lengths at transition and fracture. The crack lengths at the critical points were consistent regardless of the applied stress amplitude.

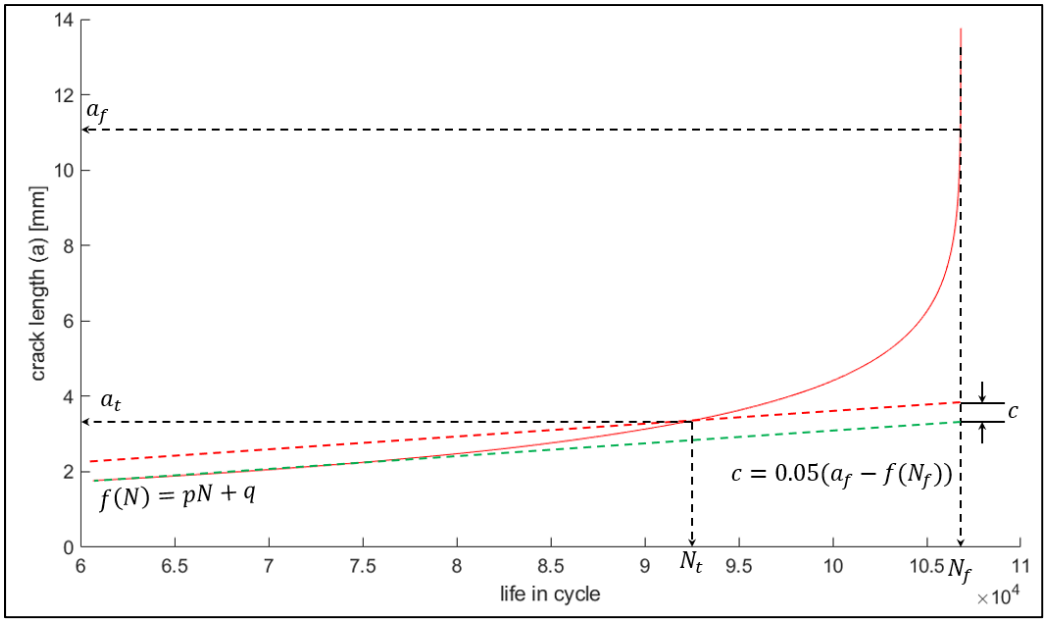

Figure 27. Graphical estimation of lives at transition and fracture (test: 8VA45). The fracture point was found from the nearly vertical crack growth curve at the end of the test, and the transition point was picked up by the offset method.

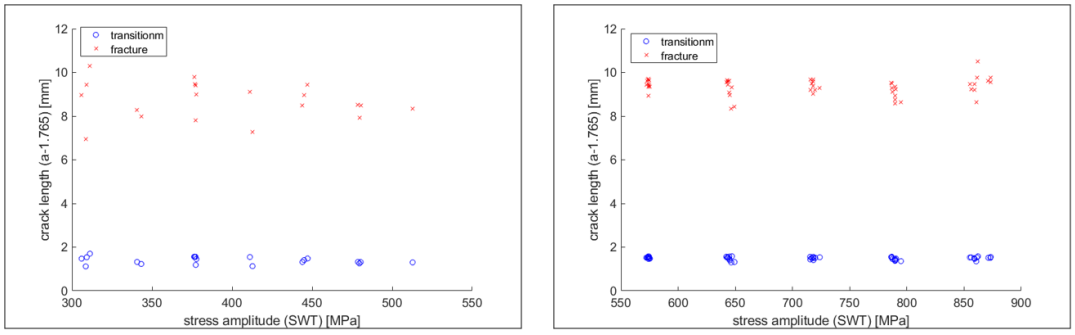

(**a**) (**b**)

Figure 28. Estimated transition and fracture crack lengths. (a) Crack lengths from AA7075-T6 fatigue tests and (b) crack lengths from AA304L fatigue tests.

Table 6 and **Table 7** present the estimated lives determined by the crack lengths and crack growth behaviors. The estimated lives are used in the entropic approaches for damage assessment, as the research flow chart described in **Figure 6**.

Table 6. Lives in the number of cycles determined by initiation, the specific crack lengths, transition, and fracture.

Test ID	Initiation	250 µm	500 µm	1000 µm	transition	fracture
7VA03	4387	5811	6864	8259	8831	10411
7VA04	5050	5748	6306	7123	7658	8935
7VA06	7040	8323	9359	10903	11888	14542
7VA07	9853	11362	12503	14064	14732	16729
7VA08	8628	9974	11117	12946	14437	18791
7VA09	2552	3596	4370	5399	5827	7002
7VA10	2037	2430	2719	3098	3245	3663
7VA11	3633	4491	5125	5966	6310	7261
7VA12	8499	9305	9981	11043	11907	14182
7VA13	15251	16643	17783	19513	20677	23909
7VA14	6652	7361	7956	8890	9642	11646
7VA16	4508	5159	5575	6026	6095	6424
7VA17	12041	12673	13112	13644	13794	14273
7VA18	15477	16780	17635	18605	18748	19553
7VA19	5703	6646	7269	7978	8135	8685
7VA20	14689	15555	16271	17375	18217	20379
7VA21	17469	18787	19924	21780	23704	28451
7VA22	5449	5978	6414	7078	7596	8817
7VA23	4437	5160	5722	6518	6953	8060
7VA24	2871	3148	3348	3606	3691	3967
8VA03	10599	11796	12763	14206	15216	17630
8VA04	13734	15186	16359	18109	19372	22264
8VA05	8467	9548	10416	11700	12567	14650
8VA06	7014	8441	9581	11261	12542	15054
8VA07	8972	10117	11055	12481	13574	16149
8VA08	13005	14505	15713	17510	18769	21720
8VA09	9831	11210	12316	13948	14996	17661
8VA10	12263	13586	14673	16329	17557	20637
8VA11	10391	11424	12289	13642	14692	17579
8VA12	7776	9138	10165	11560	12195	13898
8VA13	14872	16656	18095	20237	21658	25268
8VA14	16944	18479	19752	21721	23255	27158
8VA15	10327	12154	13613	15755	17092	20525
8VA16	17411	18826	20010	21861	23356	27238
8VA17	8656	11425	13531	16427	17793	21485

Table 7. Lives in the number of cycles determined by initiation, the specific crack lengths, transition, and fracture (continued).

Test ID	Initiation	250 µm	500 µm	1000 µm	transition	fracture
8VA18	13913	16330	18204	20848	22172	25898
8VA19	12996	14777	16247	18505	20167	24545
8VA20	11905	13844	15373	17581	18945	22193
8VA21	15253	17342	19008	21450	22868	26825
8VA22	12087	14399	16194	18734	20110	23636
8VA23	29516	31674	33459	36213	38236	43701
8VA24	24285	27473	30050	33898	36576	43055
8VA25	23245	25544	27443	30365	32653	38258
8VA26	20897	25620	29273	34411	37188	44143
8VA27	26309	30082	33033	37249	39709	45705
8VA28	23159	24947	26441	28776	30590	35509
8VA29	21814	24093	25979	28887	31153	36818
8VA30	22282	24824	26928	30170	32726	39011
8VA31	25934	28299	30214	33080	35054	39965
8VA32	26179	29087	31439	34956	37419	43374
8VA33	30228	34199	37377	42059	44994	52601
8VA34	42093	46058	49111	53380	55620	61287
8VA35	32079	35637	38542	42936	46173	53993
8VA36	46514	49136	51376	54981	58096	66925
8VA37	41309	45186	48340	53091	56457	64813
8VA38	40493	45025	48701	54217	58208	67635
8VA39	39640	42820	45479	49638	53050	61725
8VA40	34982	38021	40559	44518	47710	55910
8VA41	41672	49550	55321	62872	65760	74049
8VA42	29257	34104	37707	42514	44499	50091
8VA43	58309	63342	67431	73576	77564	88554
8VA44	66771	71957	76290	83056	88604	102597
8VA45	60675	68857	75402	85034	91318	106674
8VA46	74630	84205	92046	103960	112943	134514
8VA47	72346	79338	85002	93480	99540	113920
8VA48	77281	81977	85774	91447	95348	104977
8VA49	75822	80247	83870	89377	93387	103485
8VA50	92957	98052	102303	108928	114364	127918
8VA51	52881	56421	59403	64113	68019	78417
8VA52	97347	103370	108316	115862	121360	135495

5.5 Assessment of the crack growth model estimation

The assessment of the crack growth model estimation was approached by investigating the stress-life model. This model is a traditional empirical fatigue life model [60]. By fitting the life data at the fracture to this model, the validity of the crack growth model was determined. Stress-life model relates the stress amplitude to life, as shown in Equation (13):

$$S = AN^b, \tag{13}$$

where S is the stress amplitude, A and b are the parameters of the model. Using the number of cycles to fracture, this stress-life model was estimated. In this process, stress amplitude, according to Smith-Watson-Topper (SWT) equation, was used [60,78]. **Figure 29** presents the estimation results for both materials, and the life estimated from the crack growth model presents the consistency.

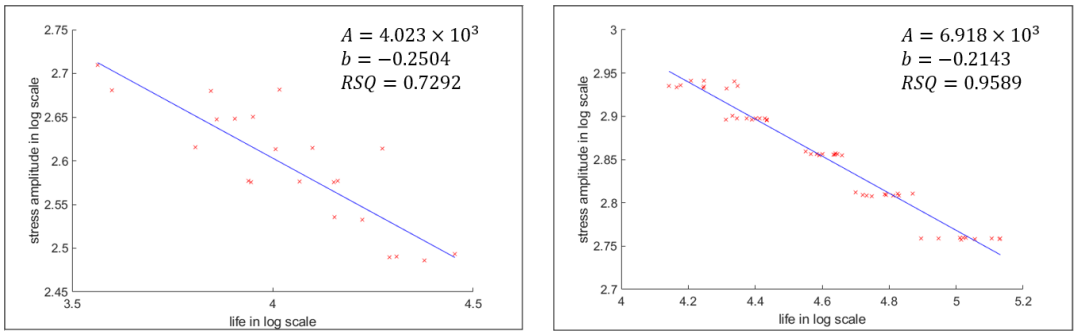

(a) **(b)**

Figure 29. Stress-life model fitting results for (a) AA7075-T6 and (b) SS304L.

Chapter 6: Entropic Approaches Characterizing Fatigue Damage

This chapter reports the results of the overall entropic approached. From multiple uniaxial fatigue tests, three sorts of energy dissipations were collected, i.e., mechanical strain energy, heat (temperature), and acoustic emission (AE). Classical thermodynamic entropy, Jeffreys divergence, and AE entropies are presented with both computation results and evaluations. Mechanical strain energy was computed only from the tests of SS304L specimens, and this chapter reports within the tests.

6.1 Classical thermodynamic entropy (CTE)

6.1.1 Entropy calculation process

As described in Equation (2), thermodynamic entropy generation is computed by the bilinear equation of force and flux for each energy dissipation mode. In the fatigue damage process, mechanical work is the dominating term, as experimentally proved from previous studies [3,26,33]. Plastic strain energy is computed numerically using discrete stress-strain data. The stress and strain data were computed from the load cell and the extensometer. Load data were converted to stress by using the cross-sectional area, considering crack growth. In converting strain from the extension, initial gauge length (25 mm) was used. **Figure 30** illustrates the process of plastic strain energy calculation for each cyclic loading. Summation of the forward and reverse work (strain energy) makes up the plastic strain energy. This forward/reverse work convention is further used in the JD calculation. The calculation process is coded using Matlab [72], and the script is provided in A.1.2.

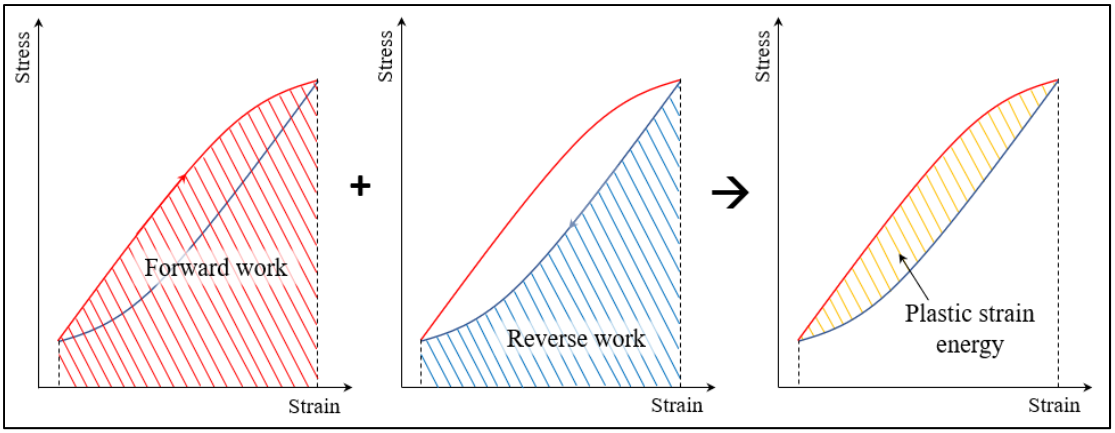

Figure 30. Strain energy calculation procedure. For each cyclic loading, the stress-strain path is divided into forward/reverse work processes, and strain energy is separately computed. The summation of two works is the plastic strain energy or hysteresis.

Temperature, measured by the thermocouple, was recorded every half second during each test. As an example, **Figure 31** shows the temperature measurement of the test 8VA03. After acquiring both strain energy and temperature, classical thermodynamic entropy was calculated based on the third term of Equation (3) for each cycle. The calculation process is described in A.1.3 that was written in the Matlab script [72].

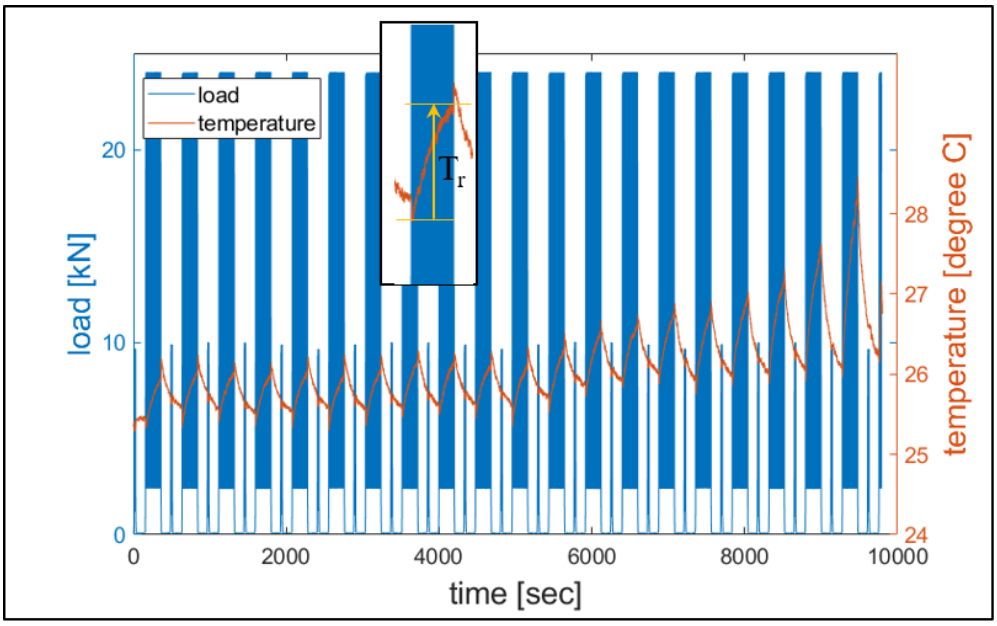

Figure 31. Temperature monitoring during the overall test (8VA10). The ninth damaging loading process is magnified to highlight the temperature rise measurement.

6.1.2 Results and evaluation of classical thermodynamic entropy

Figure 32(a) presents the cumulative classical thermodynamic entropy for a series of ten tests with 22 kN maximum loading (i.e., tests 8VA13 - 22). For each cumulative entropy plot, the initial trend is nearly linear, then the slope rapidly increases. Using the calculated life data determined by crack length, the cumulative entropy for each life was identified, as shown in **Figure 32**(b).

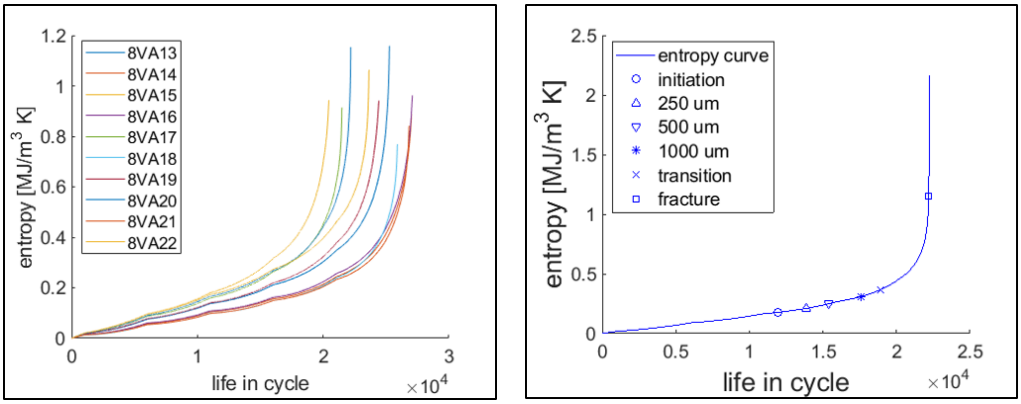

(**a**) (**b**)

Figure 32. (a) Cumulative classical thermodynamic entropy for ten tests with 22 kN maximum load. (b) The cumulative entropy measured by crack growth (test 8VA20). Every 1000 cycles, the cyclic loading process was stopped to perform some measurements. The effect of this is seen as a slight discontinuity in the plotted curves.

Figure 33 presents the cumulative entropy at each defined life by the crack length, with respect to the fatigue loading conditions. Stress amplitude, according to the Smith-Watson-Topper (SWT) equation, was used as the representative fatigue loading condition [60,86]. The effect of stress amplitude (slope in the regression line) diminishes as the crack length defining failure decreases.

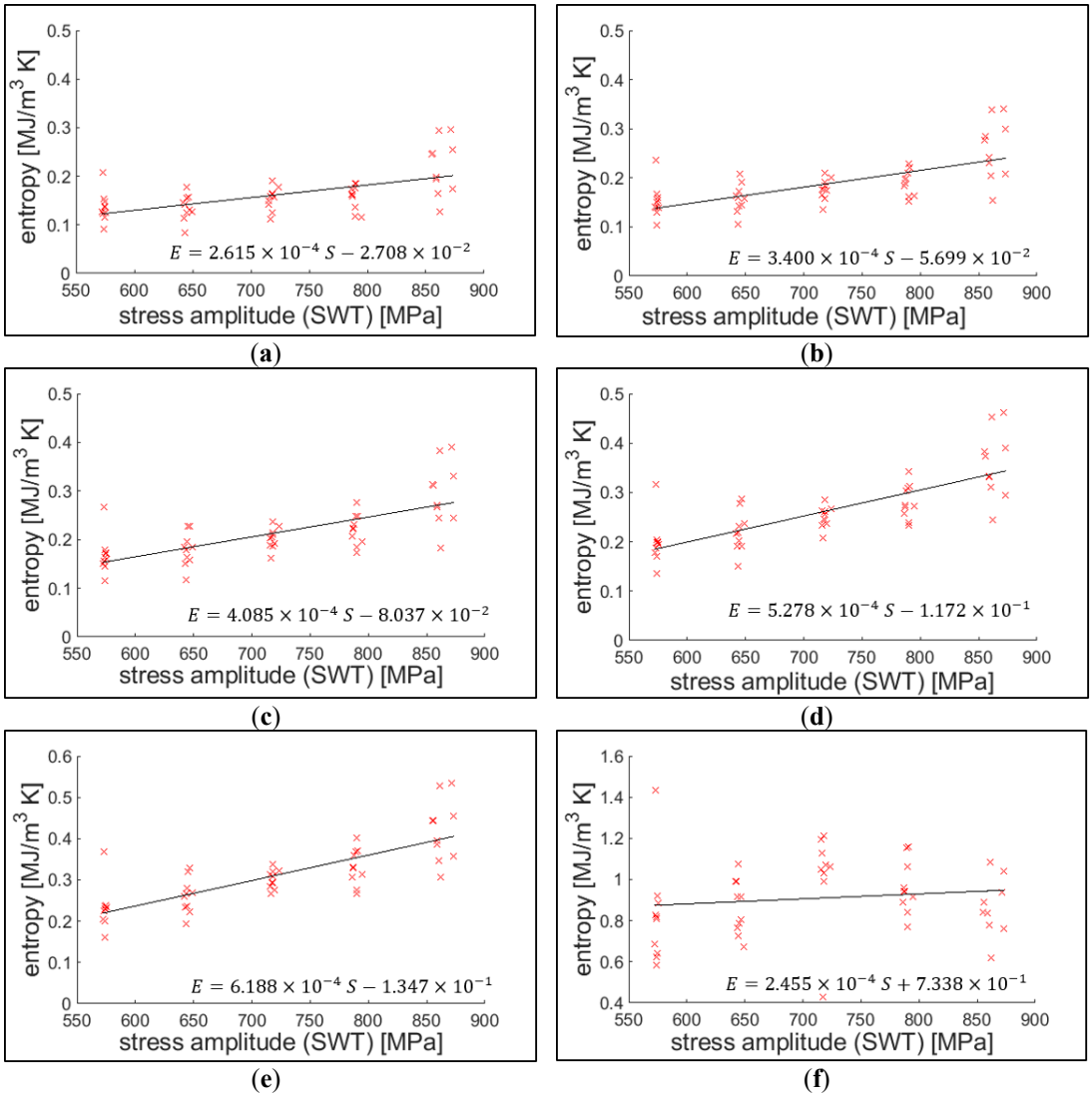

Figure 33. Classical thermodynamic entropy endurance for each defined life under crack growth. The life is determined at: (a) crack initiation, (b) 250 µm crack, (c) 500 µm crack, (d) 1000 µm crack, (e) transition, and (f) fracture, respectively.

The result indicates that entropic endurance has a small positive statistical correlation with the stress amplitude. The extensometer with 25 mm gauge length measured the strain (global strain), and the stress field is assumed to be proportional within the gauging area. This assumption is closer to reality before crack initiation. As the crack grows, the plastic zone area increases, and the stress distribution is more biased toward the plastic zone [60]. Nevertheless, endurances determined from crack length

criteria are also valid in the similar measurement setup applications. The similar entropic endurance behavior was also reported by Ontiveros et al. [3,76,87], who found that the cumulative strain energy or thermodynamic entropy at the crack initiation mildly increases with the stress amplitude.

6.2 Jeffreys divergence: the entropy of strain energy distributions

6.2.1 Analysis and results: distribution of forward/reverse work and JD calculation

The first step to calculate JD using strain energy is to develop forward and reverse work distributions. Forward/reverse work data within the same loading condition test group of fatigue tests, and strain energies with the same life ratio were gathered. In this process, the life (cycles) was determined as a function of crack length, as described in Chapter 5. Ten strain energy data (i.e., from each test group of the same loading condition and same life ratio) were fitted to the normal distribution using the maximum likelihood estimation (MLE) method. **Figure 34** shows an example of the fitted forward/reverse work normal distribution mean and standard deviation parameters with respect to the life ratio, and **Figure 35** presents an example of forward/reverse work distributions at a given life ratio. Fitting normal distribution followed the case study by Jarzynski [15] and the method of Douarche et al. [17]. More conservative and flexible fitting method such as maximum entropy distribution (MaxEnt) is also recommend [88-91].

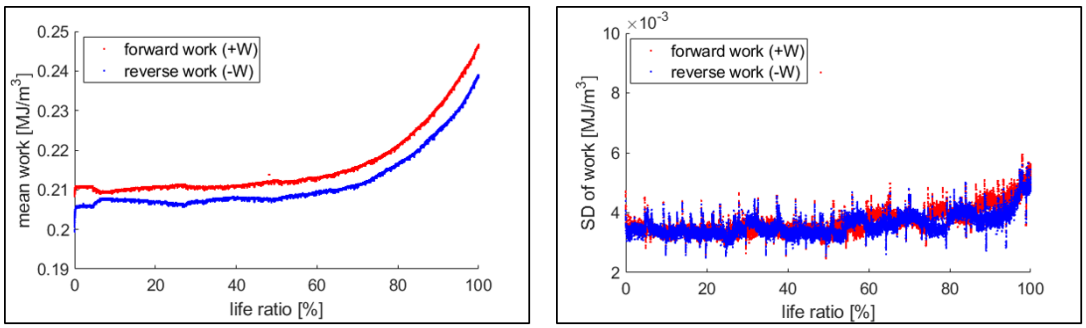

(a) (b)

Figure 34. MLE in the normal distribution of forward/reverse work distributions with respect to the life ratio. The data were collected from ten 22 kN maximum loading tests, and the failure (100 % life ratio) is determined for an initial fatigue crack length of 1000 μm. (a) Shows mean (μ), and (b) shows the standard deviation (σ). As noted, standard deviations (SD) of work for forward/reverse normal distributions have significant overlap.

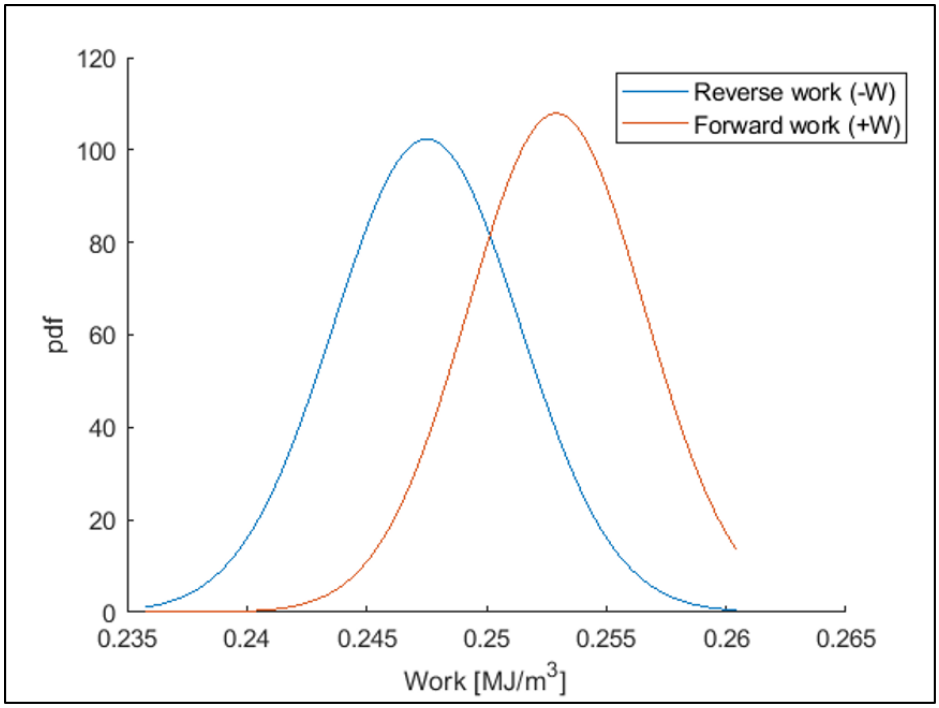

Figure 35. Forward/reverse work distributions of 22 kN maximum loading test group at 25 % of life. The distributions were fitted in the normal distribution model.

After the parametric estimation for each strain energy data set, relative entropies (both $D(\pi_f|\pi_r)$ and $D(\pi_r|\pi_f)$) were computed by using Equation (7). The cumulative JD was calculated and plotted, as shown in **Figure 36**, which presents the cumulative JD for the test group of 16 kN maximum load. Similar to the classical thermodynamic

entropy, JD is initially linear, then the slope increases as the crack grows. The computing process was executed by the Matlab script, as included in A.1.4.

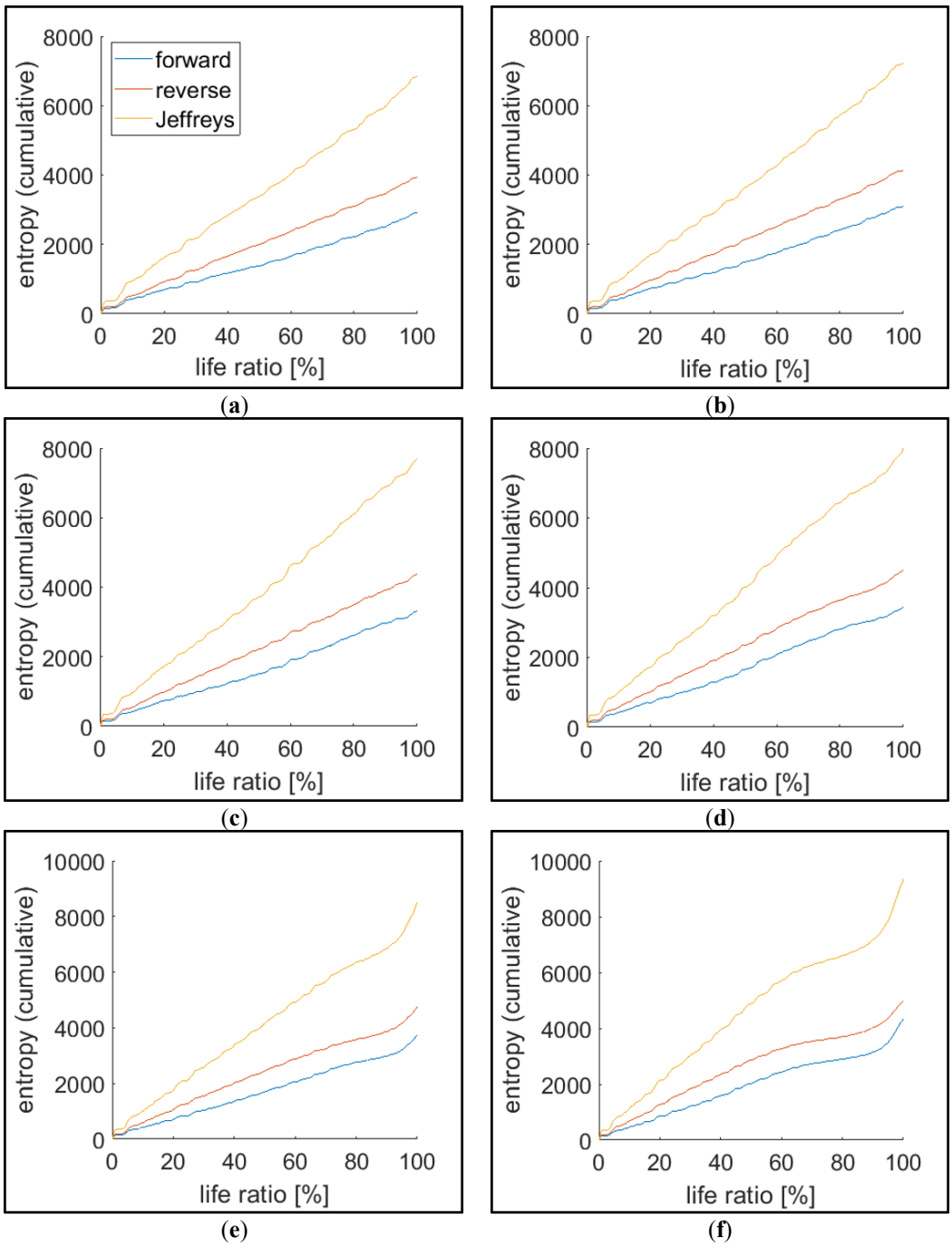

Figure 36. Cumulative relative entropy (Example: the test group with 16 kN maximum load). Each plot represents the case of normalized life at various crack lengths: (a) crack initiation, (b) 250 µm, (c) 500 µm, (d) 1000 µm, (e) transition, and (f) fracture.

6.2.2 Evaluation: Correlation to the classical thermodynamic entropy

In the evaluation of possible fatigue damage measurements, the damage is normalized according to Equation (14) [13,25]:

$$\mathrm{D} = \frac{\mathrm{M_i} - M_o}{M_f - M_o}. \tag{14}$$

Where M_o is the measured damage at time zero or the pristine state of the specimen, M_f is the damage at the failure (e.g., fracture), and M_i is the damage at a given instance (loading cycle). Depending on which crack length is used to determine the failure, M_f was differently determined, meaning, for example in case of crack initiation, M_f corresponds the measured damage at that point. The initial application of this damage measure was inspired by the Palmgren-Miner rule [60,92], in which the fatigue damage is measured in the proportion of the number of cycles. Not only the number of cycles, but also several measures such as crack length, load-carrying capacity, and elastic modulus degradation have been utilized as measures of damage in the normalized damage [18]. Normalized entropic damage was first introduced by Imanian and Modarres [25] and used by Sauerbrunn, et at. [13].

Figure 37 shows one of the five test groups (ten tests of 16 kN maximum loading) where normalized cumulative JD is linearly correlated to the normalized reference damage (classical thermodynamic entropy). The correlation between the JD and the classical thermodynamic entropy are consistent except at the point of fracture. All the loading groups present this inconsistency at the fracture failure. In case of large crack lengths, it is shown that the JD underestimates fatigue damage compared to the classical thermodynamic entropy. The cause of inconsistency needs to be further investigated.

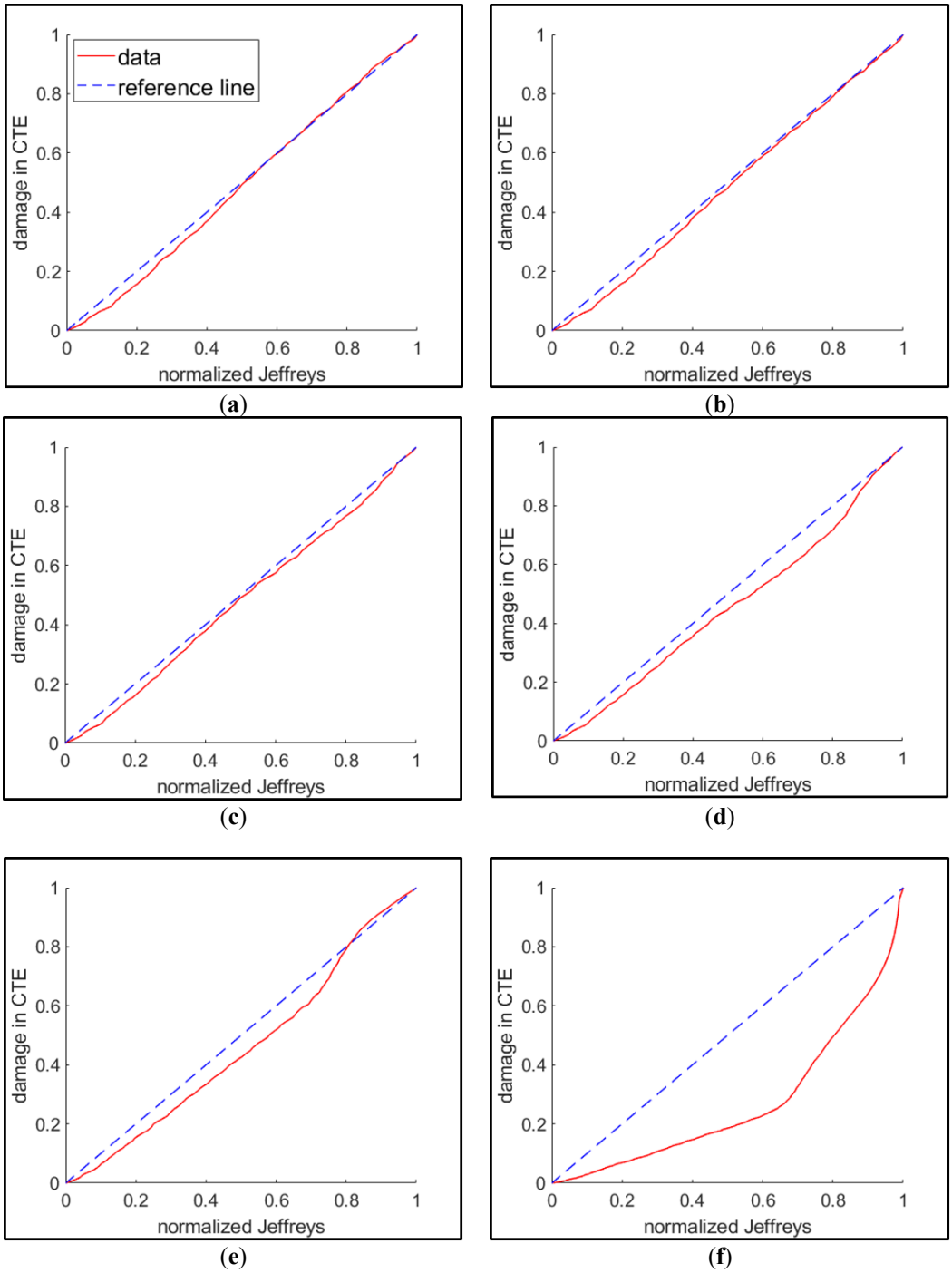

Figure 37. Evaluation of JD by correlating to the reference damage (classical thermodynamic entropy-CTE) as an example of the 16 kN maximum loading test group. The defined point of failure draws each correlation plot at (a) crack initiation, (b) 250 µm crack, (c) 500 µm crack, (d) 1000 µm crack, (e) transition, and (f) fracture.

Jeffreys divergence and thermodynamic entropy in molecular scale are related through the Boltzmann constant (k_B). However, in the context of macro-scale application in fatigue using equations (6), (8), and (9), classical thermodynamic entropy (CTE) is empirically shown to be related to JD by the means of the pseudo-Boltzmann constant, k_{pB}, wherein Equation (15), $\mathrm{k_B}$ changes to $\mathrm{k_{pB}}$.

$$\mathrm{CTE} = \mathrm{k_{pB}} \cdot JD. \tag{15}$$

The pseudo-Boltzmann constantk_{pB}, which no longer has the same interpretation and unit as the Boltzmann constant in our macro-scale application, was computed from the slope of the fitted line relating the cumulative JD to the mean classical thermodynamic entropy as shown in **Figure 38**, with the slope summarized in **Figure 39**.

The application of the fluctuation theorem to the macro-scale energy dissipation in the fatigue test has the scale limitations. The comparison of the macro-scale applications in the fatigue tests to the reported RNA test is detailed in **Table 8**. In our experiments, the fluctuation source was extended from the molecular-scale to the macro-scale by changing the measurement mode from thermal to plastic strain energy in the macro-scale application. In this extension, the fluctuation was assumed to be caused by multi-scale dimensional variability. In our experimental investigations, the fluctuation was presented by the formation of forward/reverse strain energy distributions. Furthermore, the converting factor (namely, pseudo-Boltzmann constant) shows statistical consistency that further supports our assumption that JD can be empirically applied as an alternative damage measurement. Further empirical surveys need to consider other conditions such as material, geometry, damage mode, and stress conditions.

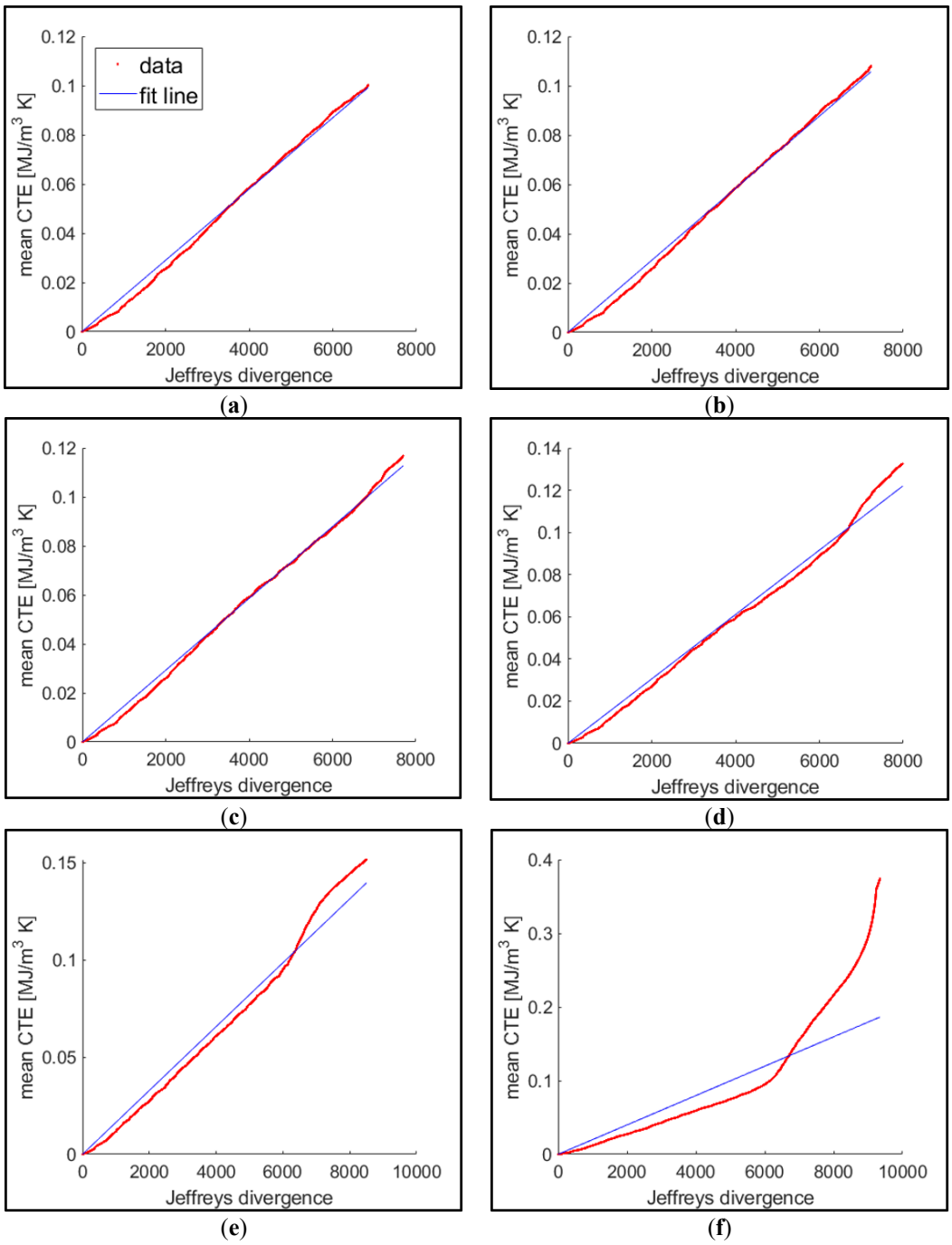

Figure 38. Linear correlation (with the zero intercept) between mean CTE and JD (for the ten tests of 16 kN maximum loading group). Using this correlation, the slope is estimated to correspond to k_{pB}. Failure defined at: (a) crack initiation, (b) 250 µm crack, (c) 500 µm crack, (d) 1000 µm crack, (e) transition, and (f) fracture.

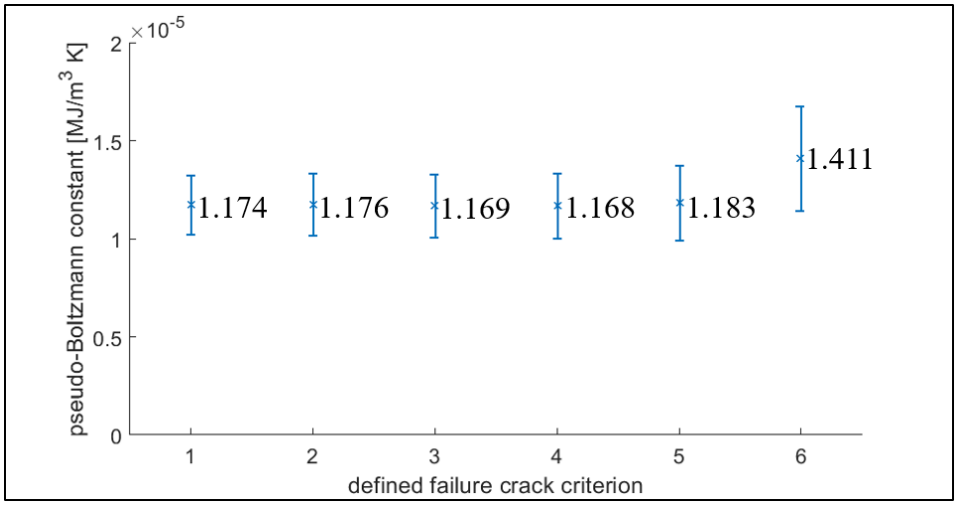

Figure 39. The slope (namely the k_{pB}) for each crack-length based failure. The bar of each data point shows one standard deviation above and below the mean shown. Failure is defined as (1) crack initiation, (2) 250 μm crack, (3) 500 μm crack, (4) 1000 μm crack, (5) transition, and (6) fracture.

Table 8. Comparison of Crooks fluctuation theorem application to RNA and metal fatigue test.

	RNA [16]	Metal Fatigue Test
Purpose	• Finding Helmholtz free energy	• Assessing the amount of damage
Source of fluctuation	• Thermal energy • Fluctuation in atomic distance	• Plastic strain energy • Multi-scale defects (e.g., point defect, dislocation, volumetric defect, inclusions, and grain structure variability)
Test control	• Controlled in displacement • Thermal equilibrium at both end of displacement points	• Controlled tensile load • The thermal equilibrium not controlled
Test repetition	• Hundreds of times • A specimen was repeated with unfolding/folding process without regarding damage	• Ten fatigue tests repeated with fixed loading condition, and strain energy data grouped in the corresponding damage
Correlating constant (JD to CTE)	• Boltzmann constant (1.381×10^{-23} J/K)	• Pseudo-Boltzmann constant estimated from tests ($1.168 - 1.411 \times 10^{-5}$ J/m^{3}K, range of the mean values)

6.3 AE entropy: information entropy and relative entropy

AE sensors, attached on the specimen surface, collected acoustic energy dissipation in the form of elastic AE signals (waveform) represented by digitized voltage data. Each waveform file is transformed into its equivalent discrete probability distribution represented by a histogram and used to quantify the information and relative entropies as expressed by Equations (3) and (4).

6.3.1 Analysis of information entropy (IE)

To calculate information (Shannon) entropy from AE waveform data, the process followed the approach reported by Sauerbrunn et al. [13] and Kahirdeh et al. [93], where information entropy is calculated from the discrete histogram of waveforms. **Figure 40** presents the procedure for AE information entropy calculation. Variations in the bin size parameter showed that the selected bin size would achieve the maximum entropy. The sampling process was based on using a parametric normal distribution under the assumption that the random AE waveforms distribute symmetrically. More flexible fitting method to the measured data is also possible such as the MaxEnt [88-91].

Figure 41 presents an example of the individual and cumulative information entropies. On the cumulative entropy plot, the crack-length points were marked. It is observed that the cumulative entropy trend becomes far steeper around the point of crack initiation. This is useful information for PHM applications.

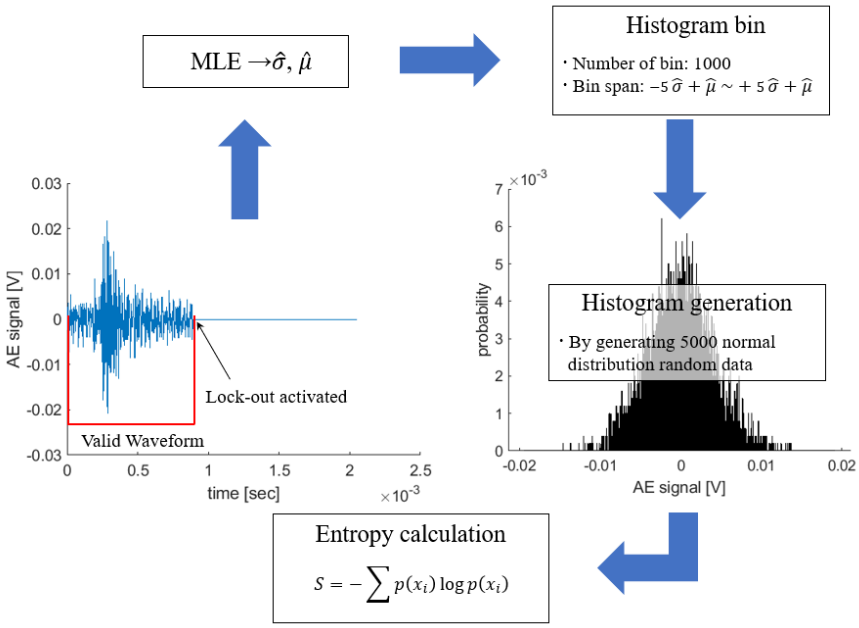

Figure 40. The procedure of AE information entropy calculation. By using the digitized waveform signal data, information entropy is calculated from the generated histogram.

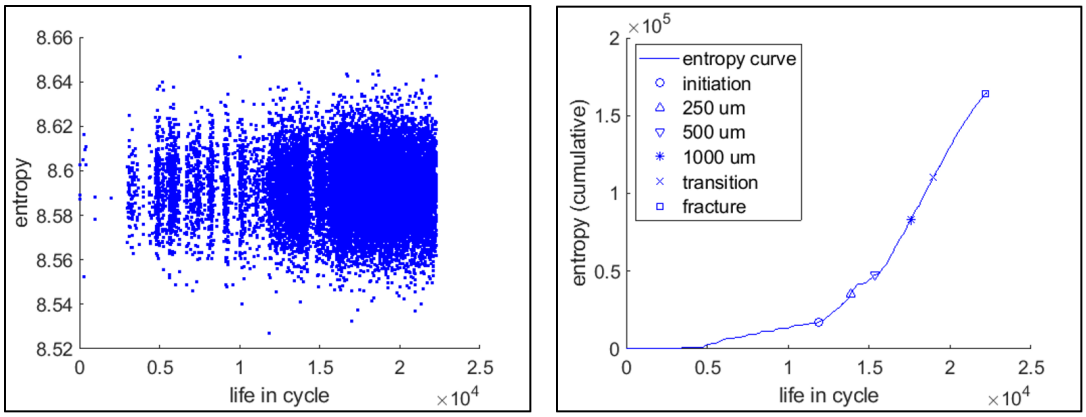

(a) **(b)**

Figure 41. AE information entropy (example: 8VA20). (a) Individual entropies for the collected waveforms. (b) Cumulative entropy through the life in cycle.

6.3.2 Analysis of relative entropy (RE)

AE relative entropy was computed by using Equation (4). In this computation, a reference distribution was determined from the waveform that exhibited the lowest information entropy throughout the test, assuming that the least information entropy was related to a background noise that caused the least damage. **Figure 42** shows when

the minimum information entropy appeared. The lowest information entropy has no particular indication of life or damage.

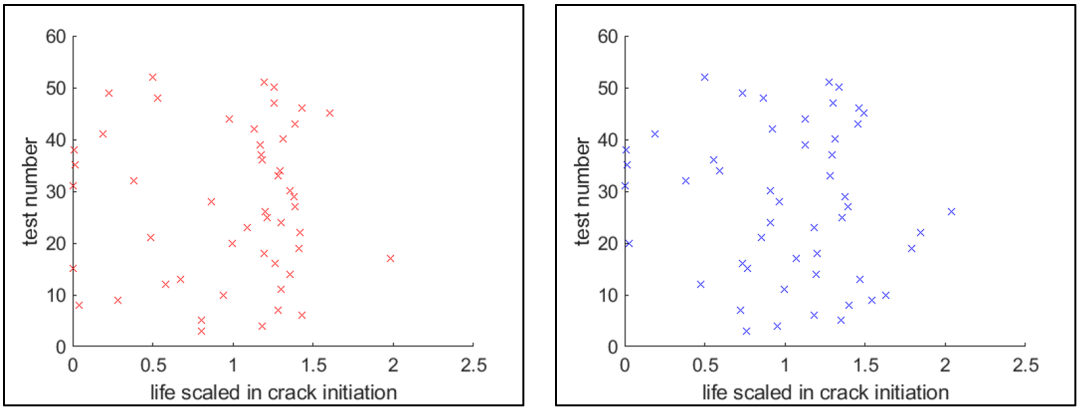

(a) (b)

Figure 42. The entropy scatters showing when the minimum information entropy appears for each test. The time of minimum entropy had no consistency to the proportion of life expended. The life at the lowest information entropy from the sensors (a) Channel 1 and (b) Channel 2.

In the calculation of relative entropy by using two AE waveforms (observed/reference), distributions were assumed as continuous (normal distribution), and computed using the numerical integration method as described by Equation (4). **Figure 43** shows the individual and cumulative relative entropies, and the cumulative entropy presents a similar trend as that of information entropy. The calculation was performed by the Matlab script, included in A.1.6.

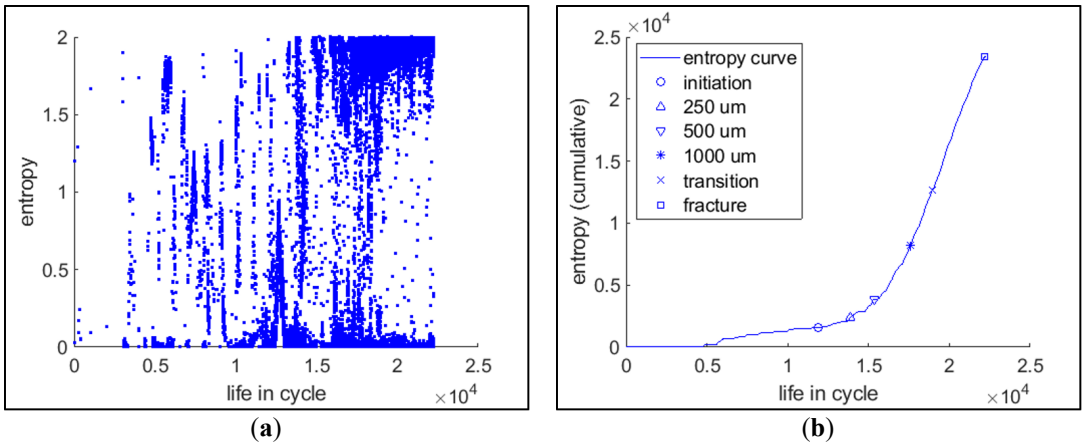

(a) (b)

Figure 43. AE relative entropy (example: 8VA20). (a) Individual entropy for each collected waveform. (b) Cumulative entropy through the life in cycle.

6.3.3 Evaluation of AE entropies and correlation with fatigue damage

After the calculation of information and relative entropies from each test, the entropic endurance from cumulative entropy was surveyed. However, the quantitative entropic endurance values were not consistent, as shown in **Figure 44**. Two plots in **Figure 44** show that cumulative entropies at the failure for both information and relative entropy have very high variabilities. Therefore, another assessment was utilized using AE entropies rather than the quantitative assessments, by comparing with several AE features in correlating to the normalized damage.

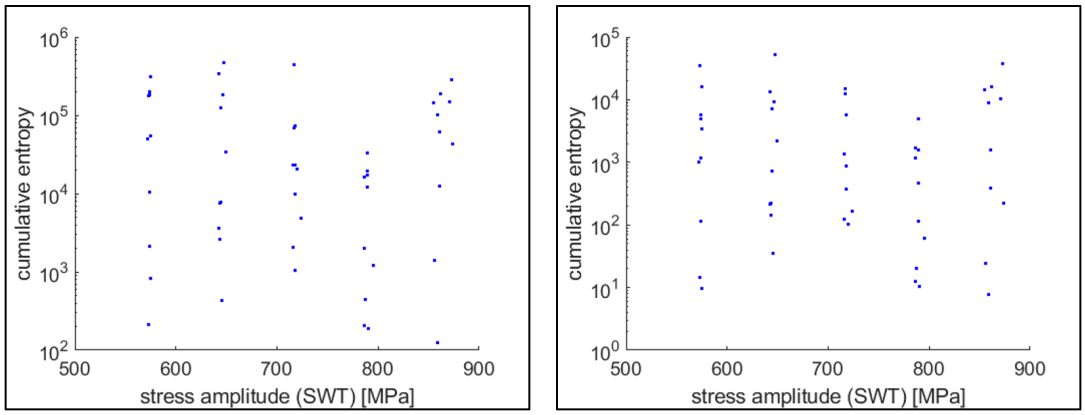

Figure 44. Cumulative AE entropy with failure defined at crack initiation. (a) Information entropy (mean: 4.8×10^4, standard deviation: 1.2×10^5) and (b) relative entropy (mean: 5.9×10^3, standard deviation: 1.1×10^4).

The AE entropic measures, AE count, and absolute energy are compared to the classical thermodynamic entropy, as shown in **Figure 45** where failure is defined at the crack initiation. The overall at-a-glance observation shows that the AE information entropy is the closest to the CTE damage. The mean deviation (mean absolute distance from CTE damage to an AE feature) was computed for each test. The sign test was used to assess AE entropy performance by using the mean deviation.

The sign test is a nonparametric statistical test measure consistent differences between pairs of observations and calculates the tests statistic from the difference in the median of the two populations [94]. In this sign test, the left tail mode was utilized, and the entailed hypotheses are shown in Equation (16) (the sign test expressed in sign-test(**a**,**b**)):

$$H_0: a - b \geq 0; H_1: a - b < 0. \quad (16)$$

When the p-value from this statistic is less than a significance level (10 % in this test), the null hypothesis is rejected, and the result concludes that the median of a is less than that of b.

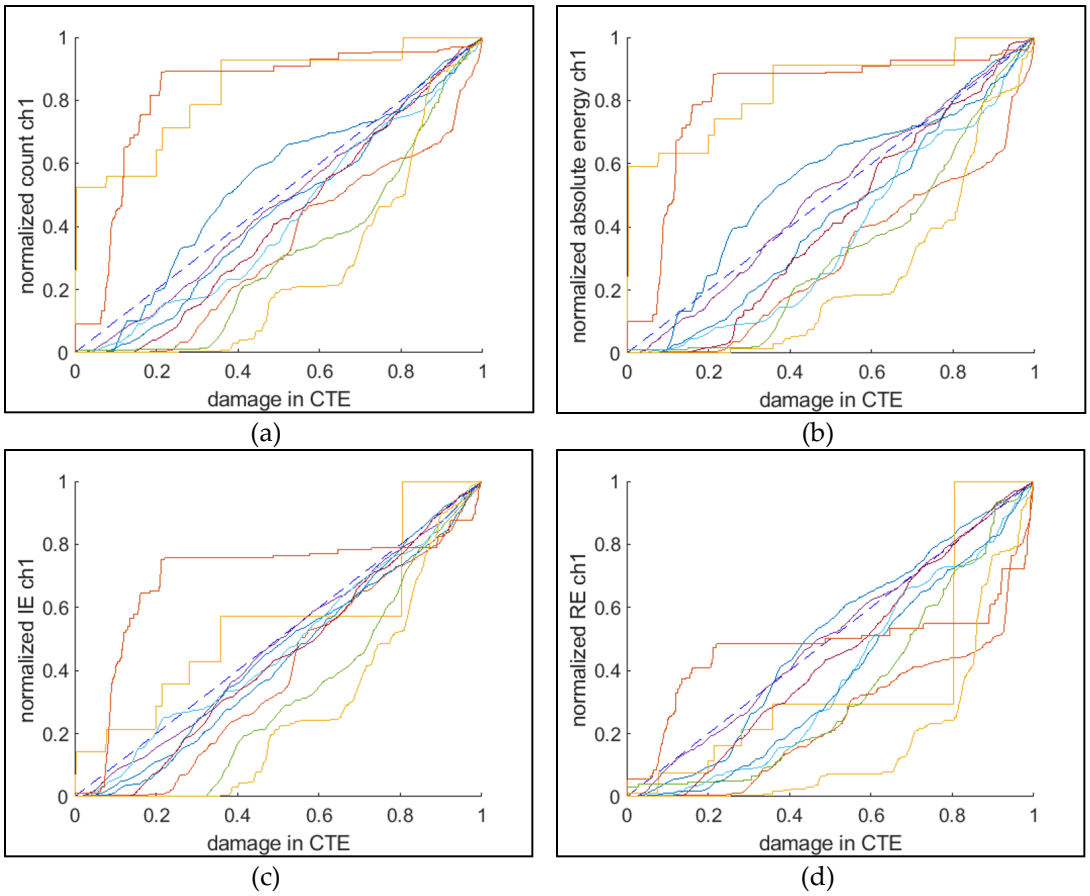

Figure 45. Correlation of AE features to the measured damage (classical thermodynamic entropy). The correlated features are (a) count, (b) absolute energy, (c) information entropy, and (d) relative entropy. These correlation plots were drawn from the 24 kN maximum loading group and AE sensor channel 1 (the sensor more adjacent to the loading actuator).

Table 9 presents the sign test results for all the cases (failure defined by the crack length and AE sensor channel). From the results, one can conclude that the information entropy is better than the count and absolute energy except for the case of fracture failure, and this result is also consistent with Sauerbrunn et al.'s [13] conclusions. However, relative entropy presents no advantage over other AE features. As discussed using **Figure 41**, the definition of the reference distribution denoising AE signal needs further surveys.

Table 9. Sign test results represented in p-value. The sign test rejects the null hypothesis (the former is not less than the later) when the p-value is less than the significance level. In the 10 % significance level, the case of not rejecting the null hypothesis is underlined.

Failure defined at	a: information entropy b: absolute energy		a: information entropy b: count		a: relative entropy b: absolute energy		a: relative entropy b: count	
	ch1	ch2	ch1	ch2	ch1	ch2	ch1	ch2
Initiation	5.9E-2	1.6E-2	5.9E-2	3.2E-2	7.7E-3	1.6E-1	1.6E-2	3.3E-3
250 μm	3.3E-3	3.3E-3	3.2E-2	1.6E-2	5.9E-2	1.6E-1	1.6E-1	4.4E-1
500 μm	1.3E-3	3.3E-3	7.7E-3	3.2E-2	5.9E-2	3.3E-1	6.6E-1	9.0E-1
1000 μm	1.5E-4	1.5E-4	1.6E-2	3.2E-2	1.6E-2	1.6E-1	7.7E-1	8.4E-1
Transition	1.5E-4	1.3E-3	3.2E-2	3.2E-2	4.5E-5	3.2E-2	1.6E-1	6.6E-1
Fracture	2.4E-1	1.0E-1	5.9E-2	3.4E-1	5.6E-1	9.4E-1	4.4E-1	7.6E-1

6.4 Summary and comparison

In sections 6.1 to 6.3, four entropic approaches were reported for applications to fatigue damage assessment. Classical thermodynamic entropy was assessed in terms of the DEG theorem by presenting the existence of an entropic endurance indicating fatigue failure. The assessments of Jeffreys divergence and AE entropies were followed using the CTE as the reference damage. From the assessment results, JD and AE information entropy exhibit reasonable correlations to the fatigue damage. Furthermore, JD quantitatively correlates with CTE through the pseudo-Boltzmann constant (k_{pB}).

Correlation analyses show that JD has a better correlation to the reference damage than the AE information entropy. The analyzed entropic approaches are compared and summarized in **Table 10**. It is noted that the simulation of the entropic prediction model, for example, through a finite element approach is more applicable to CTE and JD than the AE information entropy. For example, similar to Mozafari et al. [95], fatigue damage simulation modeling using mechanical plastic deformation, can be equally applicable to CTE and JD.

Table 10. Comparison of entropic approaches and efficacy as the measure of fatigue damage.

	Classical thermodynamic entropy (CTE)	**Jeffreys divergence (JD)**	**AE information entropy (IE)**	**AE relative entropy (RE)**
Analysis source data	• Plastic strain energy • Surface temperature	• Plastic strain energy	• AE waveform	
Calculation method	• Bilinear irreversible thermodynamic entropy • Equation (2)	• Fluctuation theorem and relative entropy • Equations (8), (9), and (10)	• Information theory • Equation (3)	• Relative entropy • Equation (4)
Evaluation	• Consistent entropic endurance • Used as the reference damage	• Correlation to normalized measured damage • Pseudo-Boltzmann constant (k_{pB})	• Correlation to normalized measured damage	
Effect	• Endurance verified • Linear relation to stress amplitude	• Endurance verified • Consistent k_{pB}	• Better than AE count and absolute energy. Useful for early life in pre-crack initiation	• Better than AE count and absolute energy for only a few particular cases

Chapter 7: STLP and Temperature Measurements

7.1 STLP and damage

For each fatigue test, short-term loading process (STLP) was applied, as shown in **Figure 14** (step 2). During the STLP or the so-called excitation process, AE waveforms were generated and received by the AE sensors. Among the AE features, information entropy of waveform was used in the STLP assessment according to the approach outlined in **Chapter 6**, where it was shown that information entropy represents fatigue damage better than other AE features.

7.1.1 AE entropies generated during STLP

AE information entropy during the STLP was investigated for each block (i.e., combining 1000 cyclic loadings and a series of STLP). **Figure 46** presents an example of the individual AE information entropy. At the initial stage of damage, no significant entropy was generated. After certain damage (crack growth), the entropies of the signals indicated and attributed to fatigue damage.

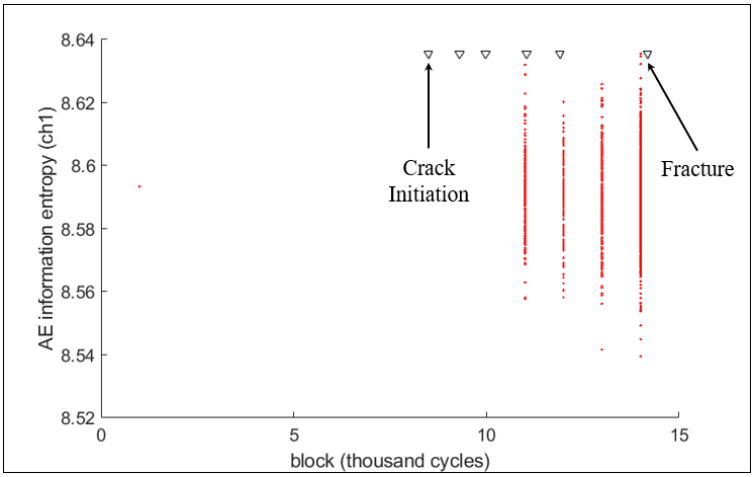

Figure 46. Individual AE information entropy (test 7VA12). The AE signals (red dots) are attributed to specific crack growth.

Throughout the investigation of all the test results, five cases representing different pattern in the STLP entropy signals were observed, (one such case is shown in **Figure 46**). In **Figure 46**, the first AE information entropy observed during the STLP intervals appears after the crack initiation. **Figure 47** presents four more cases of entropy patterns, including early signals, initial temporary STLP signals, excessive signals, and no or insignificant signals.

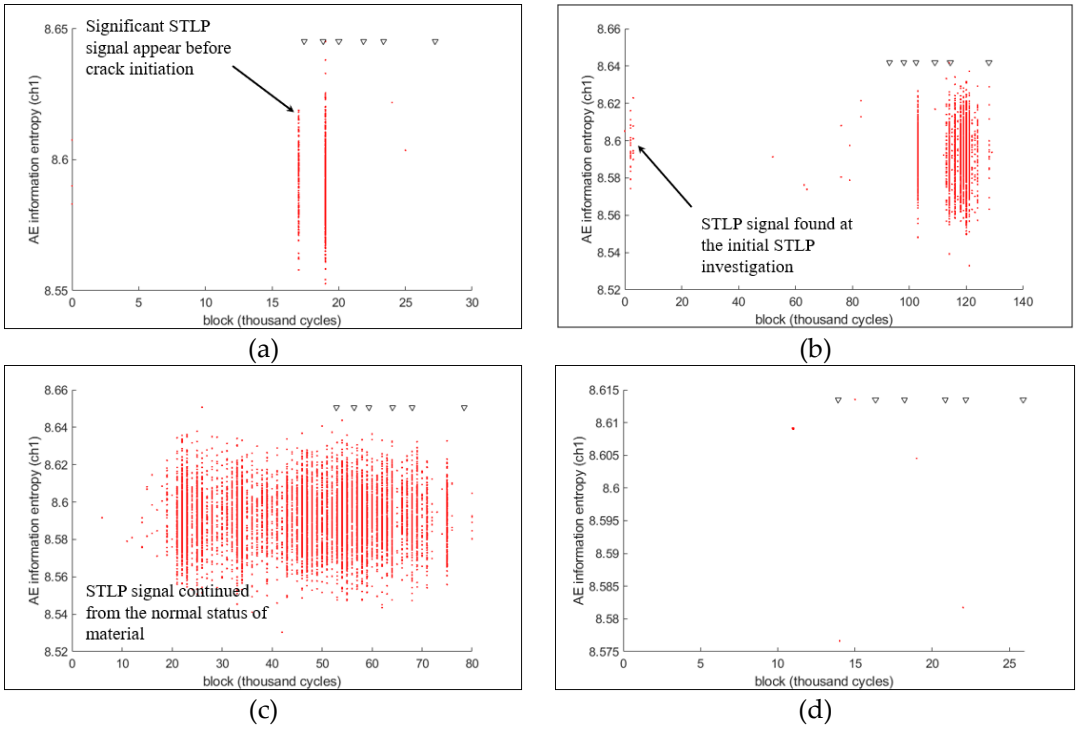

Figure 47. Four STLP AE information entropy signal patterns observed in the tests: (a) The first significant signals found before crack initiation (8VA16), (b) temporary STLP signals at the initial stage of fatigue damage (8VA50), (c) excessive signals during the test (8VA51), and (d) no or insignificant signals (8VA18).

As an alternative tool of upcoming fatigue failure detection, the STLP signals shown in **Figure 46**, **Figure 47** (a), and (b) can be used as possible evidence of fatigue damage. On the other hand, the two cases of **Figure 47** (c) and (d), provide incorrect or insufficient information to predict fatigue damage. To present detailed investigation

process in STLP, further analyses methods and quantification of the STLP signals will follow.

7.1.2 Quantification of STLP signals representing fatigue damage

The first step of STLP AE information entropy is to calculate cumulative information entropy (CIE) generated within each block. **Figure 48** shows the cumulative information entropy of the test 7VA12.

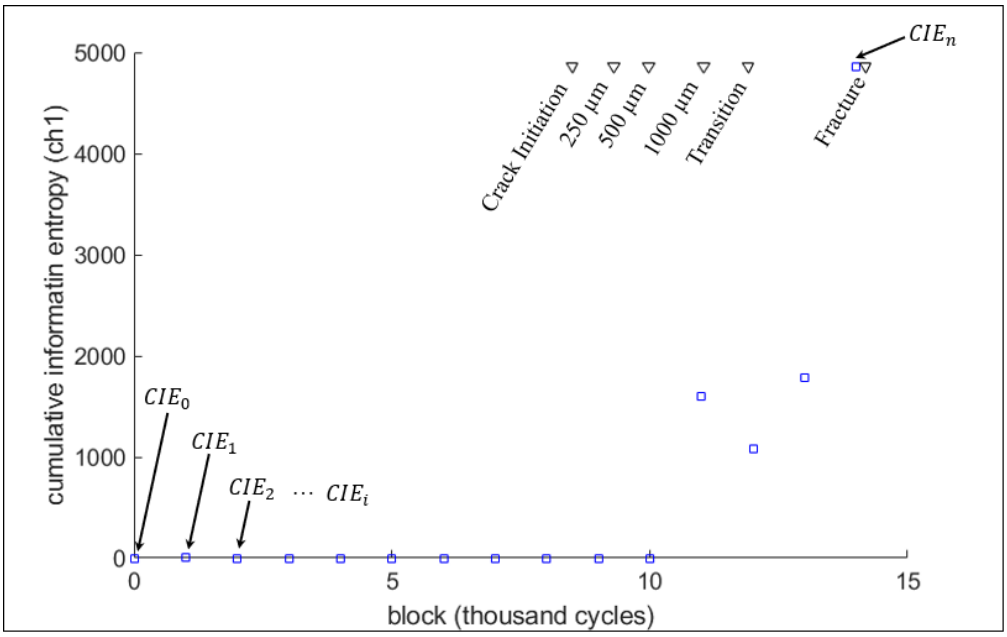

Figure 48. Cumulative AE information entropy (CIE) generated in each block's STLP (7VA12). STLP was loaded after 1000 cyclic fatigue damage loading.

As it was evident from **Figure 44**, the quantitative comparison of the cumulative information entropy showed inconsistency in crack damage representation. Likewise, information entropy during STLP also represented no quantitative consistency, as shown in **Figure 49**. In this figure, the maximum cumulative entropy for each test presents high variability. To study the signals, cumulative information entropy was converted to the criticality index (CI), considering the history of STLP signals.

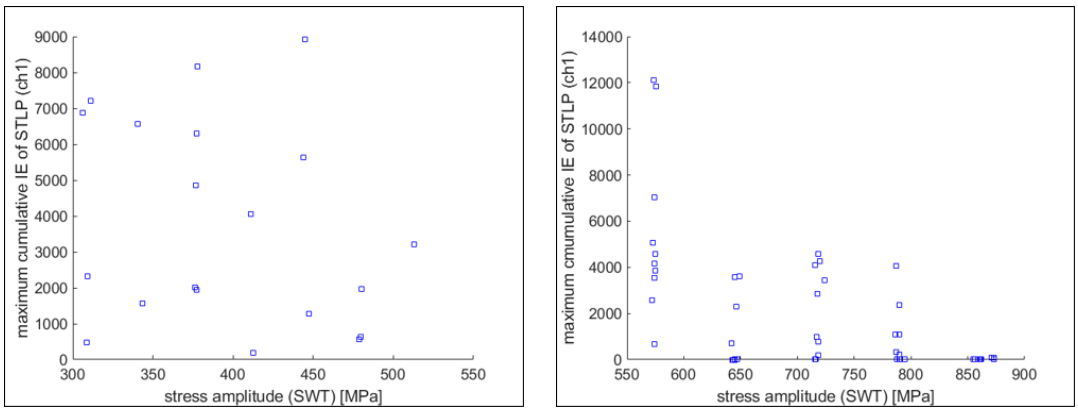

(a) (b)

Figure 49. Maximum cumulative entropy in STLP process: tests using materials (a) AA7075-T6 and (b) SS304L.

The calculation of the criticality index (CI_i) was as follows:

1. $CI_i = 0$ if $CIE_i = 0$
2. $CI_i = 0$ if CIE_i is the first non-zero cumulative entropy
3. If $CIE_i \neq 0$ and CIE_i is not the first non-zero observation, CI_i is computed by Equation (17):

$$CI_i = \frac{CIE_i}{(\sum_{k=1}^{i-1} CIE_k)/(\sum_{k=1}^{i-1} \delta_k \, (\delta_k=1 \; if \; CIE_k \neq 0, \;\; \delta_k=0 \; if \; CIE_k=0))}, \quad (17)$$

where the nominator is the current cumulative information entropy, and the denominator is the mean non-zero cumulative entropy of previous STLP's. **Figure 50** shows the plot of criticality index for a test 7VA12. In this figure, the first significant entropies of the signals in an STLP group shown in **Figure 46**, is presented.

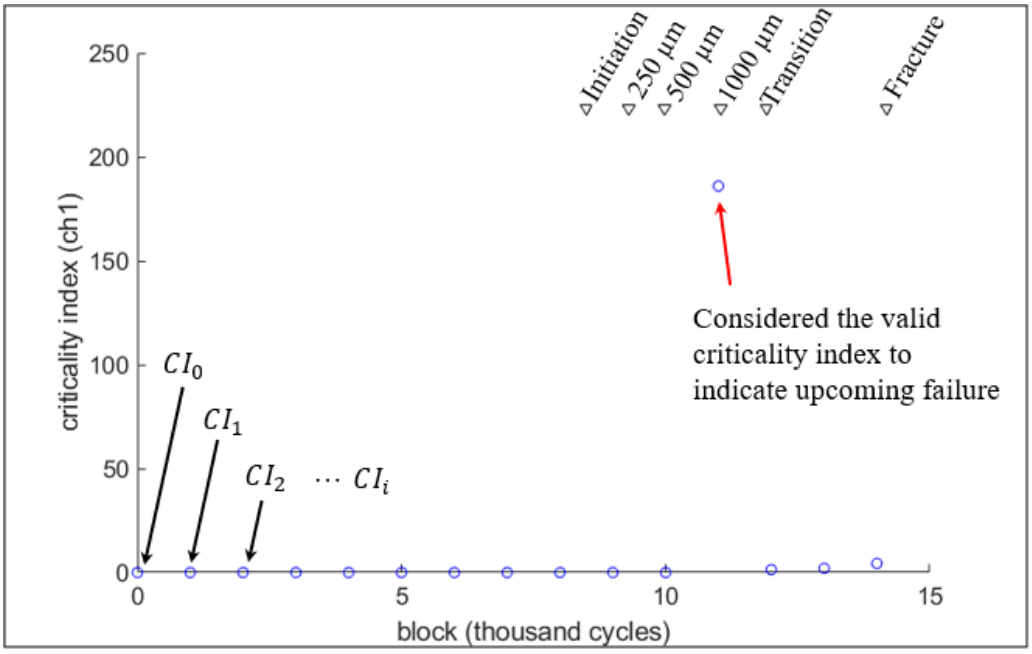

Figure 50. The criticality index (CI_i) calculated from cumulative information entropy for 7VA12. The criticality index at the first non-zero significant entropy value of a group of an STLP load is shown as a point crack growth (around 1000 μm crack length).

7.1.3 Assessment of STLP signals

STLP may be used during a macro-scale fatigue damage inspection (e.g., crack-length measurement) when a sharp rise in the criticality index in STLP is detected. For example, the valid criticality is determined by the first index exceeding a constant criticality (CI_c):

$$Valid\ criticality\ index\ \mathrm{CI_i}\colon \mathrm{CI_i} > CI_c\ . \tag{18}$$

The exceedance from criticality index indicates the high likelihood of upcoming failure. That is, the macro-scale crack measurement is nearly detectable when the first valid criticality index is detected. Even though the crack is not yet grown, the crack initiation has or will soon occur when the valid criticality index is detected.

The optimal constant criticality ($\mathrm{CI_c}$) value was found by comparing the candidate values (1 - 30). In comparison, two considerations were followed:

1. The number of successes (i.e., satisfying Equation (18), the higher number is more desirable)
2. The number of blocks from the valid criticality index to the crack initiation, if the valid criticality index was found before the crack initiation (less is better).

Figure 51 presents an example of finding the constant criticality. It was found that the optimal constant criticality is 4 for both materials.

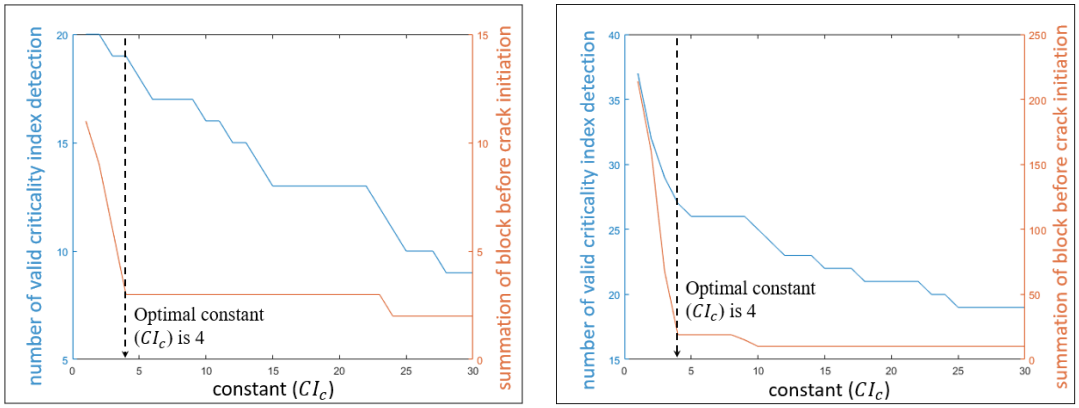

Figure 51. Plots finding the optimal constant criticality (CI_c) in STLP. The constants were compared in (1) number of tests having valid criticality index detection and (2) the summation of the remaining number of blocks to the crack initiation. Constant criticality comparisons from (a) the tests of AA7075-T6 materials and (b) the tests of SS304L materials.

After finding the optimal constant ($CI_c = 4$), the criticality index calculated from AE information entropy was assessed at each test by counting the number of success. **Table 11** and **Table 12** summarize the STLP results from the two material tests. AA7075-T6 tests showed good results in STLP that the 19 of the 20 tests (95 %) reasonably detected the upcoming failure. On the other hand, only 27 of 50 tests (54 %) were successful in the case of the SS304L tests.

Table 11. STLP test results for AA7075-T6. Nineteen out of 20 tests present successful detection on the upcoming failure. (block: the number of blocks from the test beginning to the valid criticality index detection, case: score "1" valid criticality index detected before crack initiation, score "2" indicates detected after crack initiation, and score "3" indicates failed to detect, and number of blocks from initiation: total block number from initiation to the detected valid criticality index).

Test ID	Block	Case	No. of blocks from initiation	Test ID	Block	Case	No. of blocks from initiation
7VA03	7	2	2	7VA14	7	2	0
7VA04	5	1	-1	7VA16	6	2	1
7VA06	7	1	-1	7VA17	15	2	2
7VA07	12	2	2	7VA18	18	2	2
7VA08	12	2	3	7VA19	9	2	3
7VA09	N/A	3	N/A	7VA20	17	2	2
7VA10	3	2	0	7VA21	19	2	1
7VA11	5	2	1	7VA22	9	2	3
7VA12	11	2	2	7VA23	5	2	0
7VA13	15	1	-1	7VA24	4	2	1

Table 12. STLP test results for SS304L. Twenty-seven out of 50 tests present successful detection on the upcoming failure.

Test ID	Block	Case	No. of blocks from initiation	Test ID	Block	Case	No. of blocks from initiation
8VA03	17	2	6	8VA28	20	1	-4
8VA04	N/A	3	N/A	8VA29	29	2	5
8VA05	N/A	3	N/A	8VA30	N/A	3	N/A
8VA06	N/A	3	N/A	8VA31	21	1	-5
8VA07	N/A	3	N/A	8VA32	23	1	-4
8VA08	N/A	3	N/A	8VA33	N/A	3	N/A
8VA09	N/A	3	N/A	8VA34	N/A	3	N/A
8VA10	N/A	3	N/A	8VA35	N/A	3	N/A
8VA11	N/A	3	N/A	8VA36	N/A	3	N/A
8VA12	N/A	3	N/A	8VA37	N/A	3	N/A
8VA13	N/A	3	N/A	8VA38	N/A	3	N/A
8VA14	20	2	3	8VA39	46	2	6
8VA15	N/A	3	N/A	8VA40	34	1	-1
8VA16	17	1	-1	8VA41	64	2	22
8VA17	N/A	3	N/A	8VA42	36	2	6
8VA18	N/A	3	N/A	8VA43	76	2	17
8VA19	18	2	5	8VA44	77	2	10
8VA20	14	2	2	8VA45	88	2	27
8VA21	12	1	-4	8VA46	92	2	17
8VA22	N/A	3	N/A	8VA47	80	2	7
8VA23	30	2	0	8VA48	82	2	4
8VA24	N/A	3	N/A	8VA49	78	2	2
8VA25	29	2	5	8VA50	103	2	10
8VA26	30	2	9	8VA51	N/A	3	N/A
8VA27	34	1	7	8VA52	105	2	7

It is concluded that the brittle material provides better AE-based entropic values related to fatigue damage in the form of STLP results by comparing AA7075-T6 and SS304L tests. Further investigation is recommended to assess and further generalize the STLP usefulness for the fatigue failure detection.

7.2 Temperature measurement and damage

The surface temperature was primarily measured in this research to support the calculation of the classical thermodynamic entropy (CTE). The temperature measurement throughout a fatigue test could be an independent source of detecting damages during the cyclic loading process, as shown in **Figure 31**. Hence, it is worth to relate temperature measurements to fatigue damage, as an additional detection metric.

Heat is one of the energy dissipation modes, according to the irreversible thermodynamics [1,25]. In the bilinear irreversible energy dissipation, as presented in Equation (2), The first term is the entropy generation due to heat dissipation. The heat dissipation during fatigue damage has been investigated in empirical studies [96-100]. For example, Kordatos et al. [96,100] estimated the crack-tip location by tracking the hot spot from real-time thermography studies. The prediction of fatigue life was estimated by using temperature measurements by Naderi and Khonsari [98] and Williams et al. [99]. In their studies, Naderi and Khonsari [98] used cooling rate (temperature measured right after a series of cyclic loading process), and Williams et al. [99] calculated the temperature rise rate relating to the loading condition.

In this section, the temperature measurements during our tests are evaluated by calculating the temperature rise and temperature rise rate, will be described in the following sub-section.

7.2.1 Temperature measures: rise and rise rate

At every damage loading process, the temperature rise was observed until the end of the loading process. The amount of temperature rise was measured from the beginning to the end of the damage loading for each block. Temperature rise rate was also computed at the beginning of each loading block. The measurements of both the temperature rise (T_r) and the temperature rise rate (θ_T) are described in **Figure 52**. The two temperature-related metrics were computed from the beginning to the end of the test and were reviewed to relate them to fatigue damage.

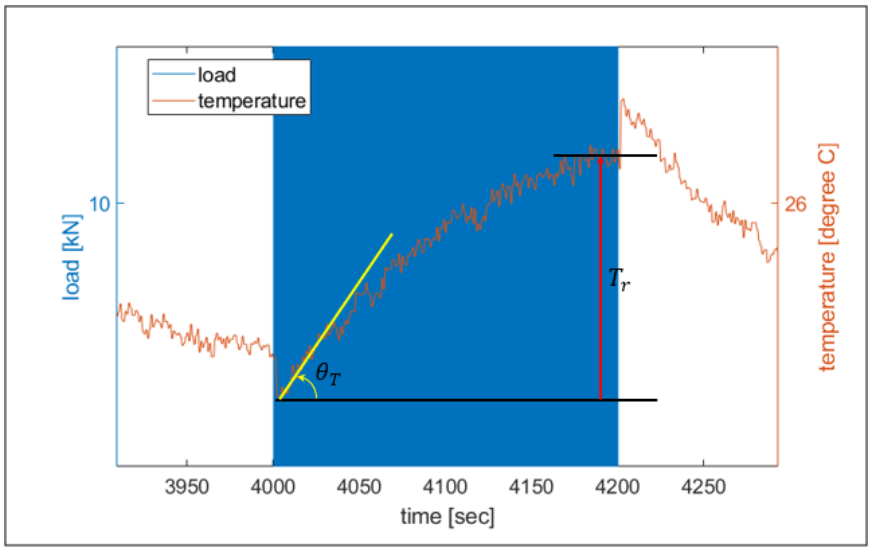

Figure 52. Two metrics of temperature measurements (test 8VA10). Temperature rise (T_r) is computed by measuring the temperature increment from the beginning to the end of the load block (1000 cycles). Temperature rise rate (θ_T) is the slope of temperature rise at the beginning of the cyclic loading block.

Two temperature metrics were calculated during all the cyclic loading blocks. As an example of AA7075-T6 tests, **Figure 53** shows T_r and θ_T measured in the test 7VA21, of which the fatigue crack initiated at the 17469th cycle (18th block). Regardless of crack growth, two temperature metrics had no significant changes in the trend.

On the other hand, 8VA10 (an SS304L test) shows a reasonably significant trend change, as shown in **Figure 54**.

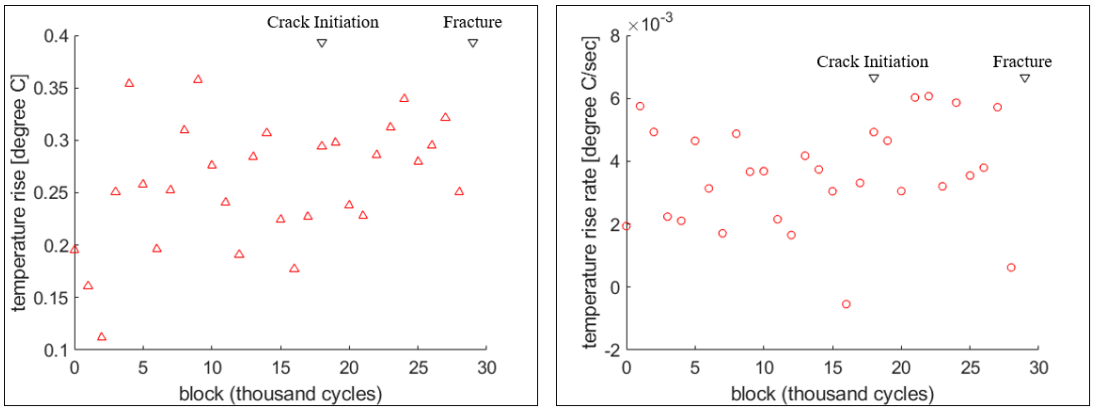

(a) (b)

Figure 53. Two temperature metrics in the test 7VA21. No particular trend change was detected during crack growth. (a) Temperature rise (T_r) and (b) Temperature rise rate (θ_T).

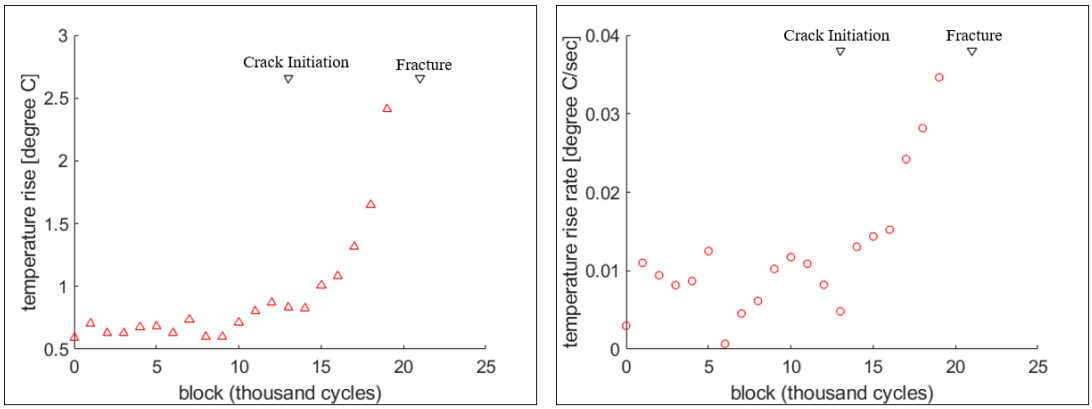

(a) (b)

Figure 54. Two temperature metrics in the test 8VA10. After crack initiation, the two metrics show the trend change to the increasing slope. (a) Temperature rise (T_r) and (b) temperature rise rate (θ_T).

7.2.2 Assessment of the temperature metrics

As observed in **Figure 54**, the two temperature-metrics increase highlights significant fatigue damage. **Figure 55** illustrates two different regions in the plot of the temperature rise rate (θ_T). The changes in the trend or transition point are significant when considerable fatigue damage (crack growth) is observed. In the analysis of finding the transition point, the dual-linear regression method, illustrated in **Figure 55**, was used.

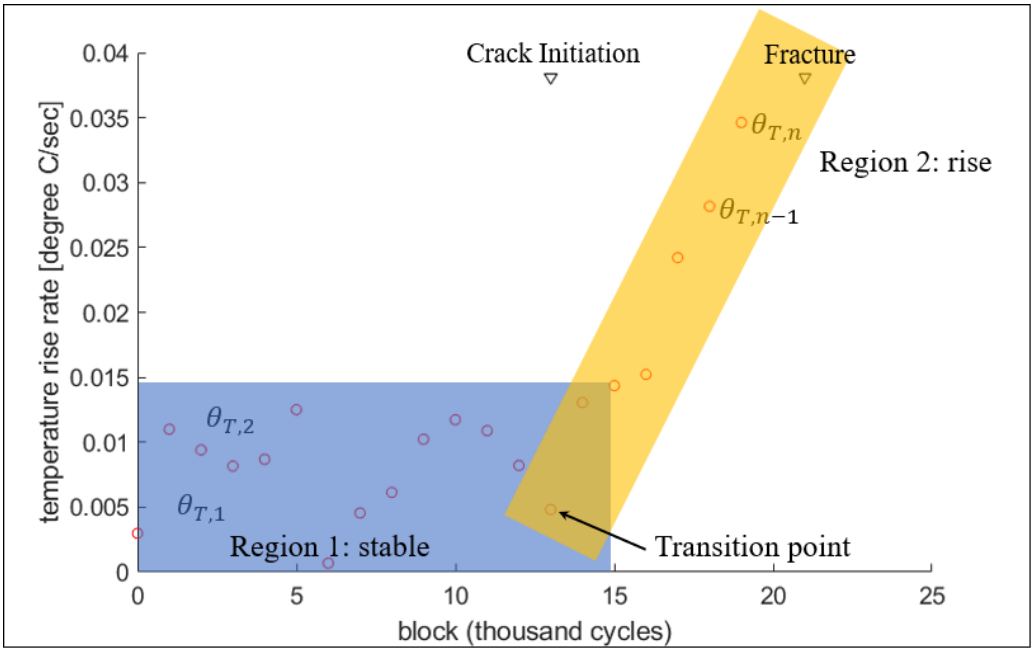

Figure 55. Illustration of two regions of temperature rise rate (θ_T) for test 8VA10. Region 1 shows stable θ_T, and Region 2 presents a substantial trend increase. The transition point may indicate the beginning of considerable fatigue damage.

The concept of dual-linear regression was used in acoustic emission and thermography analyses [96,97] during similar trend observations. In finding the appropriate block of the transition, the squared error (SE) was computed for each candidate transition point as follows:

$$SE_k = \sum_{i=1}^{k} (\hat{\theta}_{T,i}^{1} - \theta_{T,i})^2 + \sum_{i=k}^{n} (\hat{\theta}_{T,i}^{2} - \theta_{T,i})^2 \,, \tag{19}$$

where SE_k is the squared error at the k-th block, $\theta_{T,i}$ is the measured temperature rise rate at the i-th block, $\hat{\theta}_{T,i}^{p}$ is the estimated temperature rise rate at the i-th block using the regression model of the region p (p=1 or 2). The candidate transition points were considered from all the blocks except the first and the last block due to the requirement that the linear regression needs at least two data points. **Figure 56** presents the concept of the dual-linear regression process.

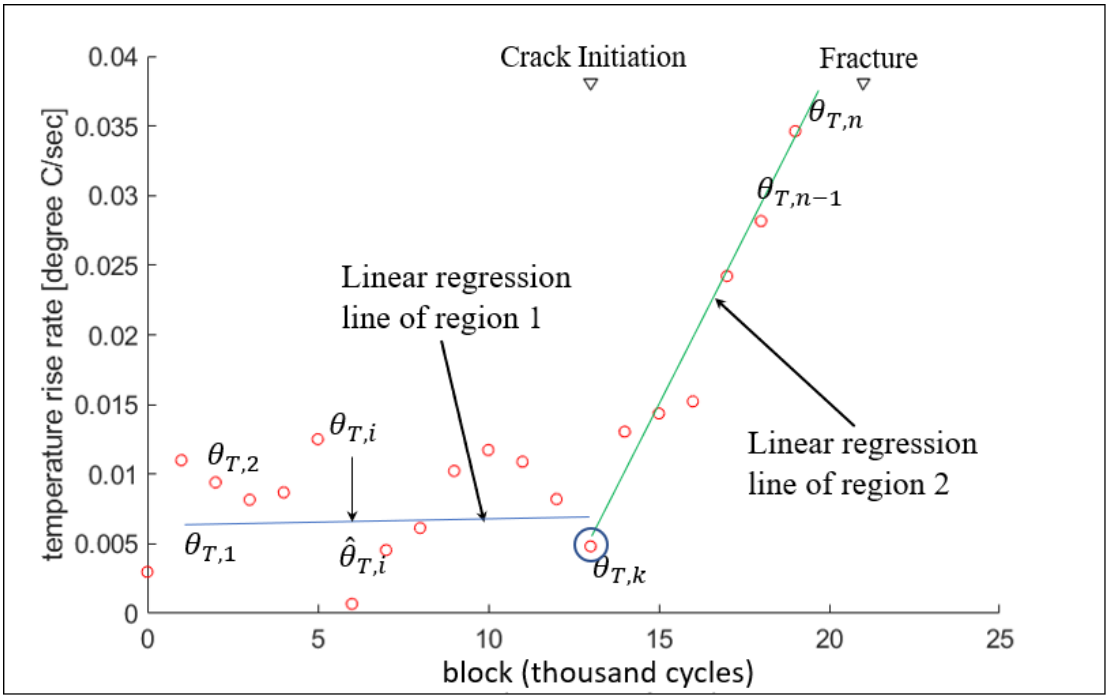

Figure 56. The process of dual-linear regression. Two linear lines were independently fitted using the least square method. Then this regression was assessed by using the squared error shown in Equation (19).

The transition point was found by minimizing the squared error (SE). As an example, **Figure 57** shows the minimum SE from both T_r and θ_T metrics in the test 8VA10. After finding the transition point for each metric, the dual-linear regression

results were compared by the test materials. In the tests of AA7075-T6, the identified transition point did not differentiate two regions, as shown in **Figure 58**. On the other hand, the transition points, in the tests of SS304L, comparably well divided two regions, as shown in **Figure 59**.

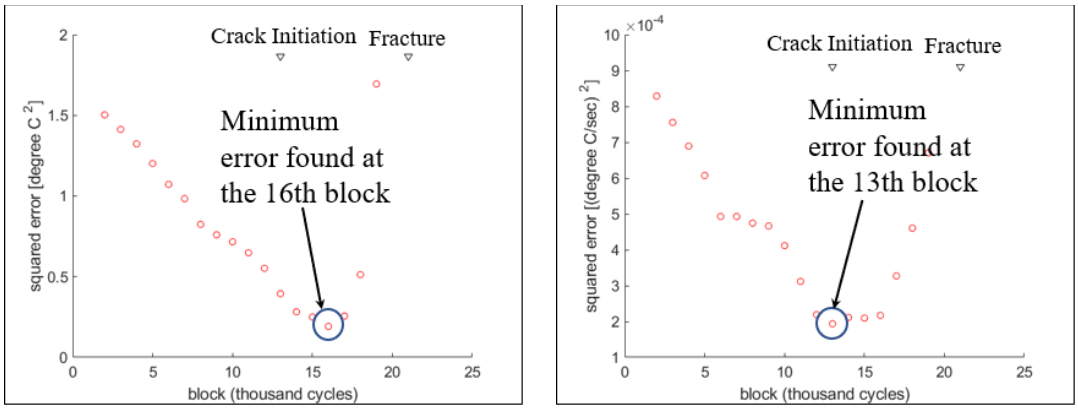

(a) (b)

Figure 57. Squared error (SE) for each candidate transition point (test 8VA10). The transition point was found at the block where the SE is minimum. SE calculated from (a) the temperature rise (T_r) and (b) the temperature rise rate (θ_T).

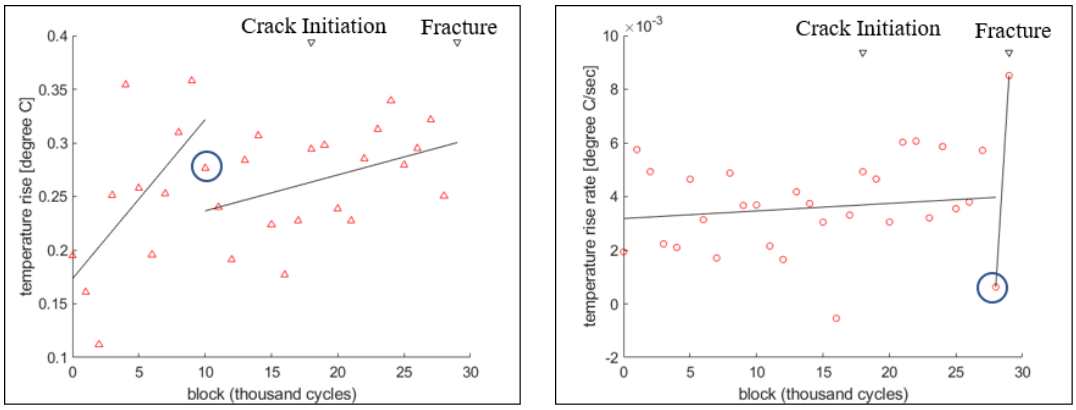

(a) (b)

Figure 58. The dual-linear regression results after finding the transition point (test 7VA21). As expected, the transition point for each temperature metric shows no particular region using (a) temperature rise (T_r) and (b) temperature rise rate (θ_T). Blue circles highlight the detected transition points identified by the minimum SE.

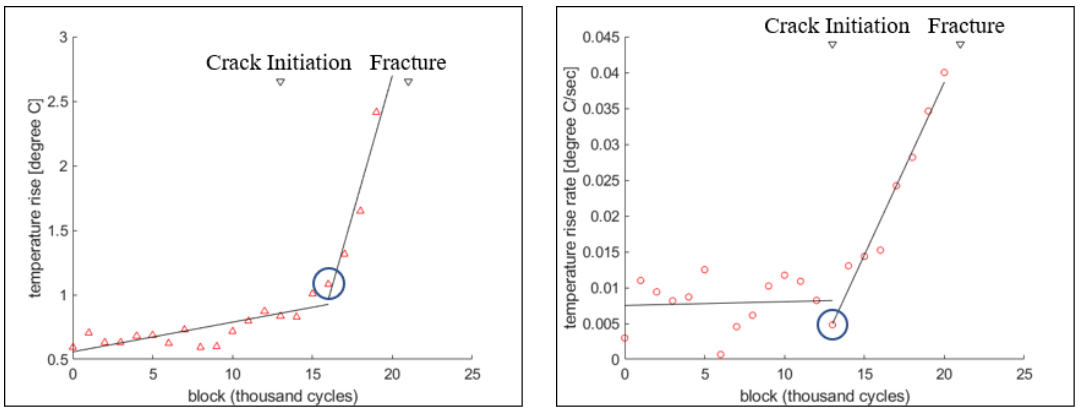

(a) (b)

Figure 59. The dual-linear regression results after finding the transition point (test 8VA10). The transition point for each temperature metric divides the two regions by (a) temperature rise (T_r) and (b) temperature rise rate (θ_T). Blue circles highlight the detected transition points.

To investigate the fatigue damage at the identified transition point, crack length for each transition point was calculated. This calculation was only possible for the SS304L tests. **Table 13** presents the crack length for each test and the corresponding temperature metrics. Majority of tests show that the transition point is related to the beginning of critical fatigue damage. Among the tests, several transition points of temperature rise rate (θ_T) were identified before crack initiation (8VA07, 14, 30, and 32), whereas some transition points were found too late (8VA42 and 48).

Crack length at the transition point, for each temperature metric, was correlated to the test conditions (i.e., stress amplitude) to investigate the effect of loading conditions, as shown in **Figure 60**. According to **Figure 60**, the transition points, from both temperature rise (T_r) and temperature rise rate (θ_T), indicate shorter crack length as the stress amplitude increases.

Table 13. The temperature metrics summary by the crack length at the transition point (tests of SS304L).

Test	Stress amplitude [MPa]	Crack length @ the transition point [mm]		Test	Stress amplitude [MPa]	Crack length @ the transition point [mm]	
		Measured in T_r	Measured in θ_T			Measured in T_r	Measured in θ_T
8VA03	872.9	0.2985	0.2985	8VA28	723.8	1.686	1.343
8VA04	861.2	0.9628	0.9628	8VA29	718.0	1.506	1.246
8VA05	858.9	0.7033	0.1162	8VA30	715.4	2.762	0
8VA06	862.1	0.9080	0.3659	8VA31	718.2	1.481	3.861
8VA07	873.3	0.4840	0	8VA32	716.8	0.341	0
8VA08	871.2	0.5677	1.6314	8VA33	644.7	1.456	0.3850
8VA09	859.1	0.6859	1.0195	8VA34	645.1	2.497	2.497
8VA10	855.1	0.8856	0.1329	8VA35	643.7	1.941	1.496
8VA11	856.1	1.163	1.7286	8VA36	647.1	2.341	3.622
8VA12	860.6	0.4549	0.2211	8VA37	643.5	2.346	3.148
8VA13	790.5	1.237	1.6244	8VA38	642.8	2.951	4.092
8VA14	786.2	1.443	0	8VA39	644.7	3.019	3.019
8VA15	787.4	1.072	0.7999	8VA40	642.0	2.823	5.048
8VA16	786.6	1.409	1.409	8VA41	646.4	2.028	2.028
8VA17	794.8	0.9090	1.424	8VA42	649.3	2.371	Fracture
8VA18	789.6	1.6806	1.681	8VA43	574.2	2.771	1.670
8VA19	786.8	1.457	1.457	8VA44	574.5	3.453	4.344
8VA20	789.5	1.124	1.483	8VA45	573.3	3.471	4.488
8VA21	789.8	1.147	1.147	8VA46	573.3	3.394	3.179
8VA22	789.8	1.068	1.768	8VA47	573.1	3.437	3.437
8VA23	719.9	2.150	2.150	8VA48	574.8	1.974	Fracture
8VA24	716.6	1.872	1.605	8VA49	572.2	2.782	3.166
8VA25	718.2	1.660	2.440	8VA50	573.8	3.285	2.981
8VA26	718.2	1.779	1.560	8VA51	573.9	3.511	1.402
8VA27	715.6	2.057	1.117	8VA52	574.2	3.678	3.678

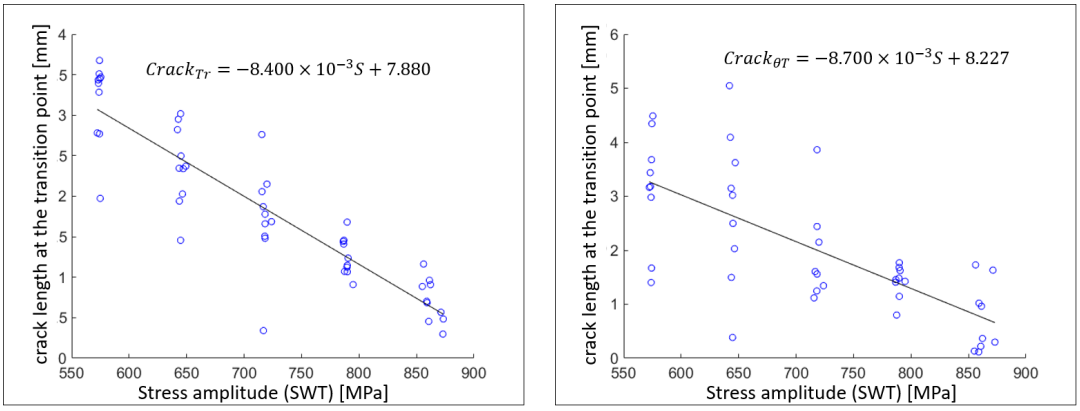

(a) (b)

Figure 60. Correlation of crack length at the transition point to the stress amplitude. Transition point found from (a) temperature rise (T_r) and (b) temperature rise rate (θ_T).

Chapter 8: Conclusion, Future Recommendation, and Publication

In this study, four entropic approaches for application to metallic material fatigue damage assessment were explored and experimentally demonstrated. Three energy dissipations resulting from mechanistic degradation phenomena-plastic mechanical strain energy, heat (temperature), and acoustic emission-were monitored in multiple uniaxial cyclic fatigue tests. Also, the concept of short-term loading process (STLP) in the context of AE was introduced and empirically demonstrated to verify that AE information entropy from STLP is an alternative method in predicting the upcoming crack initiation or fracture.

In the entropic approaches, the measured dissipations were quantified in terms of the classical thermodynamic entropy, Jeffreys divergence representing thermodynamic entropy, and AE entropies in information theorem and relative entropy. These entropic approaches were assessed along with the following findings:

- Classical thermodynamic entropy showed the endurance having a slight correlation to the cyclic stress amplitude. This entropy was shown to be an appropriate damage index.
- Jeffreys divergence in macro-scale empirically presented excellent correlation from the forward/reverse work distributions. The quantitative conversion factor (namely the pseudo-Boltzmann constant, k_{pB}) was also introduced, which showed consistency between the classical thermodynamic entropic damage and Jeffreys divergence-based entropic damage measure.

- Fatigue damage assessment using entropies of the acoustic emission waveform data, compared well with the classical thermodynamic entropy. Similarly, using statistical tests, it was shown that the AE-based information entropy of damage was consistent, compared with the two conventional AE features (i.e., count and absolute energy) used in fatigue damage assessment.
- Short-term loading process (STLP) approach provided an alternative failure prediction method by using the cumulative AE information entropy during a high-frequency/low-amplitude short term loading where no or very little damage is expected to accumulate. Partial cumulative AE information entropy collected in STLP indicated upcoming failure.
- Temperature rise (T_r) and rise rate (θ_T) provided possible alternative damage indication and can be used as precursors to crack initiation and fracture.

The findings of this dissertation provide support for innovative PHM applications, especially using the new entropic and STLP methods. To fulfill further this research, recommendations for future extensions are:

- Entropic approaches were performed for fatigue damage and proved empirically in this study. These entropic approaches need to be extended in other contexts, such as corrosion and wear failure modes, other alloys and composite materials, and more complex stress loading and environmental conditions.
- The pseudo-Boltzmann constant in JD approach will need to be generalized in the context of other alloys in fatigue and other failure mechanisms.

- In collecting and processing the AE signals, the noise reduction process is still in need of a further extension to acquire more reliable data. The suggested pre- and post-processes showed excellent results in noise elimination. Depending on the noise environment, the noise reduction strategy should be customized.
- As stated in Chapter 1 and Chapter 2, the engineering applications of this research is largely in the PHM area. From this research, multiple entropic and measurement methods were reported. Advanced data analyses techniques, such as multivariable Bayesian methods [15,101,102], can be developed in predicting RUL with less uncertainty.

The Ph.D. research achievements were documented and reported by publishing in journals and conferences. The journal papers published or under revision are listed as:

- A. Kahirdeh, C. Sauerbrunn, H. Yun, and M. Modarres, *A Parametric Approaches to Acoustic Entropy Estimation for Assessment of Fatigue Damage*, International Journal of Fatigue, 100 (2017), 2017, p. 229-237
- C. M. Sauerbrunn, A. Kahirdeh, H. Yun, and M. Modarres, *Damage Assessment Using Information Entropy of Individual Acoustic Emission Waveforms during Cyclic Fatigue Loading*, Applied Sciences, 7(6), 2017, p. 562
- H. Yun and M. Modarres, *Measures of Entropy to Characterize Fatigue Damage in Metallic Material, Entropy* (Under the second revision).

Manuscripts of two more topics (STLP fatigue damage measurement and AE noise reduction process) are also under development for the publications.

Two papers were published in conferences:

- A. Kahirdeh, H. Yun, and M. Modarres, *Degradation Entropy: An Acoustic Emission Based Approach to Structural Health Assessment*, Structural Health Monitoring 2017: Real-Time Material State Awareness and Data-Driven Safety Assurance.

- H. Yun, A. Kahirdeh, C. M. Sauerbrunn, and M. Modarres, *Entropic Approach to Measure Damage with Applications to Fatigue Failure and Structural Reliability*, Proceedings of the 2018 Annual Reliability and Maintainability Symposium (RAMS).

The research results were reported in several symposia by posters and a presentation:

- H. Yun, A. Kahirdeh, C. Sauerbrunn, and M. Modarres, *A Statistical Mechanics Approaches to Acquire Entropy Generation during the Fatigue Loading of the Material: Theory and Experiments*, International Conference on Fatigue Damage of Structural Materials XI, 18-23 September 2016, Hyannis, MA, USA (Poster section).
- A. Kahirdeh, H. Yun, C. Sauerbrunn, and M. Modarres, *Feature Extraction of the Acoustic Signals for Monitoring the Fatigue Damage of the Materials*, International Conference on Fatigue Damage of Structural Materials XI, 18-23 September 2016, Hyannis, MA, USA (Poster section).
- H. Yun and M. Modarres, *Damage Measurement with Entropic Approaches*, Engineering Mechanics Institute Conference, MIT, 2018 (Presentation section).

Appendices

A.1 Matlab scripts for data analyses

A.1.1 AE data filtering process

```
% Data filtering of AE Data
% 1. Delta T
% 2. Attenuation
% 3. Excitation and normal loading time
% 4. loading - unloading only for normal loading time
% 5. Data filter table for up to step 4

testseries='8';
t_number=3;

if t_number<10
    testnumber=strcat('0',num2str(t_number));
else
    testnumber=num2str(t_number);
end

eval(['load ',testseries,'VA00_Condition_Summary.mat p_table'])
p=p_table(t_number,1);

t_arr_max=1e-5;   % Reference time for effective maximum time inter-
val

eval(['load ',testseries,'VA',testnumber,'_paraAE.mat time_nor_AE
time_exc_AE'])

cycle_int=0.2;
k=0;
time_asc_point=zeros(1,1);
for i=1:length(time_nor_AE)-1
    k=k+1;
    time_asc_point(k,1)=time_nor_AE(i,1);
    for j=2:1000
        k=k+1;
        time_asc_point(k,1)=time_asc_point(k-1,1)+cycle_int;
    end
end
k=k+1;
time_asc_point(k,1)=time_nor_AE(end,1);
for i=2:floor(time_nor_AE(end,3)*5)
    k=k+1;
    time_asc_point(k,1)=time_asc_point(k-1,1)+cycle_int;
end
for i=1:length(time_asc_point)
    time_asc_point(i,2)=time_asc_point(i,1)+cycle_int*0.6;
end
```

```
clear i j k

for r=1:p
    if r<10
       r_ch=strcat('0',num2str(r));
    else
       r_ch=num2str(r);
    end
    eval(['load ',testseries,'VA',testnumber,'_dataAE',r_ch,'.mat
count time Abs_energy channel'])

    % Make guarentee that all data points are either of ch1 and ch2
    veri=zeros(length(count),1);
    for i=1:length(count)
        if channel(i,1)==1||2
            veri(i,1)=1;
        else
            veri(i,1)=0;
        end
    end
    dt=zeros(length(count),1);
    for i=1:length(count)
        dt(i,1)=i;
    end

    fig=figure;
    fig.Position=[100,400,800,480];
    hold on
    plot(dt,veri)
    title('Verification of Table Row with Channel')
    xlabel('Data Point')
    ylabel('1 for normal, 0 for abnormal')
    hold off

    % Allocating time and absolute energy data for ch1 and 2
    j=0; k=0;
    time_ch1_=zeros(1,1);
    Abs_energy_ch1_=zeros(1,1);
    time_ch2_=zeros(1,1);
    Abs_energy_ch2_=zeros(1,1);

    for i=1:length(count)
        if channel(i,1)==1
            j=j+1;
            time_ch1_(j,1)=time(i,1);
            Abs_energy_ch1_(j,1)=Abs_energy(i,1);
        else
            k=k+1;
            time_ch2_(k,1)=time(i,1);
            Abs_energy_ch2_(k,1)=Abs_energy(i,1);
        end
    end

    clear Abs_energy channel count dt fig time veri
```

```
    % Filtering with arrival time differece
    n1=length(time_ch1_);
    n2=length(time_ch2_);
    hit_vic=zeros(n1,2);
    Filt=zeros(n1,4);
    Filt_ID=zeros(n1,4);

    for i=1:n1
        a=find(abs(time_ch2_(:,1)-
time_ch1_(i,1))<=t_arr_max,1,'first');
        b=find(abs(time_ch2_(:,1)-
time_ch1_(i,1))<=t_arr_max,1,'last');
        if isempty(a)==1
            hit_vic(i,1)=0;
        else
            hit_vic(i,1)=a;
        end
        if isempty(b)==1
            hit_vic(i,2)=0;
        else
            hit_vic(i,2)=b;
        end
    end
    for i=1:n1
        hit_vic(i,3)=hit_vic(i,2)-hit_vic(i,1);
        a(i,1)=i;
        if hit_vic(i,1)==0
            Filt(i,1)=0;
            Filt_ID(i,1)=0;
        else
            Filt(i,1)=hit_vic(i,1);    % Effective matching data num-
ber of ch2
            Filt_ID(i,1)=1;
        end
    end
    FilterNumber(1,1)=n1;
    FilterNumber(2,1)=n2;
    FilterNumber(1,2)=sum(Filt_ID(:,1));
    FilterNumber(2,2)=sum(Filt_ID(:,1));  % First column: Before
filtering, second column: After first filtering
    clear a b
    % Filtering with energy attenuation
    ratio_E=zeros(n1,1);
    for i=1:n1
        if Filt_ID(i,1)==1
            ratio_E(i,1)=Abs_energy_ch1_(i,1)/Abs_en-
ergy_ch2_(Filt(i,1),1);
            if ratio_E(i,1)>=0.2 && ratio_E(i,1)<=5
                Filt(i,2)=Filt(i,1); Filt_ID(i,2)=1;
            else
                Filt(i,2)=0; Filt_ID(i,2)=0;
            end
        else
            Filt(i,2)=0; Filt_ID(i,2)=0;
        end
```

```
    end

    FilterNumber(1,3)=sum(Filt_ID(:,2));
    FilterNumber(2,3)=sum(Filt_ID(:,2));  % Third column: After
atenuation filtering

    % Filtering with excitation and normal loading conditon time
    cat_load=zeros(n1,2);
    Filt_ID(:,3)=zeros(n1,1);
    for i=1:n1
        if Filt_ID(i,2)==1
            for j=1:length(time_exc_AE)
                if time_ch1_(i,1)>=time_exc_AE(j,1) &&
time_ch1_(i,1)<=time_exc_AE(j,2)
                    cat_load(i,1)=j; Filt_ID(i,3)=1;  %
cat_load(:,1): excitation load and order, cat_load(:,2): normal load
and order
                end
            end
        end
    end
    for i=1:n1
        if Filt_ID(i,2)==1
            for j=1:length(time_nor_AE)
                if time_ch1_(i,1)>=time_nor_AE(j,1) &&
time_ch1_(i,1)<=time_nor_AE(j,2)
                    cat_load(i,2)=j; Filt_ID(i,3)=1;
                end
            end
        end
    end
    Filt(:,3)=zeros(n1,1);
    for i=1:n1
        if Filt_ID(i,3)==1
            Filt(i,3)=Filt(i,2);
        end
    end
    FilterNumber(1,4)=sum(Filt_ID(:,3));
    FilterNumber(2,4)=sum(Filt_ID(:,3));  % Fourth column: After ex-
citation / normal loading categorization

    % Filtering with loading / unloading conditon time (normal load-
ing)
    % dividing time slot with 1,000 cycle
    Filt_ID(:,4)=zeros(n1,1);
    Filt(:,4)=zeros(n1,1);

    for i=1:n1
        if cat_load(i,1)~=0
            Filt_ID(i,4)=1;
            Filt(i,4)=Filt(i,3);
        end
    end

    for i=1:n1
```

```
        if cat_load(i,2)~=0
            for j=1:length(time_asc_point)
                if time_ch1_(i,1)>=time_asc_point(j,1) &&
time_ch1_(i,1)<=time_asc_point(j,2)
                    Filt_ID(i,4)=1;
                    Filt(i,4)=Filt(i,3);
                    cat_load(i,3)=cat_load(i,2);   % cat_load(:,3):
loading / unloading filter with
                end
            end
        end
    end

    FilterNumber(1,5)=sum(Filt_ID(:,4));
    FilterNumber(2,5)=sum(Filt_ID(:,4));  % 5th column: After load-
ing / unloading categorization (in normal loading)

    eval(['save ',testseries,'VA',testnumber,'_dataAE',r_ch,'.mat
FilterNumber cat_load Filt Filt_ID -append'])

    clear FilterNumber Filt Filt_ID
    clear Abs_energy_ch1_ Abs_energy_ch2_ cat_load cycle_int hit_vic
i j k n1 n2 ratio_E time_ch1_ time_ch2_

end
```

A.1.2 Forward/reverse work (strain energy) calculation

```
% Loading files and renaming variables
testseries='8';
t_number=3;

if t_number<10
    testnumber=strcat('0',num2str(t_number));
else
    testnumber=num2str(t_number);
end

eval(['load ',testseries,'VA',testnumber,'_data.mat'])

% Identifying initial critical point of first cycle
figure
hold on
plot(time,load,'b')
title('Load vs Time')
xlabel('time [sec]')
ylabel('load [kN]')
hold off

% 1. Defining critical points for each cycle (normal loading)
% Converting initial / final time to data order number
num_nor_Ins=zeros(length(time_nor_Ins),1);
```

```
for i=1:length(time_nor_Ins)
    num_nor_Ins(i,1)=find(time==time_nor_Ins(i,1),1,'first');
    num_nor_Ins(i,2)=find(time==time_nor_Ins(i,2),1,'first');
end

% Finding out critical points shifting hysteresis loop direction
l_inc=zeros(length(load)-1,1);
for i=2:length(load)
    l_inc(i,1)=load(i,1)-load(i-1,1);
end

K=zeros(1,length(num_nor_Ins));
K_inc=zeros(1,1);
sign=zeros(1,1);
for i=1:length(num_nor_Ins)
    K(1,i)=num_nor_Ins(i,1);
    k=1;
    for j=num_nor_Ins(i,1):num_nor_Ins(i,2)-1  % Finding critical
points
        if l_inc(j+1,1)*l_inc(j,1)<0
            k=k+1;
            K(k,i)=j;
        end
    end
    k=k+1; K(k,i)=num_nor_Ins(i,2);
    for j=1:k-1
        K_inc(j,i)=K(j+1,i)-K(j,i);
    end
    for j=1:k-1           % Identifying critical points' direction
        if l_inc(K(j,i)+1,1)>0
            sign(j,i)=1;
        elseif l_inc(K(j,i)+1,1)<0
            sign(j,i)=-1;
        else
            sign(j,i)=0;
        end
    end
end

sign_very=zeros(1,1);
for j=1:length(sign)
    if any(sign(j,1:length(num_nor_Ins))==0)==1  % Verifying that
all critical points are valid
        if all(sign(j,1:length(num_nor_Ins)-1)==sign(j,1))==1
            sign_very(j,1)=1;
        else
            sign_very(j,1)=0;
        end
    elseif all(sign(j,1:length(num_nor_Ins)-1)==sign(j,1))==1
        sign_very(j,1)=1;
    else
        sign_very(j,1)=0;
    end
end
```

```
figure
hold on
plot(sign_very)
xlabel('loop number')
ylabel('1: okay, 0: needs correction')
hold off

%% If needs correction, manual adjustment is required

% Checking once again
for i=1:length(num_nor_Ins)
    m=find(K(:,i)~=0,1,'last');
    for j=1:m-1
        K_inc(j,i)=K(j+1,i)-K(j,i);
    end
end
for i=1:length(num_nor_Ins)
    for j=1:length(K)-1           % Identifying critical points' di-
rection
        if l_inc(K(j,i)+1,1)>0
            sign(j,i)=1;
        elseif l_inc(K(j,i)+1,1)<0
            sign(j,i)=-1;
        else
            sign(j,i)=0;
        end
    end
end
for j=1:length(sign)
    if any(sign(j,1:length(num_nor_Ins))==0)==1  % Verifying that
all critical points are valid
        if all(sign(j,1:length(num_nor_Ins)-1)==sign(j,1))==1
            sign_very(j,1)=1;
        else
            sign_very(j,1)=0;
        end
    elseif all(sign(j,1:length(num_nor_Ins)-1)==sign(j,1))==1
        sign_very(j,1)=1;
    else
        sign_very(j,1)=0;
    end
end

figure
hold on
plot(sign_very)
xlabel('critical point number')
ylabel('1: okay, 0: needs correction')
hold off

%% Verified all clear
%2. Calculating forward(+) or reverse(-) work by extension
SE=zeros(1,1);
for i=1:length(num_nor_Ins)
    m=find(K(:,i)~=0,1,'last');
```

```
    for j=1:m-1 % Work calculation based on extension
        SE(j,i)=(extension(K(j,i)+1,1)-exten-
sion(K(j,i),1))*load(K(j,i),1);
        for k=K(j,i)+1:K(j+1,i)-1
            SE(j,i)=SE(j,i)+load(k,1)*(extension(k+1,1)-extension(k-
1,1))/2;
        end
        SE(j,i)=SE(j,i)+load(K(j+1,i),1)*(extension(K(j+1,i),1)-ex-
tension(K(j+1,i)-1,1));
    end
end

%3. Allocating acquired values in forward / reverse work
p=0; q=0;
SE_F=zeros(length(SE)/2,length(time_nor_Ins));
K_F=zeros(length(SE)/2,length(time_nor_Ins));
SE_R=zeros(length(SE)/2,length(time_nor_Ins));
K_R=zeros(length(SE)/2,length(time_nor_Ins));
Error_alo=zeros(length(SE),1);
for i=1:length(SE)
    if i/2-floor(i/2)==0.5
        p=p+1;
        SE_F(p,:)=SE(i,:);
        K_F(p,:)=K(i,:);
        if all(SE(i,:)>=0)~=1
           disp('Something wrong with strain energy arrangement(+)')
           Error_alo(i,1)=1;
        end
    elseif i/2-floor(i/2)==0
        q=q+1;
        SE_R(q,:)=SE(i,:);
        K_R(q,:)=K(i,:);
        if all(SE(i,:)<=0)~=1
           disp('Something wrong with strain energy arrangement(-)')
           Error_alo(i,1)=1;
        end
    end
end
SE_P=SE_F+SE_R;

%4. Stiffness (or elastic modulus) analysis for each cycle
stiff=zeros(length(SE_P),length(time_nor_Ins));
for i=1:length(num_nor_Ins)
    m=find(K_R(:,i)~=0,1,'last');
    for j=1:m
        a=polyfit(extension(K_R(j,i)-3:K_R(j,i)),load(K_R(j,i)-
3:K_R(j,i)),1);
        stiff(j,i)=a(1,1);
    end
end

%5. Numbering in normal loading in cycle
k=0;
cyc_num=zeros(1,1);
for i=1:length(num_nor_Ins)
    m=find(K_R(:,i)~=0,1,'last');
```

```
    for j=1:m
        k=k+1;
        cyc_num(j,i)=k;
    end
end

% Cumulative strain energies
SE_F_cum_piv=0;
SE_R_cum_piv=0;
SE_P_cum_piv=0;
SE_F_cum=zeros(length(SE_P),length(time_nor_Ins));
SE_R_cum=zeros(length(SE_P),length(time_nor_Ins));
SE_P_cum=zeros(length(SE_P),length(time_nor_Ins));
for i=1:length(num_nor_Ins)
    m=find(SE_P(:,i)~=0,1,'last');
    SE_F_cum(1,i)=SE_F_cum_piv+SE_F(1,i);
    SE_R_cum(1,i)=SE_R_cum_piv+SE_R(1,i);
    SE_P_cum(1,i)=SE_P_cum_piv+SE_P(1,i);
    for j=2:m
        SE_F_cum(j,i)=SE_F(j,i)+SE_F_cum(j-1,i);
        SE_R_cum(j,i)=SE_R(j,i)+SE_R_cum(j-1,i);
        SE_P_cum(j,i)=SE_P(j,i)+SE_P_cum(j-1,i);
    end
    SE_F_cum_piv=SE_F_cum(m,i);
    SE_R_cum_piv=SE_R_cum(m,i);
    SE_P_cum_piv=SE_P_cum(m,i);
end

%6. time for each cycle
time_cri=zeros(length(SE_P),length(time_nor_Ins));
for i=1:length(num_nor_Ins)
    m=find(K_R(:,i)~=0,1,'last');
    for j=1:m
        time_cri(j,i)=time(K_R(j,i));
    end
end

figure
hold on
for i=1:length(num_nor_Ins)
    m=find(K_R(:,i)~=0,1,'last');
    scatter(cyc_num(1:m,i),stiff(1:m,i),'b.')
end
xlabel('cycle number')
ylabel('stiffness [MN/m]')
title('Stiffness for Each Cycle')
hold off

%%
eval(['save ',testseries,'VA',testnumber,'_SE_in_Extension.mat
cyc_num K_F K_R SE_F SE_R SE_P SE_F_cum SE_R_cum SE_P_cum stiff
time_cri'])

eval(['load ',testseries,'VA',testnumber,'_data.mat t W'])
```

```
eval(['load ',testseries,'VA00_Condition_Summary.mat exten-
sion_base'])
eval(['load ',testseries,'VA',testnumber,'_crack.mat DK N_life
Walker Para_W'])
t=mean(t); W=mean(W);

% Conversion from extensometer measurement

eval(['load ',testseries,'VA',testnumber,'_SE_in_Extension.mat SE_F
SE_F_cum SE_P SE_P_cum SE_R SE_R_cum stiff'])
a=2.5; r=0.4; the=pi/3; GL=25+extension_base(t_number,1); d=1.7651;

m=size(SE_P);
nz=find(SE_P(:,m(1,2))~=0,1,'last');

W_a_nz=zeros(m(1,1)*(m(1,2)-1)+nz,1);
for i=1:floor(Para_W(4,end))
    W_a_nz(i,1)=W-d;
end
for i=floor(Para_W(4,end))+1:length(W_a_nz)
    p=find(Walker(:,3)<=i,1,'last');
    ch_p=isempty(p);
    if ch_p==1
        p=1;
    end
    if p<length(Walker)
        N1=Walker(p,3); N2=Walker(p+1,3);
        a1=DK(p,2); a2=DK(p+1,2);
        a_i=(a2-a1)/(N2-N1)*(i-N1)+a1;
        W_a_nz(i,1)=W-a_i;
    else
        W_a_nz(i,1)=W_a_nz(i-1,1);
    end
end

W_a=zeros(m);
for i=1:m(1,2)-1
    W_a(:,i)=W_a_nz(1+m(1,1)*(i-1):m(1,1)*i,1);
end
W_a(1:length(W_a_nz)-m(1,1)*(m(1,2)-
1),m(1,2))=W_a_nz(1+m(1,1)*(m(1,2)-1):end,1);
A=W_a.*t;

SED_F=SE_F./A./GL.*1000; SED_F_cum=SE_F_cum./A./GL.*1000;
SED_P=SE_P./A./GL.*1000; SED_P_cum=SE_P_cum./A./GL.*1000; %MJ/m^3
SED_R=SE_R./A./GL.*1000; SED_R_cum=SE_R_cum./A./GL.*1000;
E=stiff.*GL./A; % GPa

eval(['save ',testseries,'VA',testnumber,'_SE_in_Extension.mat SED_F
SED_F_cum SED_P SED_P_cum SED_R SED_R_cum E W_a -append'])
```

A.1.3 Thermodynamic entropy calculation

```
% Loading files and renaming variables
testseries='8';
t_number=52;

if t_number<10
    testnumber=strcat('0',num2str(t_number));
else
    testnumber=num2str(t_number);
end

eval(['load ',testseries,'VA',testnumber,'_SE_in_Extension.mat SED_P
SED_P_cum'])
eval(['load ',testseries,'VA',testnumber,'_Tem.mat T_SE cyc'])

TE=SED_P./T_SE;
TE_cum=SED_P_cum./T_SE;
TE(isnan(TE))=0;
TE_cum(isnan(TE_cum))=0;

eval(['save ',testseries,'VA',testnumber,'_SE_in_Extension.mat TE
TE_cum -append'])

clear TE TE_cum SED_P SED_P_cum

eval(['load ',testseries,'VA',testnumber,'_SE_in_Position.mat SED_P
SED_P_cum'])

TE=SED_P./T_SE;
TE_cum=SED_P_cum./T_SE;
TE(isnan(TE))=0;
TE_cum(isnan(TE_cum))=0;

eval(['save ',testseries,'VA',testnumber,'_SE_in_Position.mat TE
TE_cum -append'])
```

A.1.4 Jeffreys divergence calculation

```
%% Data arrangement table for SE_F, SE_R
% In this mode, the number of data group is not determined in con-
stant but
% by the minimum life of the test group
testseries='8';
tn_ini=3;
tn_fin=12;
if tn_ini<10
    tn_ini_ch=strcat('0',num2str(tn_ini));
else
    tn_ini_ch=num2str(tn_ini);
```

```
end
if tn_fin<10
    tn_fin_ch=strcat('0',num2str(tn_fin));
else
    tn_fin_ch=num2str(tn_fin);
end

eval(['load ',testseries,'VA00_crack_growth_summary.mat
N_life_W_sum'])
eval(['load ',testseries,'VA00_Condition_Summary.mat Sa_SWT'])
Sa=mean(Sa_SWT(tn_ini:tn_fin));

SED_R_G=zeros(1,tn_fin-tn_ini+1);
SED_F_G=zeros(1,tn_fin-tn_ini+1);
TE_G=zeros(1,tn_fin-tn_ini+1);

for i=1:tn_fin-tn_ini+1
    r=tn_ini+i-1;
    if r<10
        testnumber=strcat('0',num2str(r));
    else
        testnumber=num2str(r);
    end
    eval(['load ',testseries,'VA',testnumber,'_SE_in_Extension.mat
SED_R SED_F TE'])
    m=size(SED_R); n=m(1,2); m=m(1,1);
    SED_R_G(1:m,i)=SED_R(:,1);
    SED_F_G(1:m,i)=SED_F(:,1);
    TE_G(1:m,i)=TE(:,1);
    k=m;
    for j=2:n
        k=k+m;
        SED_R_G(k-m+1:k,i)=SED_R(:,j);
        SED_F_G(k-m+1:k,i)=SED_F(:,j);
        TE_G(k-m+1:k,i)=TE(:,j);
    end
    clear TE SED_F SED_R
end

%% 1. Calculating relative entropy with up to the initiation, 250,
500, 1000, transition, fracture points
% Creating matching table with same dimension
N_life_W_sum=round(N_life_W_sum,0);
num_max=zeros(6,tn_fin-tn_ini+1);
for i=1:tn_fin-tn_ini+1
    num_max(1,i)=N_life_W_sum(i+tn_ini-1,1); % at the initiation
    num_max(2,i)=N_life_W_sum(i+tn_ini-1,2); % at 250 um
    num_max(3,i)=N_life_W_sum(i+tn_ini-1,3); % at 500 um
    num_max(4,i)=N_life_W_sum(i+tn_ini-1,4); % at 1000 um
    num_max(5,i)=N_life_W_sum(i+tn_ini-1,6); % at transition
    num_max(6,i)=N_life_W_sum(i+tn_ini-1,5); % at fracture
end

% Correcting num_max at fracture
SED_F_G(isnan(SED_F_G))=0;
```

```
for i=1:tn_fin-tn_ini+1
    if find(SED_F_G(:,i)~=0,1,'last')<num_max(6,i)
        num_max(6,i)=find(SED_F_G(:,i)~=0,1,'last');
    end
end

% Decided to compose d datapoint matching
d=zeros(6,2);
d(1,1)=min(num_max(1,:));
d(1,2)=find(num_max(1,:)==d(1,1),1,'first');
d(2,1)=min(num_max(2,:));
d(2,2)=find(num_max(2,:)==d(2,1),1,'first');
d(3,1)=min(num_max(3,:));
d(3,2)=find(num_max(3,:)==d(3,1),1,'first');
d(4,1)=min(num_max(4,:));
d(4,2)=find(num_max(4,:)==d(4,1),1,'first');
d(5,1)=min(num_max(5,:));
d(5,2)=find(num_max(5,:)==d(5,1),1,'first');
d(6,1)=min(num_max(6,:));
d(6,2)=find(num_max(6,:)==d(6,1),1,'first');

SED_R_GR_ini=zeros(d(1,1),tn_fin-tn_ini+1);
SED_F_GR_ini=zeros(d(1,1),tn_fin-tn_ini+1);
TE_GR_ini=zeros(d(1,1),tn_fin-tn_ini+1);
SED_R_GR_250=zeros(d(2,1),tn_fin-tn_ini+1);
SED_F_GR_250=zeros(d(2,1),tn_fin-tn_ini+1);
TE_GR_250=zeros(d(2,1),tn_fin-tn_ini+1);
SED_R_GR_500=zeros(d(3,1),tn_fin-tn_ini+1);
SED_F_GR_500=zeros(d(3,1),tn_fin-tn_ini+1);
TE_GR_500=zeros(d(3,1),tn_fin-tn_ini+1);
SED_R_GR_1000=zeros(d(4,1),tn_fin-tn_ini+1);
SED_F_GR_1000=zeros(d(4,1),tn_fin-tn_ini+1);
TE_GR_1000=zeros(d(4,1),tn_fin-tn_ini+1);
SED_R_GR_tra=zeros(d(5,1),tn_fin-tn_ini+1);
SED_F_GR_tra=zeros(d(5,1),tn_fin-tn_ini+1);
TE_GR_tra=zeros(d(5,1),tn_fin-tn_ini+1);
SED_R_GR_fra=zeros(d(6,1),tn_fin-tn_ini+1);
SED_F_GR_fra=zeros(d(6,1),tn_fin-tn_ini+1);
TE_GR_fra=zeros(d(6,1),tn_fin-tn_ini+1);

for i=1:tn_fin-tn_ini+1
    for j=1:d(1,1)
        a=round(num_max(1,i)*j/d(1,1),0);
        if a-1000*floor(a/1000)==0
            a=a-3;
        elseif a-1000*floor(a/1000)==999
            a=a-3;
        elseif a-1000*floor(a/1000)==998
            a=a-3;
        elseif a-1000*floor(a/1000)==1
            a=a+4;
        elseif a-1000*floor(a/1000)==2
            a=a+4;
        elseif a-1000*floor(a/1000)==3
            a=a+4;
        end
```

```
    SED_R_GR_ini(j,i)=SED_R_G(a,i);
    SED_F_GR_ini(j,i)=SED_F_G(a,i);
    TE_GR_ini(j,i)=TE_G(a,i);
end

for j=1:d(2,1)
    a=round(num_max(2,i)*j/d(2,1),0);
    if a-1000*floor(a/1000)==0
        a=a-3;
    elseif a-1000*floor(a/1000)==999
        a=a-3;
    elseif a-1000*floor(a/1000)==998
        a=a-3;
    elseif a-1000*floor(a/1000)==1
        a=a+4;
    elseif a-1000*floor(a/1000)==2
        a=a+4;
    elseif a-1000*floor(a/1000)==3
        a=a+4;
    end
    SED_R_GR_250(j,i)=SED_R_G(a,i);
    SED_F_GR_250(j,i)=SED_F_G(a,i);
    TE_GR_250(j,i)=TE_G(a,i);
end

for j=1:d(3,1)
    a=round(num_max(3,i)*j/d(3,1),0);
    if a-1000*floor(a/1000)==0
        a=a-3;
    elseif a-1000*floor(a/1000)==999
        a=a-3;
    elseif a-1000*floor(a/1000)==998
        a=a-3;
    elseif a-1000*floor(a/1000)==1
        a=a+4;
    elseif a-1000*floor(a/1000)==2
        a=a+4;
    elseif a-1000*floor(a/1000)==3
        a=a+4;
    end
    SED_R_GR_500(j,i)=SED_R_G(a,i);
    SED_F_GR_500(j,i)=SED_F_G(a,i);
    TE_GR_500(j,i)=TE_G(a,i);
end

for j=1:d(4,1)
    a=round(num_max(4,i)*j/d(4,1),0);
    if a-1000*floor(a/1000)==0
        a=a-3;
    elseif a-1000*floor(a/1000)==999
        a=a-3;
    elseif a-1000*floor(a/1000)==998
        a=a-3;
    elseif a-1000*floor(a/1000)==1
        a=a+4;
    elseif a-1000*floor(a/1000)==2
```

```
            a=a+4;
        elseif a-1000*floor(a/1000)==3
            a=a+4;
        end
        SED_R_GR_1000(j,i)=SED_R_G(a,i);
        SED_F_GR_1000(j,i)=SED_F_G(a,i);
        TE_GR_1000(j,i)=TE_G(a,i);
    end

    for j=1:d(5,1)
        a=round(num_max(5,i)*j/d(5,1),0);
        if a-1000*floor(a/1000)==0
            a=a-3;
        elseif a-1000*floor(a/1000)==999
            a=a-3;
        elseif a-1000*floor(a/1000)==998
            a=a-3;
        elseif a-1000*floor(a/1000)==1
            a=a+4;
        elseif a-1000*floor(a/1000)==2
            a=a+4;
        elseif a-1000*floor(a/1000)==3
            a=a+4;
        end
        SED_R_GR_tra(j,i)=SED_R_G(a,i);
        SED_F_GR_tra(j,i)=SED_F_G(a,i);
        TE_GR_tra(j,i)=TE_G(a,i);
    end

    for j=1:d(6,1)
        a=round(num_max(6,i)*j/d(6,1),0);
        if a-1000*floor(a/1000)==0
            a=a-3;
        elseif a-1000*floor(a/1000)==999
            a=a-3;
        elseif a-1000*floor(a/1000)==998
            a=a-3;
        elseif a-1000*floor(a/1000)==1
            a=a+4;
        elseif a-1000*floor(a/1000)==2
            a=a+4;
        elseif a-1000*floor(a/1000)==3
            a=a+4;
        end
        SED_R_GR_fra(j,i)=SED_R_G(a,i);
        SED_F_GR_fra(j,i)=SED_F_G(a,i);
        TE_GR_fra(j,i)=TE_G(a,i);
    end
end

SED_R_GR_ini=-1*SED_R_GR_ini; % Making up -W for following Crooks'
relation
SED_R_GR_250=-1*SED_R_GR_250;
SED_R_GR_500=-1*SED_R_GR_500;
SED_R_GR_1000=-1*SED_R_GR_1000;
SED_R_GR_tra=-1*SED_R_GR_tra;
```

```
SED_R_GR_fra=-1*SED_R_GR_fra;

% make the distribution with fitting in normal distribution
para_SE_R_ini=zeros(d(1,1),2);
para_SE_F_ini=zeros(d(1,1),2);
para_SE_R_250=zeros(d(2,1),2);
para_SE_F_250=zeros(d(2,1),2);
para_SE_R_500=zeros(d(3,1),2);
para_SE_F_500=zeros(d(3,1),2);
para_SE_R_1000=zeros(d(4,1),2);
para_SE_F_1000=zeros(d(4,1),2);
para_SE_R_tra=zeros(d(5,1),2);
para_SE_F_tra=zeros(d(5,1),2);
para_SE_R_fra=zeros(d(6,1),2);
para_SE_F_fra=zeros(d(6,1),2);

for i=1:d(1,1)
    para_SE_R_ini(i,1:2)=mle(SED_R_GR_ini(i,1:tn_fin-tn_ini+1),'dis-
tribution','norm');
    para_SE_F_ini(i,1:2)=mle(SED_F_GR_ini(i,1:tn_fin-tn_ini+1),'dis-
tribution','norm');
    dist_R_ini(i,1)=makedist('Norm','mu',para_SE_R_ini(i,1),'sig-
ma',para_SE_R_ini(i,2));
    dist_F_ini(i,1)=makedist('Norm','mu',para_SE_F_ini(i,1),'sig-
ma',para_SE_F_ini(i,2));
end
for i=1:d(2,1)
    para_SE_R_250(i,1:2)=mle(SED_R_GR_250(i,1:tn_fin-tn_ini+1),'dis-
tribution','norm');
    para_SE_F_250(i,1:2)=mle(SED_F_GR_250(i,1:tn_fin-tn_ini+1),'dis-
tribution','norm');
    dist_R_250(i,1)=makedist('Norm','mu',para_SE_R_250(i,1),'sig-
ma',para_SE_R_250(i,2));
    dist_F_250(i,1)=makedist('Norm','mu',para_SE_F_250(i,1),'sig-
ma',para_SE_F_250(i,2));
end
for i=1:d(3,1)
    para_SE_R_500(i,1:2)=mle(SED_R_GR_500(i,1:tn_fin-tn_ini+1),'dis-
tribution','norm');
    para_SE_F_500(i,1:2)=mle(SED_F_GR_500(i,1:tn_fin-tn_ini+1),'dis-
tribution','norm');
    dist_R_500(i,1)=makedist('Norm','mu',para_SE_R_500(i,1),'sig-
ma',para_SE_R_500(i,2));
    dist_F_500(i,1)=makedist('Norm','mu',para_SE_F_500(i,1),'sig-
ma',para_SE_F_500(i,2));
end
for i=1:d(4,1)
    para_SE_R_1000(i,1:2)=mle(SED_R_GR_1000(i,1:tn_fin-
tn_ini+1),'distribution','norm');
    para_SE_F_1000(i,1:2)=mle(SED_F_GR_1000(i,1:tn_fin-
tn_ini+1),'distribution','norm');
    dist_R_1000(i,1)=makedist('Norm','mu',para_SE_R_1000(i,1),'sig-
ma',para_SE_R_1000(i,2));
    dist_F_1000(i,1)=makedist('Norm','mu',para_SE_F_1000(i,1),'sig-
ma',para_SE_F_1000(i,2));
end
```

```
for i=1:d(5,1)
    para_SE_R_tra(i,1:2)=mle(SED_R_GR_tra(i,1:tn_fin-tn_ini+1),'dis-
tribution','norm');
    para_SE_F_tra(i,1:2)=mle(SED_F_GR_tra(i,1:tn_fin-tn_ini+1),'dis-
tribution','norm');
    dist_R_tra(i,1)=makedist('Norm','mu',para_SE_R_tra(i,1),'sig-
ma',para_SE_R_tra(i,2));
    dist_F_tra(i,1)=makedist('Norm','mu',para_SE_F_tra(i,1),'sig-
ma',para_SE_F_tra(i,2));
end
for i=1:d(6,1)
    para_SE_R_fra(i,1:2)=mle(SED_R_GR_fra(i,1:tn_fin-tn_ini+1),'dis-
tribution','norm');
    para_SE_F_fra(i,1:2)=mle(SED_F_GR_fra(i,1:tn_fin-tn_ini+1),'dis-
tribution','norm');
    dist_R_fra(i,1)=makedist('Norm','mu',para_SE_R_fra(i,1),'sig-
ma',para_SE_R_fra(i,2));
    dist_F_fra(i,1)=makedist('Norm','mu',para_SE_F_fra(i,1),'sig-
ma',para_SE_F_fra(i,2));
end

lr_1=zeros(d(1,1),1);
for i=1:d(1,1)
    lr_1(i,1)=100/d(1,1)*i;
end
lr_2=zeros(d(2,1),1);
for i=1:d(2,1)
    lr_2(i,1)=100/d(2,1)*i;
end
lr_3=zeros(d(3,1),1);
for i=1:d(3,1)
    lr_3(i,1)=100/d(3,1)*i;
end
lr_4=zeros(d(4,1),1);
for i=1:d(4,1)
    lr_4(i,1)=100/d(4,1)*i;
end
lr_5=zeros(d(5,1),1);
for i=1:d(5,1)
    lr_5(i,1)=100/d(5,1)*i;
end
lr_6=zeros(d(6,1),1);
for i=1:d(6,1)
    lr_6(i,1)=100/d(6,1)*i;
end

D_ini=zeros(d(1,1),5);
D_250=zeros(d(2,1),5);
D_500=zeros(d(3,1),5);
D_1000=zeros(d(4,1),5);
D_tra=zeros(d(5,1),5);
D_fra=zeros(d(6,1),5);

for i=1:d(1,1)
    D_ini(i,1)=min(SED_R_GR_ini(i,:));      % minimum from reverse
work
```

```
    D_ini(i,2)=max(SED_F_GR_ini(i,:));     % maximum from forware
work
    D_ini(i,3)=D_ini(i,2)-D_ini(i,1);       % distance from minimum
to maximum
    D_ini(i,4)=D_ini(i,1)-0.2*D_ini(i,3);   % 20% margin extension
from minimum
    D_ini(i,5)=D_ini(i,2)+0.2*D_ini(i,3);   % 20% margin extension
from maximum
end
for i=1:d(2,1)
    D_250(i,1)=min(SED_R_GR_250(i,:));     % minimum from reverse
work
    D_250(i,2)=max(SED_F_GR_250(i,:));     % maximum from forware
work
    D_250(i,3)=D_250(i,2)-D_250(i,1);       % distance from minimum
to maximum
    D_250(i,4)=D_250(i,1)-0.2*D_250(i,3);   % 20% margin extension
from minimum
    D_250(i,5)=D_250(i,2)+0.2*D_250(i,3);   % 20% margin extension
from maximum
end
for i=1:d(3,1)
    D_500(i,1)=min(SED_R_GR_500(i,:));     % minimum from reverse
work
    D_500(i,2)=max(SED_F_GR_500(i,:));     % maximum from forware
work
    D_500(i,3)=D_500(i,2)-D_500(i,1);       % distance from minimum
to maximum
    D_500(i,4)=D_500(i,1)-0.2*D_500(i,3);   % 20% margin extension
from minimum
    D_500(i,5)=D_500(i,2)+0.2*D_500(i,3);   % 20% margin extension
from maximum
end
for i=1:d(4,1)
    D_1000(i,1)=min(SED_R_GR_1000(i,:));     % minimum from reverse
work
    D_1000(i,2)=max(SED_F_GR_1000(i,:));     % maximum from forware
work
    D_1000(i,3)=D_1000(i,2)-D_1000(i,1);       % distance from mini-
mum to maximum
    D_1000(i,4)=D_1000(i,1)-0.2*D_1000(i,3);   % 20% margin exten-
sion from minimum
    D_1000(i,5)=D_1000(i,2)+0.2*D_1000(i,3);   % 20% margin exten-
sion from maximum
end
for i=1:d(5,1)
    D_tra(i,1)=min(SED_R_GR_tra(i,:));     % minimum from reverse
work
    D_tra(i,2)=max(SED_F_GR_tra(i,:));     % maximum from forware
work
    D_tra(i,3)=D_tra(i,2)-D_tra(i,1);       % distance from minimum
to maximum
    D_tra(i,4)=D_tra(i,1)-0.2*D_tra(i,3);   % 20% margin extension
from minimum
    D_tra(i,5)=D_tra(i,2)+0.2*D_tra(i,3);   % 20% margin extension
from maximum
```

```
end
for i=1:d(6,1)
    D_fra(i,1)=min(SED_R_GR_fra(i,:));     % minimum from reverse
work
    D_fra(i,2)=max(SED_F_GR_fra(i,:));     % maximum from forware
work
    D_fra(i,3)=D_fra(i,2)-D_fra(i,1);       % distance from minimum
to maximum
    D_fra(i,4)=D_fra(i,1)-0.2*D_fra(i,3);   % 20% margin extension
from minimum
    D_fra(i,5)=D_fra(i,2)+0.2*D_fra(i,3);   % 20% margin extension
from maximum
end

entropy_RE_F_1=zeros(d(1,1),2); % method with initiation point
entropy_RE_R_1=zeros(d(1,1),2);
entropy_RE_J_1=zeros(d(1,1),2);
entropy_RE_F_2=zeros(d(2,1),2); % method with 250 point
entropy_RE_R_2=zeros(d(2,1),2);
entropy_RE_J_2=zeros(d(2,1),2);
entropy_RE_F_3=zeros(d(3,1),2); % method with 500 point
entropy_RE_R_3=zeros(d(3,1),2);
entropy_RE_J_3=zeros(d(3,1),2);
entropy_RE_F_4=zeros(d(4,1),2); % method with 1000 point
entropy_RE_R_4=zeros(d(4,1),2);
entropy_RE_J_4=zeros(d(4,1),2);
entropy_RE_F_5=zeros(d(5,1),2); % method with transition point
entropy_RE_R_5=zeros(d(5,1),2);
entropy_RE_J_5=zeros(d(5,1),2);
entropy_RE_F_6=zeros(d(6,1),2); % method with fracture point
entropy_RE_R_6=zeros(d(6,1),2);
entropy_RE_J_6=zeros(d(6,1),2);

tic
for i=1:d(1,1)
    X=linspace(D_ini(i,4),D_ini(i,5),1000);

Y=pdf(dist_F_ini(i,1),X).*log(pdf(dist_F_ini(i,1),X)./pdf(dist_R_ini
(i,1),X));
    %  Relative entropy of forward in Normal distribution
    entropy_RE_F_1(i,1)=trapz(X,Y);
    % Relative entropy of reverse process in Normal distribution

Z=pdf(dist_R_ini(i,1),X).*log(pdf(dist_R_ini(i,1),X)./pdf(dist_F_ini
(i,1),X));
    entropy_RE_R_1(i,1)=trapz(X,Z);
    % Jeffery divergence
    entropy_RE_J_1(i,1)=entropy_RE_F_1(i,1)+entropy_RE_R_1(i,1);
    % Jeffery in Gaussian distribution
end
for i=1:d(2,1)
    X=linspace(D_250(i,4),D_250(i,5),1000);

Y=pdf(dist_F_250(i,1),X).*log(pdf(dist_F_250(i,1),X)./pdf(dist_R_250
(i,1),X));
    %  Relative entropy of forward in Normal distribution
```

```
    entropy_RE_F_2(i,1)=trapz(X,Y);
    % Relative entropy of reverse process in Normal distribution

Z=pdf(dist_R_250(i,1),X).*log(pdf(dist_R_250(i,1),X)./pdf(dist_F_250
(i,1),X));
    entropy_RE_R_2(i,1)=trapz(X,Z);
    % Jeffery divergence
    entropy_RE_J_2(i,1)=entropy_RE_F_2(i,1)+entropy_RE_R_2(i,1);
    % Jeffery in Gaussian distribution
end
for i=1:d(3,1)
    X=linspace(D_500(i,4),D_500(i,5),1000);

Y=pdf(dist_F_500(i,1),X).*log(pdf(dist_F_500(i,1),X)./pdf(dist_R_500
(i,1),X));
    %  Relative entropy of forward in Normal distribution
    entropy_RE_F_3(i,1)=trapz(X,Y);
    % Relative entropy of reverse process in Normal distribution

Z=pdf(dist_R_500(i,1),X).*log(pdf(dist_R_500(i,1),X)./pdf(dist_F_500
(i,1),X));
    entropy_RE_R_3(i,1)=trapz(X,Z);
    % Jeffery divergence
    entropy_RE_J_3(i,1)=entropy_RE_F_3(i,1)+entropy_RE_R_3(i,1);
    % Jeffery in Gaussian distribution
end
for i=1:d(4,1)
    X=linspace(D_1000(i,4),D_1000(i,5),1000);

Y=pdf(dist_F_1000(i,1),X).*log(pdf(dist_F_1000(i,1),X)./pdf(dist_R_1
000(i,1),X));
    %  Relative entropy of forward in Normal distribution
    entropy_RE_F_4(i,1)=trapz(X,Y);
    % Relative entropy of reverse process in Normal distribution

Z=pdf(dist_R_1000(i,1),X).*log(pdf(dist_R_1000(i,1),X)./pdf(dist_F_1
000(i,1),X));
    entropy_RE_R_4(i,1)=trapz(X,Z);
    % Jeffery divergence
    entropy_RE_J_4(i,1)=entropy_RE_F_4(i,1)+entropy_RE_R_4(i,1);
    % Jeffery in Gaussian distribution
end
for i=1:d(5,1)
    X=linspace(D_tra(i,4),D_tra(i,5),1000);

Y=pdf(dist_F_tra(i,1),X).*log(pdf(dist_F_tra(i,1),X)./pdf(dist_R_tra
(i,1),X));
    %  Relative entropy of forward in Normal distribution
    entropy_RE_F_5(i,1)=trapz(X,Y);
    % Relative entropy of reverse process in Normal distribution

Z=pdf(dist_R_tra(i,1),X).*log(pdf(dist_R_tra(i,1),X)./pdf(dist_F_tra
(i,1),X));
    entropy_RE_R_5(i,1)=trapz(X,Z);
    % Jeffery divergence
    entropy_RE_J_5(i,1)=entropy_RE_F_5(i,1)+entropy_RE_R_5(i,1);
```

```
    % Jeffery in Gaussian distribution
end
for i=1:d(6,1)
    X=linspace(D_fra(i,4),D_fra(i,5),1000);

Y=pdf(dist_F_fra(i,1),X).*log(pdf(dist_F_fra(i,1),X)./pdf(dist_R_fra
(i,1),X));
    %  Relative entropy of forward in Normal distribution
    entropy_RE_F_6(i,1)=trapz(X,Y);
    % Relative entropy of reverse process in Normal distribution

Z=pdf(dist_R_fra(i,1),X).*log(pdf(dist_R_fra(i,1),X)./pdf(dist_F_fra
(i,1),X));
    entropy_RE_R_6(i,1)=trapz(X,Z);
    % Jeffery divergence
    entropy_RE_J_6(i,1)=entropy_RE_F_6(i,1)+entropy_RE_R_6(i,1);
    % Jeffery in Gaussian distribution
end

toc

% Cumulative indices
entropy_RE_F_1(1,2)=entropy_RE_F_1(1,1);
entropy_RE_R_1(1,2)=entropy_RE_R_1(1,1);
entropy_RE_J_1(1,2)=entropy_RE_J_1(1,1);

entropy_RE_F_2(1,2)=entropy_RE_F_2(1,1);
entropy_RE_R_2(1,2)=entropy_RE_R_2(1,1);
entropy_RE_J_2(1,2)=entropy_RE_J_2(1,1);

entropy_RE_F_3(1,2)=entropy_RE_F_3(1,1);
entropy_RE_R_3(1,2)=entropy_RE_R_3(1,1);
entropy_RE_J_3(1,2)=entropy_RE_J_3(1,1);

entropy_RE_F_4(1,2)=entropy_RE_F_4(1,1);
entropy_RE_R_4(1,2)=entropy_RE_R_4(1,1);
entropy_RE_J_4(1,2)=entropy_RE_J_4(1,1);

entropy_RE_F_5(1,2)=entropy_RE_F_5(1,1);
entropy_RE_R_5(1,2)=entropy_RE_R_5(1,1);
entropy_RE_J_5(1,2)=entropy_RE_J_5(1,1);

entropy_RE_F_6(1,2)=entropy_RE_F_6(1,1);
entropy_RE_R_6(1,2)=entropy_RE_R_6(1,1);
entropy_RE_J_6(1,2)=entropy_RE_J_6(1,1);

for i=2:d(1,1)
    entropy_RE_F_1(i,2)=entropy_RE_F_1(i,1)+entropy_RE_F_1(i-1,2);
    entropy_RE_R_1(i,2)=entropy_RE_R_1(i,1)+entropy_RE_R_1(i-1,2);
    entropy_RE_J_1(i,2)=entropy_RE_J_1(i,1)+entropy_RE_J_1(i-1,2);
end
for i=2:d(2,1)
    entropy_RE_F_2(i,2)=entropy_RE_F_2(i,1)+entropy_RE_F_2(i-1,2);
    entropy_RE_R_2(i,2)=entropy_RE_R_2(i,1)+entropy_RE_R_2(i-1,2);
    entropy_RE_J_2(i,2)=entropy_RE_J_2(i,1)+entropy_RE_J_2(i-1,2);
```

```
end
for i=2:d(3,1)
    entropy_RE_F_3(i,2)=entropy_RE_F_3(i,1)+entropy_RE_F_3(i-1,2);
    entropy_RE_R_3(i,2)=entropy_RE_R_3(i,1)+entropy_RE_R_3(i-1,2);
    entropy_RE_J_3(i,2)=entropy_RE_J_3(i,1)+entropy_RE_J_3(i-1,2);
end
for i=2:d(4,1)
    entropy_RE_F_4(i,2)=entropy_RE_F_4(i,1)+entropy_RE_F_4(i-1,2);
    entropy_RE_R_4(i,2)=entropy_RE_R_4(i,1)+entropy_RE_R_4(i-1,2);
    entropy_RE_J_4(i,2)=entropy_RE_J_4(i,1)+entropy_RE_J_4(i-1,2);
end
for i=2:d(5,1)
    entropy_RE_F_5(i,2)=entropy_RE_F_5(i,1)+entropy_RE_F_5(i-1,2);
    entropy_RE_R_5(i,2)=entropy_RE_R_5(i,1)+entropy_RE_R_5(i-1,2);
    entropy_RE_J_5(i,2)=entropy_RE_J_5(i,1)+entropy_RE_J_5(i-1,2);
end
for i=2:d(6,1)
    entropy_RE_F_6(i,2)=entropy_RE_F_6(i,1)+entropy_RE_F_6(i-1,2);
    entropy_RE_R_6(i,2)=entropy_RE_R_6(i,1)+entropy_RE_R_6(i-1,2);
    entropy_RE_J_6(i,2)=entropy_RE_J_6(i,1)+entropy_RE_J_6(i-1,2);
end
```

A.1.5 AE information entropy calculation

```
%%% Calculating Information Entropy per Waveform: Non-parametric and
Parametric %%%%
% Parametric computation use in numerical integration
% Method5: Full numerical integration

testseries='8';
t_number=3;

if t_number<10
    testnumber=strcat('0',num2str(t_number));
else
    testnumber=num2str(t_number);
end
eval(['load ',testseries,'VA00_Condition_Summary.mat p_table'])
eval(['load ',testseries,'VA',testnumber,'_aa_wf_index.mat'])
p=p_table(t_number,1);
clear p_table

for r=1:p
    if r<10
       r_ch=strcat('0',num2str(r));
    else
       r_ch=num2str(r);
    end

    eval(['load ',testseries,'VA',testnumber,'_dataAE',r_ch,'.mat
Filt FilterNumber'])
    format shortG                                  %Formatting
    % Number of recorded waveforms for each test and for each sensor
```

```
    numberOfhits_ch1=FilterNumber(1,1);
%Input Number of files for the channel to analyze
    numberOfhits_ch2=FilterNumber(2,1);

    % Allocating matrices, not necessary to understand the idea of
the code
    entropy_IE_5_ch1=zeros(numberOfhits_ch1,1);            %Allocat-
ing, fixed bin entropy
    entropy_IE_5_ch2=zeros(numberOfhits_ch2,1);

    eval(['load ',testseries,'VA',testnumber,'_dataAE',r_ch,'.mat
para_nor_ch1 para_nor_ch2'])

    eval(['wf_index_ch1=wf_index_ch1_',r_ch,';'])
    eval(['wf_index_ch2=wf_index_ch2_',r_ch,';'])

    tic

    % IE computation
    for i=1:numberOfhits_ch1
        if Filt(i,4)~=0 && wf_index_ch1(i,1)~=0
            n=Filt(i,4);
            if wf_index_ch2(n,1)~=0
                % Analysis for ch1 data
                % entropy 5 calculation
                a=para_nor_ch1(i,1)-5*para_nor_ch1(i,2);
                b=para_nor_ch1(i,1)+5*para_nor_ch1(i,2);
                edges=linspace(a,b,1001);

mat_para=normrnd(para_nor_ch1(i,1),para_nor_ch1(i,2),[5000,1]);
                [prob] = histcounts(mat_para,edges, 'Normaliza-
tion','probability');    %Finding probability distribution with auto
binning rules
                S1_5 = zeros(length(prob),1);
%Allocating for prob matrix
                for q = 1:length(prob)
                    if prob(q)>0
                        S1_5(q) = -prob(q)*log2(prob(q));
%Calculating Shannon information content in bits
                    end
                end
                entropy_IE_5_ch1(i,1) = sum(S1_5);

                clear a b edges mat_para S1_5 q prob

               % Analysis for ch2 data
               % entropy 5 calculation
                a=para_nor_ch2(n,1)-5*para_nor_ch2(n,2);
                b=para_nor_ch2(n,1)+5*para_nor_ch2(n,2);
                edges=linspace(a,b,1001);

mat_para=normrnd(para_nor_ch2(n,1),para_nor_ch2(n,2),[5000,1]);
```

```
                [prob] = histcounts(mat_para,edges, 'Normaliza-
tion','probability');    %Finding probability distribution with auto
binning rules
                S1_5 = zeros(length(prob),1);
%Allocating for prob matrix
                for q = 1:length(prob)
                    if prob(q)>0
                        S1_5(q) = -prob(q)*log2(prob(q));
%Calculating Shannon information content in bits
                    end
                end
                entropy_IE_5_ch2(n,1) = sum(S1_5);

                clear a b edges mat_para S1_5 q prob
            end
        end
    end

    clear wf_index_ch1 wf_index_ch2
    clear Filt FilterNumber i n numberOfhits_ch1 numberOfhits_ch2
para_nor_ch1 para_nor_ch2
    eval(['save ',testseries,'VA',testnumber,'_dataAE',r_ch,'.mat
entropy_IE_5_ch1 entropy_IE_5_ch2 -append'])

    toc
end
```

A.1.6 AE relative entropy calculation

```
% 1. Finding Reference Waveform
% 2. Relative Entropy from Parametric Method (entropy 5)

testseries='8';
t_number=3;

if t_number<10
    testnumber=strcat('0',num2str(t_number));
else
    testnumber=num2str(t_number);
end
eval(['load ',testseries,'VA00_Condition_Summary.mat p_table'])
eval(['load ',testseries,'VA',testnumber,'_aa_wf_index.mat'])
p=p_table(t_number,1);
clear p_table

low_entropy_IE_5_ch1=zeros(p,2);
low_entropy_IE_5_ch2=zeros(p,2);

for r=1:p
    if r<10
       r_ch=strcat('0',num2str(r));
    else
       r_ch=num2str(r);
    end
```

```
    eval(['load ',testseries,'VA',testnumber,'_dataAE',r_ch,'.mat
entropy_IE_5_ch1 entropy_IE_5_ch2'])
    r1=find(entropy_IE_5_ch1~=0,1,'first');
    r2=find(entropy_IE_5_ch2~=0,1,'first');
    low_entropy_IE_5_ch1(r,1)=entropy_IE_5_ch1(r1,1);
    low_entropy_IE_5_ch2(r,1)=entropy_IE_5_ch2(r2,1);
    low_entropy_IE_5_ch1(r,2)=r1;
    low_entropy_IE_5_ch2(r,2)=r2;

    for j=r1+1:length(entropy_IE_5_ch1)
        if entropy_IE_5_ch1(j,1)~=0 && entropy_IE_5_ch1(j,1)<low_en-
tropy_IE_5_ch1(r,1)
            low_entropy_IE_5_ch1(r,1)=entropy_IE_5_ch1(j,1);
            low_entropy_IE_5_ch1(r,2)=j;
        end
    end

    for j=r2+1:length(entropy_IE_5_ch2)
        if entropy_IE_5_ch2(j,1)~=0 && entropy_IE_5_ch2(j,1)<low_en-
tropy_IE_5_ch2(r,1)
            low_entropy_IE_5_ch2(r,1)=entropy_IE_5_ch2(j,1);
            low_entropy_IE_5_ch2(r,2)=j;
        end
    end
    clear entropy_IE_5_ch1 entropy_IE_5_ch2
end
clear r j r1 r2

min_entropy_IE_5_ch1=min(low_entropy_IE_5_ch1(:,1));
min_entropy_IE_5_ch2=min(low_entropy_IE_5_ch2(:,1));

% Relative entropy based on ch1, method 5
% Relative entropy based on ch2, method 5

% 1. Relative entropy calculation, method 5
% For channel 1
% Figuring out the parameters of reference waveform
r=find(low_entropy_IE_5_ch1(:,1)==min_entropy_IE_5_ch1,1,'first');
if r<10
   r_ch=strcat('0',num2str(r));
else
   r_ch=num2str(r);
end
eval(['wf_index_ch1=wf_index_ch1_',r_ch,';'])
i=low_entropy_IE_5_ch1(r,2);
eval(['load ',testseries,'VA',testnumber,'_dataAE',r_ch,'.mat
para_nor_ch1'])
para_ref_ch1=para_nor_ch1(i,:);
a=para_ref_ch1(1,1)-5*para_ref_ch1(1,2);
b=para_ref_ch1(1,1)+5*para_ref_ch1(1,2);
clear para_nor_ch1
dist_ref_ch1=makedist('Normal','mu',para_ref_ch1(1,1),'sig-
ma',para_ref_ch1(1,2));
clear wf_index_ch1
```

```
tic

for r=1:p
    if r<10
        r_ch=strcat('0',num2str(r));
    else
        r_ch=num2str(r);
    end
    eval(['load ',testseries,'VA',testnumber,'_dataAE',r_ch,'.mat
Filt FilterNumber para_nor_ch1'])
    eval(['entropy_RE_5_ch1_',r_ch,'=zeros(FilterNumber(1,1),1);'])
    eval(['wf_index_ch1=wf_index_ch1_',r_ch,';'])

    numberOfFiles_ch1=FilterNumber(1,1); %Input Number of files for
the channel to analyze
    for i=1:numberOfFiles_ch1
        if Filt(i,4)~=0 && wf_index_ch1(i,1)~=0
            n=Filt(i,4);
            if wf_index_ch2(n,1)~=0
                % Calculating relative entropy
                dist=makedist('Normal','mu',para_nor_ch1(i,1),'sig-
ma',para_nor_ch1(i,2));
                c=para_nor_ch1(i,1)-5*para_nor_ch1(i,2);
                d=para_nor_ch1(i,1)+5*para_nor_ch1(i,2);
                equ_RE=@(x)
pdf(dist,x).*log2(pdf(dist,x)./pdf(dist_ref_ch1,x));
                entropy_RE=integral(equ_RE,max(a,c),min(b,d));
                eval(['entropy_RE_5_ch1_',r_ch,'(i,1) = en-
tropy_RE;'])
                clear dist c d n equ_RE entropy_RE
            end
        end
    end
    clear Filt FilterNumber numberOfFiles_ch1 wf_index_ch1
end
clear r r_ch a b

toc

% For channel 2
% Figuring out the parameters of reference waveform
r=find(low_entropy_IE_5_ch2(:,1)==min_entropy_IE_5_ch2,1,'first');
if r<10
   r_ch=strcat('0',num2str(r));
else
   r_ch=num2str(r);
end
eval(['wf_index_ch2=wf_index_ch2_',r_ch,';'])
n=low_entropy_IE_5_ch2(r,2);
eval(['load ',testseries,'VA',testnumber,'_dataAE',r_ch,'.mat
para_nor_ch2'])
para_ref_ch2=para_nor_ch2(n,:);
a=para_ref_ch2(1,1)-5*para_ref_ch2(1,2);
b=para_ref_ch2(1,1)+5*para_ref_ch2(1,2);
clear para_nor_ch2
```

```
dist_ref_ch2=makedist('Normal','mu',para_ref_ch2(1,1),'sig-
ma',para_ref_ch2(1,2));
clear wf_index_ch2

tic

for r=1:p
    if r<10
        r_ch=strcat('0',num2str(r));
    else
        r_ch=num2str(r);
    end
    eval(['load ',testseries,'VA',testnumber,'_dataAE',r_ch,'.mat
Filt FilterNumber para_nor_ch2'])
    eval(['entropy_RE_5_ch2_',r_ch,'=zeros(FilterNumber(2,1),1);'])
    eval(['wf_index_ch1=wf_index_ch1_',r_ch,';'])
    eval(['wf_index_ch2=wf_index_ch2_',r_ch,';'])

    numberOfFiles_ch1=FilterNumber(1,1); %Input Number of files for
the channel to analyze
    for i=1:numberOfFiles_ch1
        if Filt(i,4)~=0 && wf_index_ch1(i,1)~=0
            n=Filt(i,4);
            if wf_index_ch2(n,1)~=0
                % Calculating relative entropy
                dist=makedist('Normal','mu',para_nor_ch2(n,1),'sig-
ma',para_nor_ch2(n,2));
                c=para_nor_ch2(n,1)-5*para_nor_ch2(n,2);
                d=para_nor_ch2(n,1)+5*para_nor_ch2(n,2);
                equ_RE=@(x)
pdf(dist,x).*log2(pdf(dist,x)./pdf(dist_ref_ch2,x));
                entropy_RE=integral(equ_RE,max(a,c),min(b,d));
                eval(['entropy_RE_5_ch2_',r_ch,'(n,1) = en-
tropy_RE;'])
                clear dist c d n equ_RE entropy_RE
            end
        end
    end
    clear Filt FilterNumber numberOfFiles_ch1 wf_index_ch1 wf_in-
dex_ch2
end
clear r r_ch a b

toc

% Assigning computed entropy values to each AE data mat files

for r=1:p
    if r<10
       r_ch=strcat('0',num2str(r));
    else
       r_ch=num2str(r);
    end
    eval(['entropy_RE_5_ch1=entropy_RE_5_ch1_',r_ch,';'])
    eval(['entropy_RE_5_ch2=entropy_RE_5_ch2_',r_ch,';'])
```

```
    eval(['save ',testseries,'VA',testnumber,'_dataAE',r_ch,'.mat
entropy_RE_5_ch1 entropy_RE_5_ch2 -append'])
    eval(['save ',testseries,'VA',testnumber,'_aa_wf_reference.mat
low_entropy_IE_5_ch1 low_entropy_IE_5_ch2 -append'])
    clear entropy_RE_5_ch1 entropy_RE_5_ch2
end
```

A.2 Database structure

In this experimental research, multiple sources of data were collected to analyze the entropic methods as fatigue damage measurements. **Figure 61** presents the database structure to identify and track the data files to follow the analysis processes, in which the sorts of data and associated file names are described. **Table 14** presents the directory of each file. The file name and directory followed the Reliability and Mechanics Lab's database.

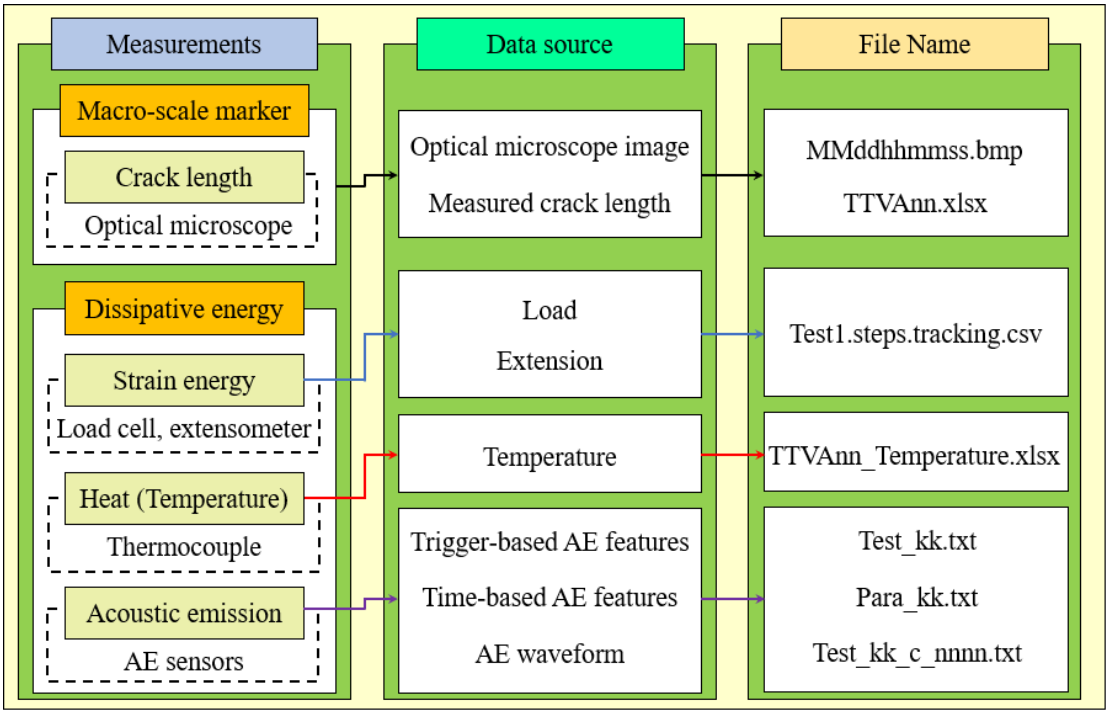

Figure 61. Data sources and associated file names for each measurement.

Table 14. Data file names and the associated directories. The symbols related to the material and specimen identification, test date and time, and AE file name are also described.

File Name	Directory
MMddhhmmss.bmp	\02_Image Files\Image_Realtime\TTVAnn_MMddYY\
TTVAnn.xlsx	\01_Data Files\Crack_data\
Test1.steps.tracking.csv	\01_Data Files\Instron_data\TTVAnn_MMddYY\Test1\
TTVAnn_Temperature.xlsx	\01_Data Files\Thermocouple_data\TTVAnn_MMddYY\
Test_kk.txt	\01_Data Files\AE_data\TTVAnn_MMddYY\
Para_kk.txt	\01_Data Files\AE_data\TTVAnn_MMddYY\
Test_kk_c_nnnn.txt	\01_Data Files\AE_data\TTVAnn_MMddYY\Waveform\
Symbols	
YY: year, MM: month, dd: day, hh: hour, mm: minute, ss: second, TT: test material (7_1: AA7075-T6, 8: SS304L), nn: test number, kk: file number in AE data, c: AE sensor channel number, nnnn: number in the order of AE waveform generation	

Bibliography

[1] M. Amiri and M. Modarres, "An Entropy-Based Damage Characterization," *Entropy,* vol. 16, pp. 6434-6463, 2014.

[2] M. Naderi, M. Amiri and M. Khonsari, "On the Thermodynamic Entropy of Fatigue Fracture," *Proceedings of the Royal Society A,* pp. 1-16, 2009.

[3] V. Ontiveros, M. Amiri, A. Kahirdeh and M. M, "Thermodynamic Entropy Generation in the Course of the Fatigue Crack Initiation," *Fatigue & Fracture of Engineering Materials & Structures,* vol. 40, pp. 423-434, 2016.

[4] B. E. Klanecki, "Wear-An Entropy Production Model," *Wear,* vol. 58, pp. 325-330, 1980.

[5] B. E. Klamecki, "Energy Dissipaton in Sliding," *Wear,* vol. 77, pp. 115-128, 1982.

[6] B. E. Klamecki, "An Entropy-Based Model of Plastic Deformation Energy Dissipation in Sliding," *Wear,* vol. 96, pp. 319-329, 1984.

[7] A. Zmitrowicz, "A Thermodynamical Model of Contact, Friction and Wear: I Governing Equations," *Wear,* vol. 114, pp. 135-168, 1987.

[8] A. Zmitrowicz, "A Thermodyanmical Model of Contact, Friction and Wear: II Constitutive Equations for Materials and Linearized Theories," *Wear,* vol. 114, pp. 169-197, 1987.

[9] A. Zmitrowicz, "A Thermodynamical Model of Contact, Friction and Wear: III Constitutive Equations for Friction, Wear and Frictional Heat," *Wear,* vol. 114, pp. 199-221, 1987.

[10] K. L. Doelling, F. F. Ling, M. D. Bryant and B. P. Heilman, "An Experimental Study of the Correlation between Wear and Entropy Flow in Machinery Components," *Journal of Applied Physics,* vol. 88, no. 5, pp. 2999-3003, 2000.

[11] M. D. Bryant, "Modeling Degradation Using Thermodynamic Entropy," in *Annual Conference of the Prognostics and Health Management Society*, 2014.

[12] M. Nosonovsky and B. Bhushan, "Themodynamics of Surface Degradation, Self-organization and Self-healing for Biomimetic Surface," *Philosophical Transactions of The Royal Society,* vol. 267, pp. 1607-1627, 2009.

[13] C. M. Sauerbrunn, A. Kahirdeh, H. Yun and M. Modarres, "Damage Assessment Using Information Entropy of Individual Acoustic Emission Waveforms during Cyclic Fatigue Loading," *Applied Science,* vol. 7, no. 6, p. 562, 2017.

[14] G. E. Crooks, "Entropy Production Fluctuation Theorem and the Nonequilibrium Work Relation for Free Energy Difference," *Physical Review E,* vol. 60, no. 2, pp. 2721-2726, 1999.

[15] C. Jarzynski, "Equality and Inequalities: Irreversibility and the Second Law of Thermodynamics at the Nanoscale," *Annual Review of Condensed Matter Physics,* vol. 2, pp. 329-351, 2011.

[16] D. Collin, F. Ritort, C. Jarzynski, S. Smith, I. J. Tinoco and C. Bustamante, "Verification of the Crooks Fluctuation Theorem and Recovery of RNA Folding Free Energies," *Nature,* vol. 437, no. 8, pp. 231-234, 2005.

[17] F. Douarche, S. Ciliberto, A. Petrosyan and I. Rabbiosi, "An Experimental Test of the Jarzynski Equality in a Mechanical Experiment," *Europhysics Letters,* vol. 70, no. 5, pp. 593-599, 2005.

[18] J. Lemaitre, A Course on Damage Mechanics, 2 ed., Berlin: Springer, 1990.

[19] K. L. Tsui, N. Chen, Q. Zhou, Y. Hai and W. Wang, "Prognostics and Health Management: A Review on Data Driven Approaches," *Mathematical Problems in Engineering,* pp. 1-17, 2015.

[20] N.-H. Kim, D. An and J.-H. Choi, Prognostics and Health Management of Engineering Systems: An Introduction, Switzerland: Springer, 2017.

[21] S. Ekwaro-Osire, F. M. Alemayehu and A. C. Goncaleves, Probabilistic Prognostics and Health Management of Energy Systems, Cham, Switzerland: Springer, 2017.

[22] X.-S. Si, Z.-X. Zhang and C.-H. Hu, Data-Driven Remaining Useful Life Prognosis Techniques, Berlin, Gemany: Springer, 2017.

[23] G. Niu, Data-Driven Technology for Engineering Systems Health Management, Beijing, China: Springer, 2017.

[24] V. Weiss and A. Ghoshal, "On the Search for Optimal Damage Precursors," *Structural Health Monitoring,* vol. 13, no. 6, pp. 601-608, 2014.

[25] A. Imanian and M. Modarres, "A Thermodynamic Entropy Approach to Reliability Assessment with Applications to Corrosion Fatigue," *Entropy,* vol. 17, pp. 6995-7020, 2015.

[26] M. Bryant, M. Khonsari and F. Ling, "On the Thermodynamics of Degradation," *Proceedings of the Royal Society A,* vol. 464, pp. 2001-2014, 8 4 2008.

[27] C. Basaran and S. Nie, "An Irreversible Thermodyanmics Theory for Damage Mechanics of Solids," *International Journal of Damage Mechanics,* vol. 13, no. 3, pp. 205-223, 2004.

[28] A. Kahirdeh and M. Khonsari, "Energy Dissipation in the Course of the Fatigue Degradation: Mathematical Derivation and Experimental Quantification," *International Journal of Solids and Structure,* vol. 77, pp. 75-85, 2015.

[29] G. E. Crooks and D. A. Sivak, "Measures of Trajectory Ensemble Disparity in Nonequilibrium Statistical Dynamics," *Journal of Statistical Mechanics: Theory and Experiment,* pp. 1-10, 2011.

[30] J. Blitz, Electrical and Magnetic Methods of Non-destructive Testing, Dordrecht: Springer Netherlands, 1997.

[31] J. J. Burke and V. Weiss, Sagamore Army Materials Research Conference Proceedings on the Nondestructive Characterization of Materials, Raquette Lake: Plaenum, 1979.

[32] C. Basaran and R. Chandaroy, "Mechanics of Ph40/Sn60 Near-eutectic Solder Alloys Subjected to Vibrations," *Applied Mathematical Modelling,* vol. 22, no. 8, pp. 601-627, 1998.

[33] A. Imanian and M. Modarres, "A Thermodynamic Entropy-based Damage Assessment with Applications to Prognostics and Health Management," *Structural Health Monitoring,* vol. 17, no. 2, pp. 240-254, 2018.

[34] A. Keshtgar and M. Modarres, "Acoustic Emission-Based Fatigue Crack Growth prediction," in *Reliability and Maintanability Symposium (RAMS)*, St. Louis, 2013.

[35] P. Vanniamparambil, U. Guclu and A. Kontsos, "Identification of Crack Initiation in Aluminum Alloys Using Acoustic Emission," *Experimental Mechanics,* vol. 55, no. 5, pp. 837-850, 2015.

[36] A. Berkovits and D. Fang, "Study of Fatigue Crack Characteristics by Acoustic Emission," *Engineering Fracture Mechanics,* vol. 51, pp. 401-416, 1995.

[37] K. Mathis and F. Chmelik, "Exploring Plastic Deformation of Metallic Materials by the Acoustic Emission Technique," in *Acoustic Emission*, Rijeka, Intechopen, 2011, pp. 23-48.

[38] A. Keshtgar, C. M. Sauerbrunn and M. Modarres, "Structural Reliability Prediction Using Acoustic Emission-Based Modeling of Fatigue Crack Growth," *Applied Science,* vol. 8, no. 8, p. 1225, 2018.

[39] M. Hughes, "Analysis of Ultrasonic Waveforms Using Shannon Entropy," in *IEEE 1992 Ultrasonics Symposium Proceedings*, Tucson, 1992.

[40] A. Caticha, Entropic Inference and the Foundations of Physics, Albany, 2012.

[41] S. Lin, s. Goa, Z. He and Y. Deng, "A Pilot Directional Protection for HVDC Transmission Line Based on Relative Entropy of Wavelet Energy," *Entropy,* vol. 2015, no. 17, pp. 5257-5273, 2015.

[42] H. He, Y. Tan and Y. Wang, "Optimal Based Wavelet Selection for ECG Noise Reduction Using a Comprehensive Entropy Criterion," *Entropy,* vol. 2015, no. 17, pp. 6093-6109, 2015.

[43] C. Maes, "The Fluctuation Theorem as a Gibbs Property," *Journal of Statistical Physics,* vol. 95, no. 1-2, pp. 367-392, 1999.

[44] C. Maes and K. Netocny, "Time-Reversal and Entropy," *Journal of Statistical Physics,* vol. 110, no. 1-2, pp. 269-310, 2003.

[45] P. Gaspard, "Time-Reversed Dynamical Entropy and Irreversiblity in Markovian Random Processes," *Journal of Statistical Physics,* vol. 117, no. 314, pp. 599-615, 2004.

[46] A. G. Evans, M. Linzer and L. R. Russell, "Acoustic Emission and Crack Propagration in Polycrystalline Alumina," *Materials Science and Engineering,* vol. 15, pp. 253-261, 1974.

[47] C. R. Heiple, S. H. Carpenter and R. L. Thomas, "Acoustic emission produced by defromation of metals and alloys," *Journal of Acoustic Emission,* vol. 6, pp. 177-204, 1987.

[48] K. Ono and M. Yamamoto, "Anisotropic Mechanical and Acoustic Emission Behavior of A533B Steels," *Materials Science and Engineering,* vol. 47, pp. 247-263, 1981.

[49] M. L. Rosinberg and E. Vives, Metastability, hysteresis, avalanches, and acoustic emission: Martensitiic transitions in functional materials, Egidelberg: Springer, 2012.

[50] Y. Li and M. Enoki, "Twinning behaviro of pure magnesium quantitatively investigated by acoustic emission," *Materials Science and Engineering A,* vol. 536, pp. 8-13, 2012.

[51] O. Muransky, M. R. Barnett, D. G. Carr, S. C. Vogel and E. C. Oliver, "Investigation of deformation tweinning in a fin-grained and coarse-grained ZM20 Mg alloy: Combined in situ neutron diffraction and acoustic emission," *Acta Materialia,* vol. 58, pp. 1503-1517, 2010.

[52] T. M. Morton, R. M. Harrington and J. G. Bjeletich, "Acoustic Emissions of Fatigue Crack Growth," *Engineering Fracture Mechanics,* vol. 5, pp. 691-697, 1973.

[53] R. Miller, *Acoustic emission: an applicatyion to fracture mechanics,* West Lafayette, IN: Purdue University, 1979.

[54] C. M. Sauerbrunn , *Evaluation of Information Entropy from Acoustic Emission Waveforms as a Fatigue Damage Metric for AL7075-T6,* College Park, MD: University of Maryland, 2016.

[55] M. G. Baxter, R. Pullin, K. M. Holford and S. L. Evans, "Delta T source location for acoustic emission," *Mechanical Systems and Signal Processing,* vol. 21, pp. 1512-1520, 2007.

[56] L. Gao, F. Zai, S. Su, H. Wang, P. Chen and L. Liu, "Study and Applicaiton of Acoustic Emission Testing in Fault Diagnosis of Low-Speed Heavy-Duty Gears," *Sensors,* vol. 11, pp. 599-611, 2011.

[57] T. Matsuo and H. Cho, "Development of AE Monitoring System with Noise Reduction Function by Spectral Subtraction," *Maerials Transactions,* vol. 53, no. 2, pp. 342-348, 2012.

[58] Z. Parsons and W. J. Staszewski, "Nonlinear acoustics with low-profile piezoceramic excitation for crack detection in etallic structures," *Smart Materials and Structures,* vol. 15, pp. 1110-1118, 2006.

[59] M. Amiri and M. M. Khonsari, "Nondestructive Estimation of Remaining Fatigue Life: Thermography Techniques," *Journal of Failure Analysis and Prevention,* vol. 12, no. 6, pp. 683-688, 2012.

[60] J. A. Bannantine, J. J. Comer and J. L. Handrock, Fundamentals of Metal Fatigue Analysis, 1 ed., Englewood Cliffs, Jew Jersey: Prentice Hall, 1990.

[61] *ASTM E466 Standard Practice for Conducting Force Controlled Constant Amplitude Axial Fatigue Tests of Metallic Materials.*

[62] I. ANSYS, *ANSYS Workbench Release 16.2,* 2016.

[63] I. Autodesk, *AutoCAD 2018,* 2018.

[64] Instron Inc., *8800 System Console Version 8.4,* 2011.

[65] Illinois Tool Works Inc., *WaveMatrix V1.5,* 2010.

[66] Mistras Group, *AEwin for PCI2 Version E5.60,* 2014.

[67] Physical Acoustics Corporation, *PCI-2 Based AE System User's Manual Rev 3,* Princeton Junction: Physical Acoustics Corporation, 2007.

[68] ASTM, *ASTM E650M-17 Standard Guide for Mounting Pezoelectric Acoustic Emission Sensors,* 2017.

[69] ASTM, *ASTM E976-99 Standard Guide for Determining the REproducibility of Acoustic Emission Sensor Response,* 1999.

[70] S. V. Ranganayakulu, B. S. Goud and B. R. Kumar, "Calibration of Acoustic Emission System for Materials Characterization," *Universal Journal of Materials Science,* vol. 3, no. 4, pp. 62-69, 2015.

[71] S. K. Al-Jumaili, M. R. Pearson, K. M. Holford, M. J. Eaton and R. Pullin, "Acoustic emission source location in complex structures using full automatic delta T mapping technique," *Mechanical Systems and Signal Processing,* Vols. 72-73, pp. 513-524, 2016.

[72] I. The Mathworks, *Matlab 2019a,* 2019.

[73] Omega Engineering, "Ready-Made Insulated Thermocouples," Omega Engineering, [Online]. Available: https://www.omega.com/en-us/search/?text=5TC-TT-K-40-36. [Accessed 16 May 2019].

[74] National Instrument, *Labview 2017.*

[75] TShow Software, *OCView Version 7.1.1.2.*

[76] V. L. Ontiveros, *Strain Energy Density and Thermodynamic Entropy as Prognostic Measures of Crack Initiation in Aluminum,* College Park, Maryland: Unitversity of Maryland, 2013.

[77] T. Anderson, Fracture Mechanics, Fundamentals and Applications, 3 ed., Boca Raton, Florida: CRC Press, 2005.

[78] N. Iyyer, S. Sarkar, R. Merrill and N. Phan, "Aircraft life management using crack initiation and crack growth models - P-3C Aircraft experience," *International Journal of Fatigue,* vol. 29, no. 9-11, pp. 1584-1607, 2007.

[79] J. Schijve, Fatigue of Structures and Materials, Delft: Springer, 2009.

[80] L. Pook, Metal Fatigue: What it is, why it matters, Dordrecht: Springer, 2007.

[81] U. Krupp, Fatigue Crack Propagation in Metals and Alloys: Microstructural Aspects and Modelling Concepts, Wiley-VCH Verlag GmbH & Co. KGaA, 2007.

[82] Adobe, *Photoshop CC,* 2017.

[83] S. M. Beden, S. Sbdullah and A. K. Ariffin, "Reveiw of Fatigue Crack Propagation Models for Metallic Componets," *European Journal of Scientific Research,* vol. 28, no. 3, pp. 364-397, 2009.

[84] P. Paris and F. Erdogan, "A critical analysis of crack propagation laws," *Journal of Basic Engineering, Transaction of the American Society of Mechanical Engineers,* pp. 528-534, 1963.

[85] W. D. Calister and D. G. Rethsisch, Materials Science and Engineering: An Introduction, Hoboken: Wiley, 2014.

[86] N. E. Dowling, "Mean Stress Effects in Stress-Life and Strain-Life Fatigue," in *Second SAE Brasil International Conference on Fatigue*, 2004.

[87] V. L. Ontiveros, M. Modarres and M. Amiri, "Estimation of reliability of structures subject to fatigue loading using plastic strain energy and thermodynamic entropy generation," *Proceedings of the Institution of Mechanical Engineerings, Part O: Journal of Risk and Reliability,* vol. 229, no. 3, pp. 220-236, 2015.

[88] X. Guan, R. Jha and Y. Liu, "Probabilistic fatigue damage prognosis using maximum entropy approach," *Journal of Intelligent Manufacturing,* vol. 23, no. 2, pp. 163-171, 2012.

[89] H. Li, D. Wen, Z. Lu, Y. Wang and F. Deng, "Identifying the Probability Distribution of Fatigue Life Using the Maximum Entropy Principle," *Entropy,* vol. 18, no. 4, p. 111, 2016.

[90] C. Soize, Uncertainty Quantification: An Accelerated Course with Advanced Applications in Computational Engineering, Cham, Switzland: Springer, 2017.

[91] J. N. Kapur and H. K. Kesavan, Entropy optimization principles with applications, Boston: Academic Press, 1992.

[92] M. A. Miner, "Cumulative Damge in Fatigue," *Journal of Applied Mechanics,* vol. 3, pp. 159-164, 1945.

[93] A. Kahirdeh, C. Sauerbrunn, H. Yun and M. Modarres, "A Parametric Approach to Acoustic Entropy Estimation for Assessment of Fatigue Damage," *International Journal of Fatigue,* vol. 100, no. 1, pp. 229-237, 2017.

[94] J. D. Gibbons and C. S., Nonparametric Statistical Inference, Boca Raton, FL: Chapman & Hall/CRC Press, Taylor & Francis, 2011.

[95] F. Mozafari, P. Thamburaja, A. R. Srinivasa and N. Moslemi, "A rate independent inelasticity model with smooth transition for unifying low-cycle and high-cycle fatigue life prediction," *International Journal of Mechanical Sciences,* vol. 159, no. 2019, pp. 325-335, 2019.

[96] E. Z. Kordatos, K. G. Dassios, D. G. Aggelis and T. E. Matikas, "Rapid evaluation of the fatigue limit in composites using infrared lock-in thermography and acoustic emission," *Mechanics Research Communications,* vol. 54, pp. 14-20, 2013.

[97] J. Fan, X. Guo, C. Wu, Y. Zhao and Q. Guo, "Stress assessment and fatigue behavior evaluation of components with defects based on the finite element method and lock-in thermography," *Journal of Mechanical Engineering Science,* vol. 229, no. 7, pp. 1194-1205`, 2015.

[98] M. Naderi and M. M. Khonsari, "Thermodynamics analysis of fatigue failure in a composite lamintate," *Mechanics of Materials,* vol. 46, no. 2012, pp. 113-122, 2012.

[99] P. Williams, M. Liakat, M. M. Khonsari and O. M. Kabir, "A thermographic method for remaining fatigue life prediction of welded joints," *Materials and Design,* vol. 51, no. 2013, pp. 916-923, 2013.

[100] E. Z. Kordatos, D. G. Aggelis and T. E. Matikas, "Monitoring mechanical damage in structural materials using complimentary NDE techniques based on thermography and acoustic emission," *Composites: Part B,* vol. 43, no. 2012, pp. 2676-2686, 2012.

[101] P. M. Djuric and M. F. Bugallo, "Particle filtering for multivariate state-space models," in *Forty Sixth Asilomar Conferece on Signals, Systems and Computers (ASILOMAR)*, Pasific Grove, 2012.

[102] T. Yang, R. S. Laugesen, P. G. Mehta and S. P. Meyn, "Multivariable feedback particle filter," *Automatica,* vol. 71, pp. 10-23, 2016.